Nonlinear Control for High Precision Motion and Energy Saving in Multi-Axis Industrial Systems

August, 2013

Doctor of Engineering

Abd El Khalick Mohammad Ahmad Mohammad

Toyohashi University of Technology

Declaration of Authorship

I, Abd El Khalick Mohammad Ahmad Mohammad, declare that this thesis titled,
' Nonlinear Control for High Precision Motion and Energy Saving in Multi-Axis
Industrial Systems' and the work presented in it are my own. I confirm that:

- This work was done wholly or mainly while in candidature for a research
  degree at this University.

- Where any part of this thesis has previously been submitted for a degree or
  any other qualification at this University or any other institution, this has
  been clearly stated.

- Where I have consulted the published work of others, this is always clearly
  attributed.

- Where I have quoted from the work of others, the source is always given.
  With the exception of such quotations, this thesis is entirely my own work.

- I have acknowledged all main sources of help.

- Where the thesis is based on work done by myself jointly with others, I have
  made clear exactly what was done by others and what I have contributed
  myself.

Signed:
_____

Date:
_____

TOYOHASHI UNIVERSITY OF TECHNOLOGY

Abstract

Graduate School of Engineering
Department of Mechanical Engineering

Doctor of Engineering

**Nonlinear Control for High Precision Motion and Energy Saving in
Multi-Axis Industrial Systems**

by Abd El Khalick Mohammad Ahmad Mohammad

High-precision machining of complex-shaped such as dies, molds, and aerospace parts with sculptured surfaces requires multi-axis feed drive systems to accurately follow specified contours. In addition, because computer numerical controlled (CNC) machines are widely used night and day in manufacturing all over the world, not only high-speed and high-precision control but consumed energy control is required. In practice, the tool motion deviates from the desired trajectory due to the limited bandwidth of the servo drives, as well as disturbances originating from cutting forces and guide-way friction. For machining, reduction of contour error is an important issue. Contour error is defined as the component orthogonal to the desired contour curve, and it represents better indicator of precision machining. In addition, it is too difficult to calculate the contour error in real time because it requires solving nonlinear equations in real time. In order to improve tracking=contouring performance for multi-axis feed drive systems, this thesis presents several approaches for the following feed drive systems:

1. Single-axis feed drive system

   We presented a novel sliding mode controller with a non-linear sliding surface to improve the machining accuracy of ball-screw feed drive systems. Unlike the conventional sliding mode control design, the proposed non-linear sliding surface varies according to the output (controlled variable) so that the closed loop system simultaneously achieves low overshoot and a small settling time, resulting in a smaller error and small energy consumption. The consumed energy and control input variation were reduced by about 12.9% and 19.1%, respectively.

2. Biaxial feed drive system

   In this section, we have presented a novel algorithm to model predictive contouring control for biaxial feed drive systems. Model predictive control (MPC) refers to a class of model-based controllers that uses an explicit process model and tracking error dynamics to predict the future behavior of a plant, making it effective for machine tool feed drive systems that must achieve high-precision motion and are severely affected by friction, cutting force and changes in the workpiece mass. To improve contouring performance, we propose a new performance index in which error components orthogonal to the desired contour curve are given more importance than tracking errors with respect to each feed drive axis. The effectiveness of the proposed control approach is demonstrated with an experimental biaxial feed drive system for circular and non-circular trajectories. The proposed contouring controller allows the feed drive to follow smooth curves and reduces contour error. In addition, We proposed a novel sliding mode contouring controller with a nonlinear sliding surface to improve the machining accuracy and reduce the consumed energy of the biaxial feed drive systems. The advantage of including the contour error in the proposed sliding surface is that the damping ratio of the system changes from its initial low value to its final high value as the contour error changes from high value to small value and vice versa. The proposed approach reduced the control input variance and consumed energy on average by about 41.2% and 14.9% (for x and y-axis, respectively) and 23.6% and 5.5% (for x and y-axis, respectively), respectively.

3. Three-axis feed drive systems

We presented a new contour error estimation model for three dimensional machining tasks. The model is based on estimation of the instantaneous curvature of the reference trajectory and a coordinate transformation approach. This algorithm is based on an iterative desired contour curve approximation by circular curves. We extended the approach of sliding mode contouring controller for biaxial feed drive system to the three-axis case. In this approach, the normal and bi-normal error components are given more importance than the tangential component. By using the proposed method, simulation and experimental results for a desktop three-axis machine show a significant performance improvement in terms of the contour error.

4. Five-Axis Machines

Conventionally, five-axis machines do its control efforts to minimize the error components along the driving axis independently. Although many effective controllers have been applied to the individual axis control loops, elimination of the tracking errors of each individual axis in multi-axis feed drive systems may not guarantee the desired contouring accuracy. Even if the tool tip contour error and tool orientation contour error are very small, a mismatch between the observed tool tip position and tool-orientation will cause an over-cut or undercut when these errors are treated independently. To avoid this mismatch, we present a new definition of the tool orientation contour error to consider synchronization between the tool-tip contour error and tool-orientation contour error. Experimental results demonstrate that the proposed tool orientation contour error reduction is more important than the reduction of the conventional tool orientation contour error. Based on the tool orientation contour error estimation method, we designed a novel sliding mode contouring controller with nonlinear sliding surface and disturbance observer for five-axis machines. The proposed controller considering the synchronization of the tool tip and orientation contour errors...

Acknowledgements

First of all, I like to express my thanks to ALLAH, the most beneficent the most merciful, the Lord of the Worlds, for his many and uncountable blessings upon us. Without his blessing, this work would not be done.

I would like to express my deep appreciation to Prof. Dr. Naoki Uchiyama for his willingness to take me into his research group and for the wonderful opportunity and passionate guidance, he gave me during the three-years researching. His enthusiasm and interest for science are contagious. I have learned not only scientific techniques from him, but also more importantly, the method of scientific thinking, how to identify a research problem, how to form and carry out a research plan and how to get results.

I am grateful to my committee members, Prof. Dr. Hideki Yanada, Prof. Dr. Kazuhiko Terashima and Prof. Dr. Shinchi Suzuki for their great support and constructive comments. In addition I would like to thank Assistant Prof. Dr. Shigenori Sano for giving me valuable discussion and suggestion to complete this work. I also extend my thanks to all members of the Robotics and Mechatronics Laboratory for their assistance and friendship during my graduate study.

Furthermore, I thank MEXT(Ministry of Education, Culture, Sports, Science and Technology, Japan), Toyohashi University of Technology, The Hori Sciences and Arts Foundation and Yamazaki MAZAK Corporation for their financial support and thanks for all Toyohashi University of Technology staff members for their assistance and friendship.

With my endless love, I would like to thank my wife Noran Elhoussieny. Her encouragement, support, quiet patience and unwavering love are undeniably. Her tolerance of my occasional vulgar moods is a testament in itself of her unyielding devotion and love.

I extend most heartfelt thanks to my parents for their endless support, sacrifice, and unconditional love. I also thank my sisters, brothers, sisters-in-law, and brothers-in-law, and for their constant understanding and encouragement. The warm love of my family motivates me to go on.

Contents

List of Figures

List of Tables

Abbreviations

CCC	Cross-Coupled Control
CNC	Computer Numerical Controlled
DC	Direct Current
AC	Alternating Current
NC	Numerical Controlled
CNC	Computer Numerical Controlled
PID	Proportional-Integral-Derivative
ZPETC	Zero Phase Error Tracking Control
LSS	Linear Sliding Surface
NLSS	Nonlinear Sliding Surface
SMC	Sliding Mode Control
CNF	Composite Nonlinear Feedback

To my Parentes with my love . . .

Chapter 1

Introduction

1.1   Introduction

In the aerospace industry, die and mold manufacturing and semiconductor manufacturing fields, the need for fast response and high precision becomes the concern of the machine tool community. In the aerospace industry, high speed machine tools is required to enable complex parts to be produced in one piece within the shortest possible time. On the other hand, the die and mold industry demands machine tools that can cut complex 3-D shapes with speed, accuracy and high-quality surface finishes. Similarly, automotive manufacturers need high-precision machines that can perform point-to-point cutting operations in the possible shortest time [1]. In order to achieve such high accurate machining, computer numerical controlled (CNC) machines is an essential key.

1.1.1   Computer Numerical Control Machines

CNC is one in which the motions and functions of a machine tool are controlled by means of a storage program. This program contains coded alphanumeric data, which is used to control the motions of the workpiece or tool. In addition, the program includes some input parameters such as feed, depth of cut, speed of the spindle, and the on/off functions such as turning spindle and turning coolant..

CNC machines have several advantages over the conventional manufacturing machines such as high accuracy in manufacturing, short production time, greater

FIGURE 1.1: Application of ball screw feed drive in CNC machines

manufacturing flexibility, simpler fixturing, contour machining (2 up 5-axis machining), reduced human error, etc. Due to these advantages, CNC machines are widely used for machine tool area such as milling machine, drill press, lath, grinding, laser cutting machines, sheet-metal press working machine etc. In addition, they are used for other areas such as welding machines (including arc and resistance), electronic assembly, coordinate measuring machine, tape laying and filament winding machines for composites, etc. However, CNC has some drawbacks such as high cost, maintenance, and the requirement of a skilled part programmers.

1.1.2 Feed drive system

Generally, CNC machines consist of a group of axes, also known as feed drives, each axis consists of a driving motor which provides the driving forces (for linear axes) or torques (for rotary axes). This force or torque is transmitted to the axis through a train of mechanical transmission elements such as gears.
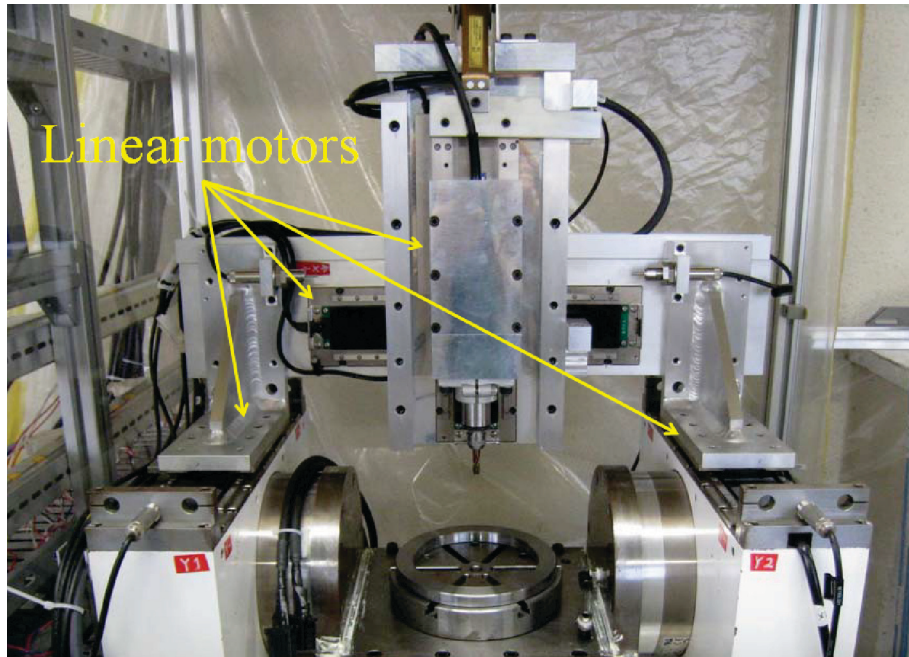
FIGURE 1.2: Application of linear motor in CNC machines

The ball screw feed drives are very commonly used in machine tools because of their relatively high stiffness to cutting force, disturbances, table load variations and this is due to the gear reduction ratio. They provide thrust and linear motion of the feed drive by transmitting power from the driving motor through a ball screw mechanism. In the ball screw feed drive system, the servomotor torque is transmitted to the ball screw shaft through some transmission mechanism such as gears. The screw-nut mechanism converts the servomotor rotational motion into a linear motion and moves the table that holds the workpiece or cutting tool and attached to the nut as shown in Fig. 1.1. The different shafts in the system are coupled together through elastic couplings, and bearings are used to support the shafts and allow the smooth rotational movement [2].

Another method to provide the linear motion of the feed drive is to employ a direct drives such as linear motors as shown in Fig. 1.2. In which, the linear motion and thrust directly supplied to the machine tool table without any need of an intermediary conversion mechanism. Therefore, they have an advantage over ball screw drives because they involve fewer components and are thus less susceptible to the influence of undesirable structural modes [1]. Another advantage of the linear actuators is that they can achieve higher speeds and accelerations with minimal backlash and friction. On the other hand, direct drives suffer from some significant drawbacks such as high sensitivity to changes in workpiece mass. In
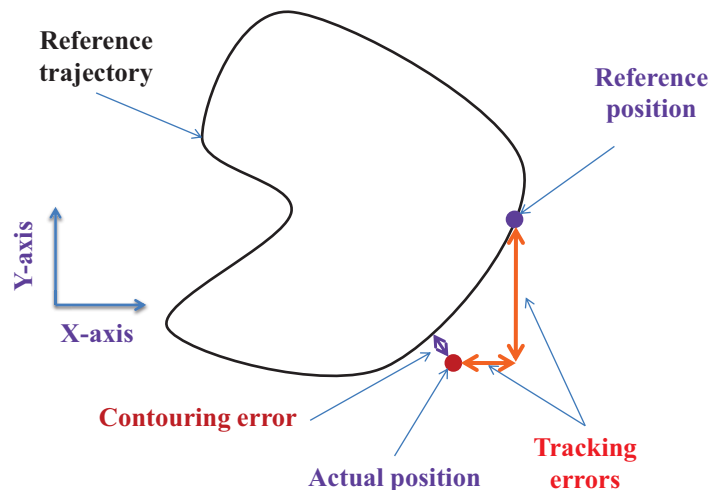
FIGURE 1.3: Contour error in two dimensional machining

addition, their dynamic stiffness depends mainly on the controller settings; it has little reinforcement from the mechanical structure. As a result, the large forces that occur during machining could easily excite the dynamics of the control loop and cause instability in both the controller and the metal cutting process. In order to mitigate the effects of cutting forces and workpiece mass variations on the control of direct-driven machines, they are typically over-sized by increasing the mass of the table and the power of the linear motors. This in turn reduces the achievable bandwidth and increases the cost of direct-driven machine tools, both of which are undesirable[1].

In machining applications, the interpolator generates the desired tool motion relative to workpiece and then decomposes the desired motion into reference position commands for the individual driving axes. In order to achieve high-speed, high-precision position control, full-closed feedback control is applied. Several control approaches have been proposed for such a system. In general, proportional position control or proportional plus integral velocity control or integral plus proportional velocity control (P,PI/I-P), which are specific types of proportional plus integral plus differential control (PID), is applied in many industrial applications. However, in the case of changing mechanical characteristics of the control target, the parameters of P,PI/I-PI control must also change in order to maintain good motion performance [3].
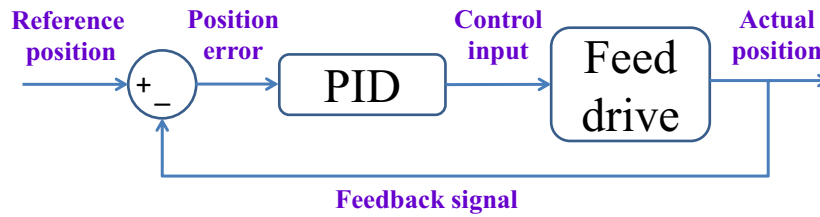
FIGURE 1.4: Feedback controller for a single axis drive system

1.1.3 Control of Multi-Axis Feed Drive Systems

High-precision machining requires multi-axis feed drive systems to accurately follow specified contours [4, 5]. Tracking errors usually appear in many industrial applications such as X-Y tables, computer numerical control (CNC) machines and industrial manipulators. For machining, error components orthogonal to the desired contour curve represent better indicators of the precision of machining, and are defined as "contour error". Tracking and contour errors as shown in Fig. 1.3, are important aspects that significantly affect machining accuracy.

Two main control approaches are used to improve contouring performance: tracking control approach and contouring control approach [6–9]. For the tracking control approach, the control law of each drive axis control loop attempts to minimize the tracking error independent of other control loops. In addition, disturbances in one control loop are compensated only by that particular loop. Other control loops do not receive any information about the disturbance, and they run as if the disturbed control loop is functioning normally. This lack of coordination causes error in other axes. However, the contour error of the desired path is evaluated in real time, and this error is eliminated by feedback control in contouring control systems.

Research efforts to improve the contouring accuracy in the modern manufacturing systems have brought out many efficient methodologies in the past years such as:

1.1.3.1 Feedback Controllers

In order to reduce the tracking errors, various control approaches based on the feedback principle have been developed. A typical feedback controller, proportional-integral-derivative (PID) controller is shown in Fig. 1.4. In the PID controller, the

correction signal is a combination of three components: proportional, integral, and derivative of the position error. The advantage of the PID controller is that it is simple to install and easily understood by most engineers. The main problem with the PID controller in contouring applications is the poor tracking performance at corners and for nonlinear contours.

1.1.3.2 Feed-forward Controllers

To decrease the tracking errors, a feed-forward controller can be added to the control loop. To improve the tracking accuracy in each individual axis by elimination of the servo-lag phenomenon, Masory proposed a feed-forward controller [10], and Tomizuka proposed the zero phase error tracking control [11]. The above approaches can be applied to effectively reduce tracking errors for single axis or decoupled motion applications. However, they do not guarantee contouring performance when applied to multi-axis contour-following tasks.

1.1.3.3 Robust Controllers

Examples of robust controllers are the sliding mode controller [12, 13] and the H_∞ controllers [14]. These focus on making the control system robust against uncertainties in the drive parameters, maximizing the bandwidth within the physical limitations of the system, and compensating for external disturbances. However, these controllers still focus on the improvement of the individual axis performance only. The main drawback of these methods, which consider the performance of each axis separately during contouring, is that reducing the individual axis errors does not necessarily reduce the contour error.

1.1.3.4 Cross Coupling Controllers

The main idea of the cross coupling controller is that the elimination of the contour error is the controller objective, rather than the reduction of the individual axis errors. Therefore, the cross coupling controller requires the construction of a contour error model in real time, and its utilization in a control law that reduces the contour error. By calculating the contour error from the tracking error in biaxial contour-following tasks, Koren proposed a cross coupled controller (CCC)
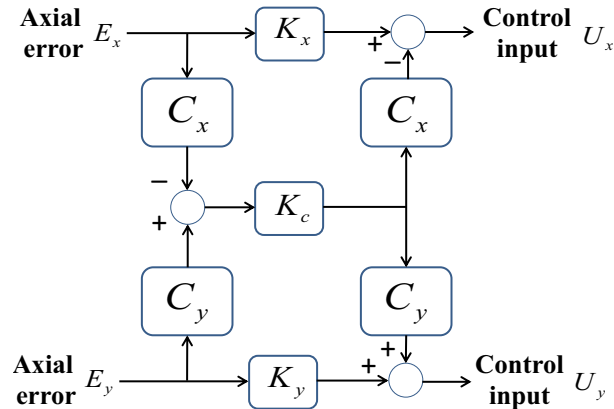
FIGURE 1.5: Cross coupling controller for a biaxial feed drive system

[15]. Yeh *et al.* employed a cross-coupled fuzzy logic controller for improving the contouring accuracy [16]. They utilized a new fuzzy rule-generated method which is based on a performance index of the contour error model. A block diagram of a basic biaxial cross coupling controller is shown in Fig. 1.5. The axial position errors E_x and E_y are used to calculate the contour error ε by being multiplied by the variable gains, C_x and C_y. The output of the proper control law is decomposed into two axial components by multiplying by C_x and C_y. These axial components are then inserted into the individual axis loops with the appropriate sign ensuring that contour error correction is executed in the proper direction. However, minimization of the tracking error in CCC achieved by the axial controller dose not reduce the contour error, and hence, force the contour controller to contradict it. As a result, it is difficult to judge which controller dominates the contour error, hence, some difficulties in adjusting controller parameters will appear.

1.1.3.5 Contouring Controllers

Reduction of error components orthogonal to desired contour curves is an effective tool for contour following in multi-axis machining tasks. Ho *et al.* decomposes the contour error into normal tracking error and advancing tangential error, following which a dynamic decoupling procedure is applied to the system dynamics [17]. By transforming the machine tool feed drive dynamics into a moving-task coordinate frame attached to the desired contour, Chiu and Tomizuka proposed the task coordinate frame approach [18]; Cheng *et al.* [19] proposed an integrated control scheme that consists of a feedback controller, a feed-forward controller and a modified contour error controller (i.e. a CCC equipped with a real-time contour error

estimator). In addition, they proposed a fuzzy-logic-based feed-rate regulator to further reduce the contour error. Su and Cheng [20] proposed a position error compensator (PEC) by compensating position errors in advance. To further reduce the contour error, they employed an integrated motion control scheme consisting of PEC, a modified version of CCC, and a fuzzy-logic-based feed rate regulator. Lo and Chung proposed tangential contouring controller for biaxial motion [21]. The proposed controller is based on a coordinate transformation between the X-Y frame and a tangential-contouring (T-C) frame defined along the contour. Cheng and Lee proposed a real-time contour error estimation algorithm [22]. Ye *et al.* proposed a new cross-coupled path pre-compensation algorithm for rapid prototyping and manufacturing systems [23]. To reduce the contour error by optimizing controller parameters using a genetic algorithm, Tarng *et al.* presented a cross-coupled fuzzy-feedrate control scheme [24]. Chin *et al.* proposed a fuzzy-logic controller to a proven algorithm in the cross-coupled pre-compensation method, and using both position and contour error to generate compensation term [25]. Yeh and Hsu [26] proposed an adaptive federate interpolation algorithm based on the geometric relationship between chord error and curvature constraints. Jee and Koren proposed an adaptive fuzzy logic controller to reduce contour error [27]. They adjusted both input and output membership functions simultaneously within a stable range derived from a stability analysis.

1.2 Sliding Mode Control

1.2.1 Introduction

Sliding mode control (SMC) is a special class of variable structure control with a high speed, nonlinear feedback that switches discontinuously in time on a specified sliding surface. SMC originated in the Soviet Union in the late 1950s, however it was not published outside the Soviet Union until the publications [28] and [29]. After these publications, the list of publications concerning SMC grew rapidly and SMC has been receiving increasing attention in many control fields such as electromechanical systems, robotic manipulators and servo systems.
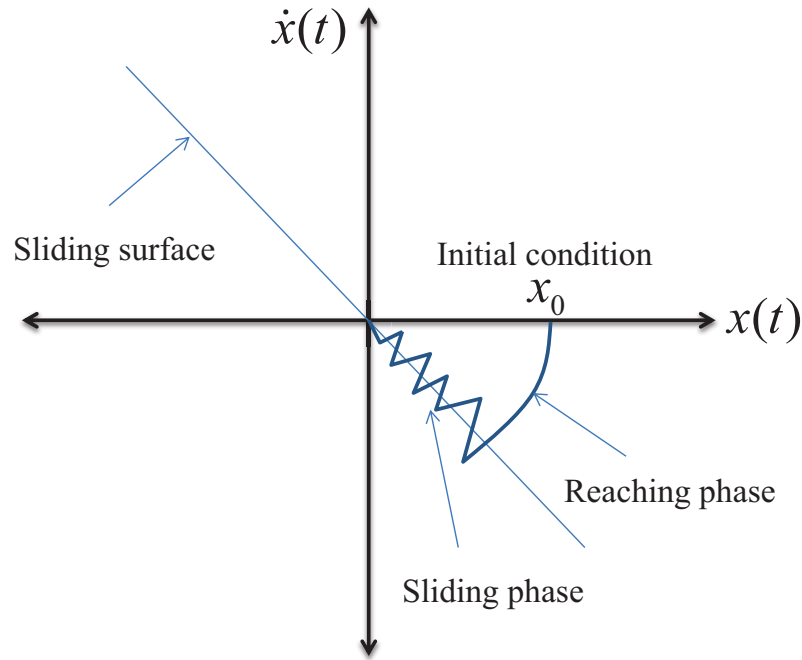
FIGURE 1.6: State trajectory during reaching phase and sliding phase in sliding
mode control

Sliding mode control has several attractive interests. Among them, its relative
simple design, invariance to systems dynamics characteristics and external dis-
turbances, control of independent motion (as long as sliding conditions are main-
tained), wide variety of operational modes such as regulation, trajectory control
[30], model following [31] and observation [32]. Although SMC has already been
studied in many researches [33–36], surveys [37], or books [38–40], it still remains
many study subjects from the theoretical and applications viewpoints [41].

In order to explain the sliding mode control approach, let us consider the following
first order uncertain system [42]:

$$\dot{x}(t) = ax(t) + bu(t) + \rho(x,t). \qquad (1.1)$$

where $x(t) \in R$, $u(t) \in R$ are the control variable and control input, respectively.
a and b are known nonzero constants. $\rho(x,t) \in R$ refers to unknown uncertainty
and only the bounds of this uncertainty are known. In order to stabilize the system
in (1.1), if the initial value of $x(t)$ is positive then $\dot{x}(t)$ should be negative and vice
versa. Therefore, depending on the sign of $x(t)$, control law should be altered to

ensure stabilization of $x(t)$. Consider the following control law:

$$u(t) = -b^{-1}(ax(t) + Q\text{sgn}(x)). \tag{1.2}$$

where $sgn(.)$ denotes the sign function, and $Q > 0$ is chosen such that

$$Q \geq \rho_{max}. \tag{1.3}$$

where ρ_{max} represents the upper bound of the uncertainty $\rho(x,t)$. With control law (1.2), system (1.1) becomes

$$\dot{x}(t) = -Q\text{sgn}(x(t)) + \rho(x,t). \tag{1.4}$$

In order to analyze the above closed loop system, consider the following three different cases; First if the initial condition $x(0) > 0$. From (1.4) we can see that $\dot{x}(t) < 0$. Therefore, $x(t)$ is decreasing and moving towards the origin $x(t) = 0$. Second if the initial condition $x(0) < 0$, then using (1.4), it implies that $\dot{x} > 0$. Therefore $x(t)$ increasing and approaches $x(t) = 0$. Third case when $x(t) = 0$, the discontinuous part of the control law is not defined. However, the moment the trajectory crosses the surface $x(t) = 0$ from either direction, again it is forced back on $x(t) = 0$ according to the above mentioned two cases. Therefore in all cases $x(t)$ is moving towards the point $x(t) = 0$. Thus, the control law (1.4) forced the system state $x(t) = 0$ regardless of the initial conditions.

In order to understand more physically what is happening during sliding mode control, let us consider the following sliding surface for a second order system:

$$s(x,t) = kx + \dot{x}. \tag{1.5}$$

where x and $\dot{x}$ are the states of the system and k is a positive constant. Figure 1.6 shows the state trajectories in the vicinity of the sliding surface $s(x,t) = 0$. The sliding mode control has two phases as shown in Fig. 1.6; the initial phase when the trajectory is forced towards $s(x,t) = 0$ and it is called the *reaching phase*; and the second phase when $s(x,t) = 0$ is called the *sliding phase* or *sliding mode*. During the reaching phase, external disturbance can affect the system performance while during the sliding phase system motion is insensitive to external disturbance. Because the control law is discontinuous about $s(x,t) = 0$ it requires switching

at very high frequency to maintain the system on the desired sliding surface. If this switching occurs at a very high frequency then $s(x,t) = 0$ can be consistently maintained with this discontinuous control law.

1.2.2 Nonlinear sliding surface design

Generally, designing of sliding mode control consists of two main steps. The crucial and most important step of sliding mode control design is the construction of the sliding surface which is expected to response desired control specifications and performance [43]. The second step in sliding mode control design procedure is to determine a control law that force the system dynamics the sliding surface within finite time and then remain on it for a subsequent time. Generally, the sliding control law consists of two term; the continuous control law that control the system on the sliding surface; and the discontinuous control law to guarantee the stability against disturbance effect.

In the conventional sliding mode controller design, a linear sliding surface is utilized which gives a constant damping ratio. In many control applications such as robotics, electric drives, machine tool control, vehicle and motion control, the most important requirements are fast response and small overshoot. However, quick response produces high overshoot, which causes contour errors and also increases the consumed energy. On the other hand, low overshoot means slow response, which leads to significant contour errors. Thus, it is very difficult to achieve small overshoot with a fast response using the conventional linear SMC method. This particular problem can be solved by employing the composite nonlinear feedback (CNF) technique [44]. The nonlinear sliding surface consists of a linear term and a nonlinear term. The linear term comprises a gain matrix that has a very low damping ratio, thereby facilitating a fast response [45]. The nonlinear term is introduced to provide a variable damping ratio in order to achieve a small overshoot and settling time of the closed loop system as the contour error converges to zero.

1.3 Energy Saving in Manufacturing

Manufacturing, the core of industrial activities, has been an essential source of energy consumption. Hence, it becomes a focal point in environmental impacts

studies [46]. Reducing the energy consumption of machine tools can significantly improve the environmental performance of manufacturing processes and systems. The cutting energy used in the machine tool in material removal process accounts for 15-25% of the whole energy consumed by the machine [47–49]. This energy consumption can be categorized as that consumed by the main spindle and by the feed drives. Recently, researchers have developed several approaches in the process control level to reduce the energy consumption in machining by improvement in toolchip contact mechanics.

For example, Zolgharni *et al.* proposed Diamond-Like Carbon deposited tools to improve the energy efficiency of machine tools [50]. However, the feed drives have mean power consumption smaller than the power consumed by the spindle during roughing operations; they have in-negligible power consumption compared to the spindle during the finishing operations. In addition, the feed drive is used for other operations such as returning motion of the tool. Hence, we focus on the feed drive motion in this study. Moreover, this idea can be applied to most industrial robots where the energy consumed by the feed drives contributes a large proportion of the total power consumption

1.4 Study Objectives

This thesis gives a comprehensive discussion on the issue of improving the tracking and contouring performance for multi-axis feed drive systems. As mentioned in the previous section, the high accurate motion of the feed drive-axis is highly demanded to insure high precession machining. In addition, reduction of the consumed energy of the feed drive system contributes to environmental, natural resources and energy problems. This thesis presents a novel sliding mode control design with a nonlinear sliding surface for feed drive systems with single, two, three and five-axis as follows:

(1) Based on model predictive control, a contouring controller for biaxial feed drive systems is presented. To improve contouring performance, a new performance index in which error components orthogonal to the desired contour curve are given more importance than tracking errors with respect to each feed drive axis.

(2) A novel sliding-mode controller with a non-linear sliding surface to improve the machining accuracy of ball-screw feed drive systems is presented. Unlike the conventional sliding-mode control design, the proposed non-linear sliding surface varies according to the output (controlled variable) so that the damping ratio of the system changes from its initial low value to its final high value as the output changes from its initial value to the reference point.

(3) Based on the contour error estimation by coordinate transformation approach, we proposed a novel sliding mode contouring controller with non-linear sliding surface to improve the machining accuracy of the biaxial feed drive systems.

(4) New contour error estimation model for three dimensional machining tasks to improve the machining quality is presented. The model is based on estimation of the instantaneous curvature of the reference trajectory and coordinates transformation approach. Then a sliding mode contouring controller with nonlinear sliding surface to improve the machining accuracy for three-dimensional machining is presented.

(5) Experimental verification of proposed definition of the tool orientation contour error in five-axis machines is conducted. The proposed definition considers synchronization between the tool-tip contour error and tool-orientation contour error.

(6) A novel sliding mode contouring controller with a nonlinear sliding surface for five-axis machining tasks is presented. The controller aims to reduce the tool tip and tool orientation contour errors. In addition, a design of disturbance observer to compensate for the effect of modeling error and external disturbance is introduced.

1.5   Thesis Outline

The reset of this thesis is organized as follows: In Chapter 3, an algorithm to model predictive contouring control for biaxial feed drive systems is presented. It should be noted that this is extension of my Master work [51]. In Chapter 2, a novel algorithm to sliding mode control with nonlinear sliding surface is presented. Chapter 4 presents a new sliding mode contouring controller with nonlinear sliding

surface for biaxial feed drive systems. We have extended the proposed controller presented in Chapter 4 to the three-dimensional machining tasks and presented it in Chapter 5. Chapter 6 presents a new definition of the tool orientation contour error to consider synchronization between the tool-tip contour error and tool-orientation contour error and experimental verification. Base on the definition of the tool orientation contour error presented in Chapter 6, we presented a novel sliding mode contouring controller with nonlinear sliding surface and disturbance observer in Chapter 7. Conclusions and future work are given in Chapter 8.

Chapter 2

Sliding Mode Controller Design with A Nonlinear Sliding Surface for Feed Drive Systems

2.1 Introduction

A ball-screw-driven mechanism actuated by servo drives is commonly used in many industrial applications such as computer numerical control (CNC) machines, precision assembly equipments and industrial robots to provide high-speed motion and positioning accuracy. Because most of these applications run for a long time all over the world, a huge amount of electrical energy is consumed by these application. Hence, reduction of the consumed energy by feed drive systems has become an important issue in modern machining technology.

One important source of increase in energy consumption is torsional and axial vibrations of the ball screw which result in oscillatory behaviour when the bandwidth of the control loop is increased [52]. Feed-forward pre-filtering of trajectory commands [53–55] or notch filtering of the control signal [56] helps to partially alleviate this problem by reducing the excitation delivered through the control signal. However, this attenuation is not perfect, as structural frequencies can also be excited by external disturbances such as cutting forces or sudden friction transients. Hence, the control law needs to be robust against varying or unmodelled axis dynamics [14], as well as the ability to attenuate structural vibrations [57]

and counteract external disturbances, such as cutting forces [58] and friction [59]. Erkorkmaz and Kamalzadeh proposed a bandwidth control scheme for ball screw drives [60]. They modelled and identified the dynamics of the drive system, which is comprised of rigid body motion, friction, and torsional vibrations.

The main issue in servo applications is position control, which is essential for many mechanical motion systems. A positional servo system in a high-performance industrial application must have fast response, preferably without overshoot, high steady-state accuracy, good external disturbance rejection, and robustness to parameter perturbations [61]. Sliding-mode control (SMC), a class of variable structure control [62], provides a viable and effective method with a strong robustness property and fast error convergence characteristics for non-linear systems subjected to external disturbances and parameter variations by emulating a prescribed reduced-order system [63]. In the recent few decades, the SMC with linear sliding surface technique for mechanical systems has been extensively studied by many researchers [64–67]. Altintas *et al.* proposed an SMC applied to a ball-screw feed drive system [12]. The control system is capable of coping with changing friction and external disturbances, and uncertainties in the drive inertia. Chen *et al.* designed an SMC method to reject system disturbances and uncertainties for ball screw feed drives [68]. To avoid the chattering effect of conventional SMC, they used an integral-type SMC. Braembussche *et al.* proposed an H_∞ and a sliding-mode controller for a prototype machine tool axis with a linear motor [69]. Yau and Yan [70] proposed a proportional-integral switching surface to design an adaptive sliding-mode controller in the static and dynamic regimes to achieve improved precision performance.

However, to ensure high performance, the system should settle quickly without any overshoot, which can not be achieved with a linear sliding surface. One strategy of the sliding surface design is the use of non-linear sliding surfaces instead of linear surfaces of a classical SMC as it is first reported by Rimarez and Bolnar [71], however the design algorithm was not provided in their study. Jabbari *et al.* employed parabolic sliding surfaces to achieve near-minimum time control [72]. In order to improve the transient response, Lee proposed cubic polynomials [73]. Chu *et al.* proposed a technique to design SMC based on non-linear sliding surface that guarantees asymptotic stability [74]. However finding non-linear functions causes some analytical difficulties such as choosing structure of the non-linear function and defining parameters for the non-linear function [75].
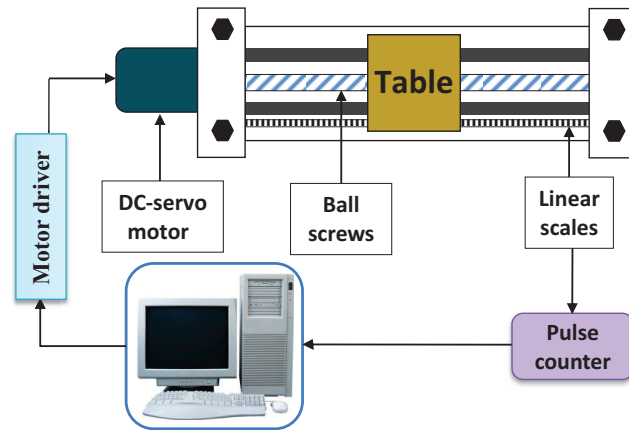
FIGURE 2.1: Typical ball-screw feed drive system

In this chapter, we propose the application of a sliding-mode controller with a non-linear sliding surface [42] to a general feed drive mechanism, for its practical application and understanding. The performance of a classical sliding-mode controller with a constant, linear sliding surface is improved by using a non-linear function that has the effect of changing the system closed-loop damping ratio from its initial low value to its final high value. The variable system closed-loop damping ratio results in low energy consumption because it provides a fast response with small overshoot. Furthermore, the non-linear function has a simple geometric interpretation and its parameters can be tuned easily. In addition, the stability analysis of the system as well as the stability in the sliding-mode is presented.

2.2 System Modelling and Control Design

2.2.1 System modelling

This study considers a typical ball-screw feed drive system, which is shown in Fig. 2.1. A DC servo motor, which is commonly used in industrial applications, is used to drive the feed drive system. The feed drive system is generally represented by the following second-order system:

$$m\ddot{x} + g\dot{x} = f - d, \tag{2.1}$$

TABLE 2.1: Experimental parameter values

Parameter	M		C	
Value	16.0	Vs^2/m	180	Vs/m

where $m(>0)$, $g\ (\geq 0)$, d and f are the mass of the load, viscous friction coefficient, disturbance with known bounds and driving force along the drive axis, respectively, and x is the position of the feed drive. A ball-screw is used to convert the angular motion of the motor to the linear motion of the table. The motor dynamics for driving the feed drive system is described as follows [76]:

$$n\ddot{\theta} + h\dot{\theta} + \tau = u, \tag{2.2}$$

where θ, $n(>0)$, $h(\geq 0), \tau$ and u are the rotational angle of the motor, motor inertia, motor viscous friction coefficient, torque needed to drive the feed drive system (Eq.(2.1)) and the motor input voltage, respectively. Here, u (V) is applied to the actuator armature current controller (i.e., the armature current is proportional to the control signal u). The current in the motor armature generates the motor torque, which is proportional to the armature current. The motor torque is equivalent to the motor inertia torque $(n\ddot{\theta})$, torque dissipated by viscous friction $(h\dot{\theta})$ and the torque to drive the ball screw (τ). The relationships between the force f and torque τ, and position x and angle θ are

$$f = \frac{2\pi\tau}{p}, \ x = \frac{p\theta}{2\pi}, \tag{2.3}$$

where p is the pitch of the ball screw. By combining Eqs. (2.1), (2.2) and (2.3), the equivalent dynamics can be obtained as follows:

$$M\ddot{x} + C\dot{x} = u - \frac{p}{2\pi}d,$$
$$M = \left(\frac{2\pi}{p}n + \frac{p}{2\pi}m\right),$$
$$C = \left(\frac{2\pi}{p}h + \frac{p}{2\pi}g\right). \tag{2.4}$$

The equivalent inertia and friction coefficients are a combination of the linear and rotary friction coefficients. The equivalent inertia and friction coefficients for the actual system are given in Table 2.1. The state space representation of the above

system is as follows:

$$\dot{z} = Az + bu - \tilde{d},$$

$$y = c^T z,$$

$$z = [z_1, z_2]^T, A = \begin{bmatrix} 0 & 1 \\ 0 & -\frac{C}{M} \end{bmatrix},$$

$$b = \left[0, \frac{1}{M}\right]^T, \tilde{d} = \left[0, \frac{pd}{2\pi M}\right]^T, c = [1, 0]^T. \tag{2.5}$$

where the state z_1 represents the position of the feed drive and it is measured by using a linear encoder with a resolution of 0.1 μm. A low-pass filter with a cutoff frequency ω_f of 75 Hz is employed to estimate the state z_2 from z_1. $\tilde{d} = [\tilde{d}_1, \tilde{d}_2]^T$ is assumed to be matched (i.e. it lies in the space range of the input matrix b).

2.2.2 Assumptions for controller design

The following items are assumed for the controller design in this study

1. Nominal parameters of M and C in (2.5) are known.

2. Position $z_1 = x$ and velocity $z_2 = \dot{x}$ are measurable.

3. d is unknown and bounded.

4. Reference signal for z_1 and z_2, z_{1ref} and z_{2ref}, are given.

2.2.3 Proposed sliding surface and its stability analysis

To introduce a general idea of the proposed approach a common second order system with different damping ratio can be used. Figure 2.2 shows the step response of three second order systems with different damping ratio; In the System (a) that has a large damping ratio, the system response is very slow with small energy consumption and large tracking error; The system (b) has a small damping ratio to make the system response very fast. The smaller damping ratio increases the overshoot and hence the energy consumption is increased as well. The system (c) is a combination of the previous two systems such that smaller damping ratio is assigned in the beginning to achieve fast response, and the larger damping ratio is
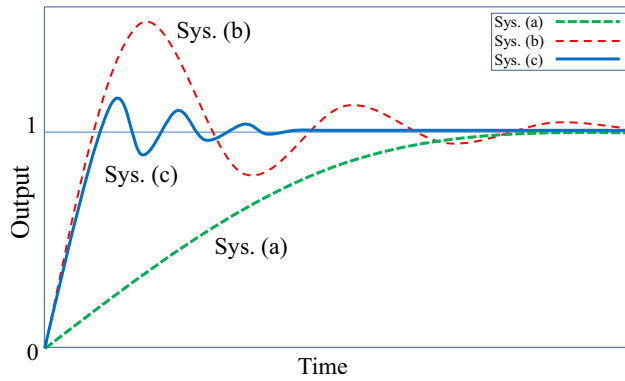
FIGURE 2.2: System response with different damping ratios; Sys.(a) with high damping ratio, Sys.(b) with low damping ratio and Sys.(c) with non-linear damping ratio

assigned when the output value is close to the reference to prevent the high over-shoot. The advantage of this combination is to reduce the energy consumption in most electro-mechanical and robotics systems which are used all over the world night and day. In this subsection, the design of the sliding-mode controller with a non-linear sliding surface for ball-screw feed drive systems will be considered. Using a non-linear sliding surface, the damping ratio of the closed-loop system can be changed from its initial low value to a final high value. The initial low value of the damping ratio results in a quick response, while the subsequent high damping avoids overshoot to minimize energy consumption. The objective of this study is to show that the significant energy reduction is possible while maintaining the control performance by selecting the sliding surface appropriately. If the sliding surface has a similar property with the proposed design, energy reduction may be possible even by using the standard sliding surface. On the basis of the system dynamics in (2.5), we propose the following non-linear sliding surface:

$$
\begin{aligned}
S &= \begin{bmatrix} F - \Psi P & 1 \end{bmatrix} e, S \in R, \\
e &= [e_1, e_2]^T = z_{ref} - z, z_{ref} = [z_{1ref}, z_{2ref}]^T.
\end{aligned} \tag{2.6}
$$

Here e is the tracking error vector of the feed drive system. z_{ref} is the desired trajectory vector. $P \in R$ is a positive constant to adjust the damping ratio. $F \in R$ is the linear term of the sliding surface, which is chosen such that the dominant poles have small damping ratios to achieve a fast response. $\Psi \in R$ is a non-positive non-linear function that depends on the output and desired velocity, and was used to change the damping ratio of the system. However, the choice of Ψ is not unique, the function Ψ should has the following properties:

1. It varies from 0 to a certain negative value $(-\beta)$, as the error varies from large value to zero to change the system damping ratio.

2. It is differentiable with respect to z_1.

In this study, we have extended the nonlinear function presented in [42] for a step type reference trajectory and generalized it to the systems with time-variant reference trajectories as follows:

$$\Psi = \frac{-\beta}{1 - \exp(-1)}\left[\exp(-(1 - \zeta^2)) - \exp(-1)\right] \tag{2.7}$$

where β is a tuning parameter that is used to adjust the weight of the non-linear term. ζ indicates how much the system output changes with respect to the desired reference. In [42], $\zeta = (z_1 - z_{1o})/(z_{1ref} - z_{1o})$ where z_{1o} is the initial position. In this study, we have generalized this function where $\zeta = (z_1(iT) - z_1((i-1)T))/(z_{1ref}(iT) - z_1((i-1)T))$ where i and T are the sampling instant and sapling time, respectively. Here, the function ζ represents how much the system output changes with respect to the desired reference at a certain time iT. When the system output achieves the desired reference, ζ becomes one, and $\Psi = -\beta$ results in increase of the damping ratio to prevent the overshoot. On the other hand, if the system output is far from the desired reference, the magnitude of ψ becomes very small, and it provides small damping ratio to speed up the system response. Because Eq. (2.7) is not defined for $z_{1ref}(i) - z_1(i-1)=0$, we employ the linear sliding surface (i.e., $\Psi=0$) when $|z_{1ref}(i) - z_1(i - 1)|$ is very small. In this case, because the control objective is almost satisfied, the linear sliding surface may be sufficient.

By applying some control law, which will be presented later, the system can be forced to the sliding surface. During the sliding-mode $S = 0$, we have

$$\dot{e}_1 = (-F + \Psi P)e_1. \tag{2.8}$$

The above equation includes the time variant parameter Ψ.

In order to show the stability of the proposed sliding dynamics, we consider a Lyapunov function candidate for the system in Eq. (2.8) as follows:

$$V_1 = \frac{1}{2}e_1^2. \tag{2.9}$$

TABLE 2.2: Controller parameter values

Parameter		K	F	P	β	Q
		s^{-1}	s^{-1}	s^{-1}	-	ms^{-2}
Case No. 1	LSS	80	100	1.5	-	0.3
	NLSS	80	100	1.5	175	0.3
Case No. 2	LSS	80	137	1.5	-	0.3
	NLSS	80	100	1.5	175	0.3

Using Eq. (2.8), the time derivative of the Lyapunov function candidate becomes

$$\dot{V}_1 = (-F + \Psi P)e_1^2. \tag{2.10}$$

Since $\Psi \leq 0$, $F > 0$ and $P > 0$, we have

$$\dot{V}_1 < 0. \tag{2.11}$$

and this ensure the system stability during the ideal sliding-mode. In addition, comparing the convergence rate between the above function (Eq. (2.10)) and that without the non-linear term ΨP, we can see that the non-linear term accelerates the convergence speed of the error e_1 than the conventional sliding surface when the error magnitude is large. On the other hand, when it becomes small, the convergence speed decreases to reduce the consumed energy.

2.2.4   Controller Design and Stability Analysis

In this subsection, we design a controller to enforce the system Eq. (2.5) to move from any initial conditions to the desired sliding surface and thereafter remain on it. Assuming that the reference position, velocity and acceleration are given, and considering the feed drive dynamics, we design the following controller:

$$\begin{aligned} u &= -M\left[\Gamma\left\{\dot{z}_{ref} - Az\right\} + KS + Q\mathrm{sgn}(S) - \frac{d\Psi}{dt}Pe_2\right], \\ \Gamma &= [F - \Psi P, 1]. \end{aligned} \tag{2.12}$$

where K is the controller gain. Q is chosen from the maximum bound of the uncertainty as follows:

$$Q \geq \max(\tilde{d}_2). \tag{2.13}$$

For asymptotic stability and to force the tracking error onto the desired sliding surface as $t \to \infty$, the time derivative of the following Lyapunov function must be negative:

$$V = \frac{1}{2}S^2. \tag{2.14}$$

The time derivative of the Lyapunov function candidate is

$$\dot{V} = S\left\{\Gamma\dot{e} - \frac{d\Psi}{dt}Pe_1\right\}. \tag{2.15}$$

Using the system (2.5), the tracking error dynamics is

$$\dot{e} = \dot{z}_{ref} - Az - bu + \tilde{d}. \tag{2.16}$$

Substituting Eq. (2.16) into Eq. (2.15) leads to

$$\dot{V} = S\left[\Gamma\{\dot{z}_{ref} - Az - bu + \tilde{d}\} - \frac{d\Psi}{dt}Pe_1\right]. \tag{2.17}$$

Using control law (2.12), it can be seen that

$$\dot{V} = S\left[-KS - Q\text{sgn}(S) + \tilde{d}_2\right] \tag{2.18}$$

Thus, with (2.13), it is easy to show that

$$\dot{V} < 0. \tag{2.19}$$

2.3 Simulation results

To verify the effectiveness of the proposed controller, a computer simulation is conducted for the following reference trajectory:

$$x = 4\cos\left(\frac{\pi}{10}t\right)(\text{mm}). \tag{2.20}$$

In order to consider the vibration in ball screw and effects of the disturbance force due to the change of the load, we consider the following for simulation:
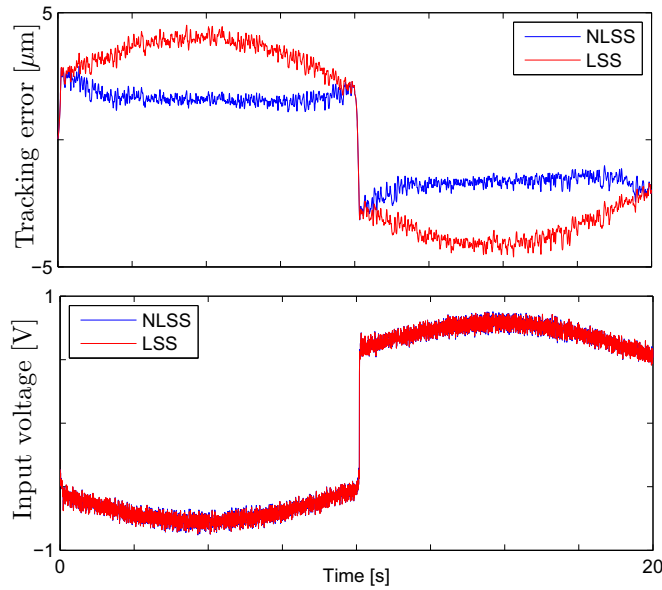
FIGURE 2.3: Simulation results; Linear sliding surface (LSS) vs Non-linear
sliding surface (NLSS)

1. A model of screw drive including a higher frequency mode in [76] is used for
   simulation model instead of Eq. (2.5). The feed drive is modeled as a two
   mass system (m_1 and m_2) connected by a damper (viscous friction coefficient
   c) and a spring (spring constant k). Mass m_1 and m_2 are subjected to viscous
   friction with coefficients b_1 and b_2, respectively. The control input force is
   given to the mass m_1, and the mass m_2 is subjected to external disturbance
   d_2. The output of the feed drive system is considered as the position of mass
   m_2. The system dynamics can be represented by the following fourth order
   system:

$$
\begin{bmatrix} \dot{x}_2 \\ \ddot{x}_2 \\ \dot{x}_1 \\ \ddot{x}_1 \end{bmatrix} = \begin{bmatrix} 0 & 1 & 0 & 0 \\ \frac{-k}{m_2} & \frac{-c-b_2}{m_2} & \frac{k}{m_2} & \frac{c}{m_2} \\ 0 & 0 & 0 & 1 \\ \frac{k}{m_1} & \frac{c}{m_1} & \frac{-k}{m_1} & \frac{-c-b_1}{m_1} \end{bmatrix} \begin{bmatrix} x_2 \\ \dot{x}_2 \\ x_1 \\ \dot{x}_1 \end{bmatrix} + \begin{bmatrix} 0 \\ 0 \\ 0 \\ \frac{u}{m_1} \end{bmatrix}
$$

$$
+ \begin{bmatrix} 0 \\ \frac{-d_2}{m_2} \\ 0 \\ 0 \end{bmatrix}. \tag{2.21}
$$

2. Disturbance force is added to the control input such that the actual control
   input applied to Eq. (2.22) is $u = u_{con} + u_{dis}$ where u_{con} is generated by Eq.
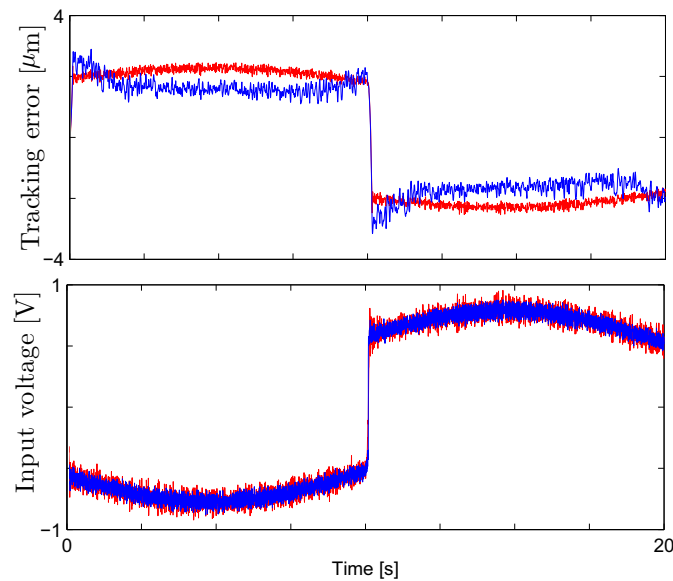
FIGURE 2.4: Simulation results; PD controller vs Proposed controller

(2.12) and $u_{dis} = 5.0 \times 10^{-3} \sin(\text{rand}(10))$ (V) is a disturbance term. Here, rand(10) refers to a random number from 1 to 10.

3. 50% reduction in the inertia and viscous friction coefficients from those used in the controller design is applied.

4. Coulomb friction of 0.5V equivalent magnitude is added to Eq. (2.22) used for simulation.

The proposed controller with a non-linear sliding surface (Eq. (2.12)) and the controller with a linear sliding surface (i.e., $\Psi=0$ in Eq. (2.7)) are compared. To verify the effectiveness of the non-linear term, the controller gain K and the linear term of the sliding surface F were set to the same values in both controllers. The controller gain K and the linear term of the sliding surface F were selected to be 80 s^{-1} and 100 s^{-1}, respectively, while the non-linear tuning parameter β was selected to be 175.

Figure 2.3 shows the control input and the tracking error of the feed drive system for both controllers. It can be seen that the proposed approach achieves smaller tracking error than the conventional one. In addition, the control input voltage is almost equal for both controllers.

In addition, the proposed approach is compared with a PD controller under approximately similar tracking condition as shown in Fig. 2.4. It can be seen that in
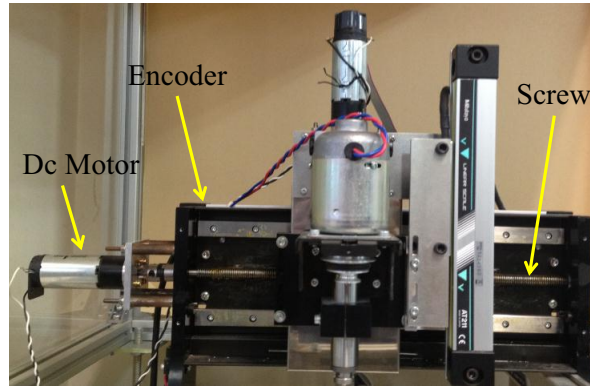
FIGURE 2.5: Experimental feed drive system

the case of the PD controller, the control input variation and magnitude is higher than the case of the proposed approach.

It should be noted that elimination of the control input chattering was not considered in the experiment because the main concern of the study is to achieve lower overshoot and small settling time, resulting in a smaller error, by changing of the systems damping ratio from its initial low value to its final high value.

2.4 Experimental Results

The proposed controller was experimentally verified with a ball-screw feed drive system driven by a DC servo motor as shown in Fig. 2.5. A linear encoder with a resolution of 0.1 μm was attached to the feed drive to measure the actual position of the feed drive system. The control law given in Eq. (2.12) was implemented using the C++ programming language on a personal computer (OS: Windows XP, CPU: 2 GHz) with a sampling time of 5 ms. In order to provide a fixed sampling period in a Windows XP environment, we employed a timer on a counter board of 24-bit up/down counters. To demonstrate the effectiveness of the proposed approach, the proposed controller was compared with the conventional one for the reference trajectory given in Eq. (2.20) based on the following two perspectives:

(1) *Case No. 1: Tracking error perspective*

First, we compared the controller with a non-linear sliding surface (i.e., Eq. (2.12)) and the controller with a linear sliding surface (i.e., Ψ=0 in Eq.
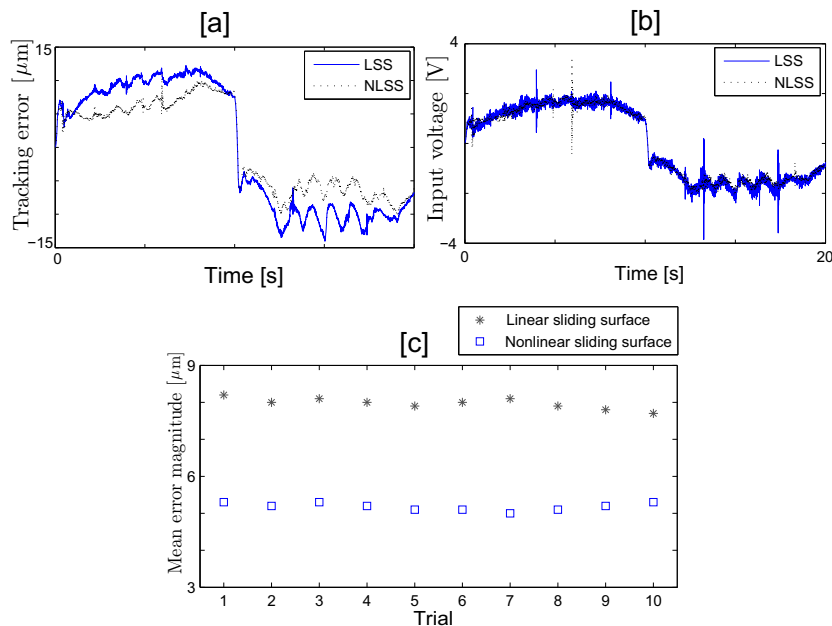
FIGURE 2.6: Experimental results for *Case No.* 1; (a) Tracking errors, (b) Control inputs and (c) Mean of the tracking error magnitude

(2.7)). The controller parameters used in this experiment are given in Table 2.2.

Figure 2.6(a) shows that the controller with the non-linear sliding surface achieved a better performance than the conventional controller with the linear sliding surface in terms of tracking error. In addition, a smaller control input was required in the case of the proposed surface, as shown in Fig. 2.6(b). To verify the repeatability of the proposed approach, the same experiments that were performed in Figs. 2.6(a) and (b) were repeated 10 times, and the mean values of the tracking error magnitude were compared in Fig. 2.6(c). Note that to avoid inaccuracies in the comparison, the running time in Fig. 2.6(c) was increased from 20 s to 180 s. It can be seen that the proposed approach reduced the mean value of the error magnitude by about 35%.

To demonstrate the ability of the proposed approach to reduce the energy consumption and the control input variance, the consumed energy was measured and the control input variance was computed for the experiments shown in Fig. 2.6(c). The consumed energy was measured by a power Hi-tester (HIOKI 3334 AC/DC), and the control input variance was calculated
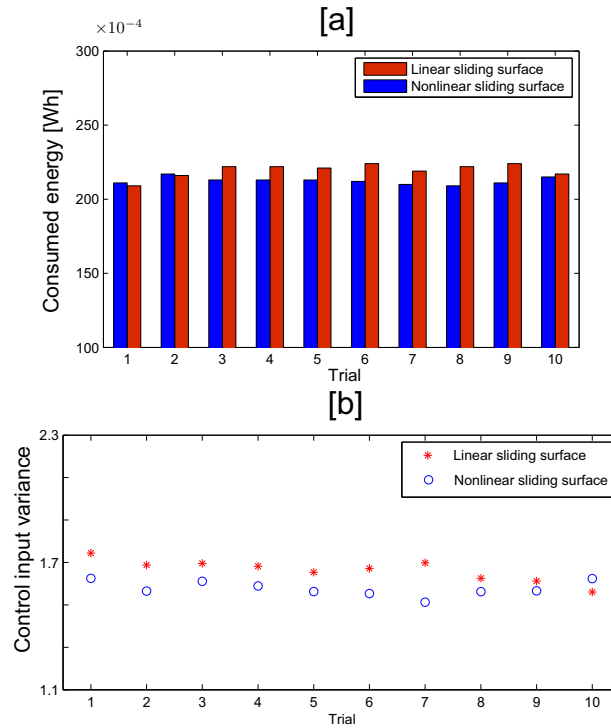
FIGURE 2.7: Experimental results for *Case No.* 1; (a) Consumed energy and (b) Control input variation

as follows:

$$\sigma^2 = \frac{\sum\limits_{i=1}^{N}(u_i - \mu)^2}{N} \tag{2.22}$$

where u_i denotes the control input value at the ith sampling instant, N is the total number of sampling instants ($i = 1, ..., N$), and μ is the mean of all of the control input values. As shown in Figs. 2.7(a) and (b), the proposed approach required about 3.2% less energy, and provided a control input variance that was about 5.1% smaller. In conclusion, the non-linear sliding surface reduced the tracking error of the feed drive system without requiring any additional electrical energy.

(2) *Case No. 2: Consumed energy perspective* In this case, the energy consumption for both controllers was compared for a roughly similar tracking error. To achieve tracking errors that are similar for both controllers, the linear term F of the controller with a linear sliding surface was increased to 137 s^{-1}, while the parameters of the proposed approach remained similar to those in *Case No.* 1 as given in Table 2.2. As shown in Fig. 2.8(a), a roughly similar tracking error was achieved for both controllers. However, achieving
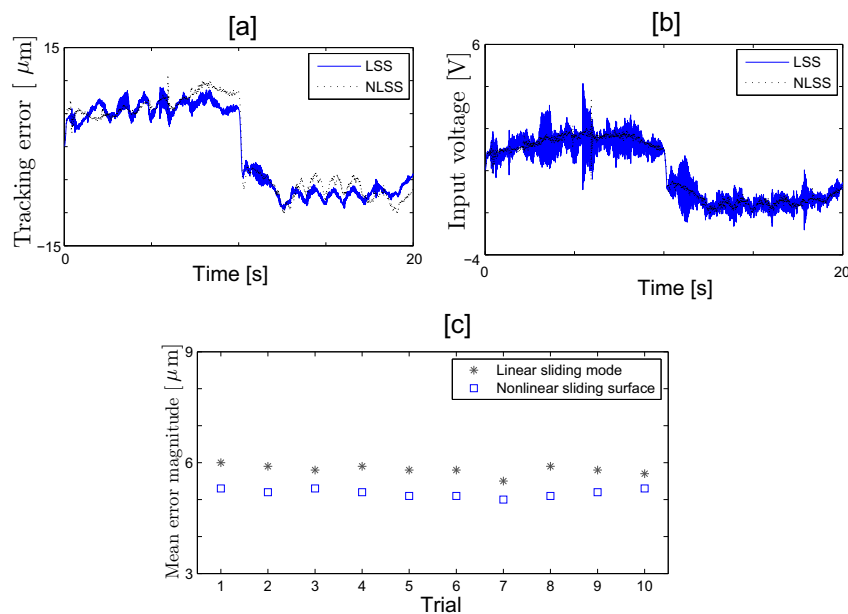
FIGURE 2.8: Experimental result for *Case No.* 2; (a) Tracking errors, (b) Control inputs and (c) Mean of the tracking error magnitude

a similar tracking performance with the linear sliding surface increased the control input, as shown in Fig. 2.8(b). Figure 2.8(c) verifies the repeatability of the proposed approach where the experiments in Figs. 2.8(a) and (b) were repeated 10 times with a running time of 180 s. It is clear that both controllers achieved roughly similar tracking performances in terms of the magnitude of the tracking error.

Now it appears fair to compare both controllers from the viewpoint of the consumed energy, as shown in Figs. 2.9(a) and (b), where the energy consumed by both controllers is compared based on similar experimental conditions, as shown in Fig. 2.8(c). The consumed energy and control input variance are reduced significantly (by 12.9% and 19.1%, respectively), with respect to the conventional linear sliding-surface. In conclusion, the proposed approach reduced the consumed energy and control input variance more significantly than the conventional method under the similar tracking performance.

Another advantage of the proposed approach is that it is easy to tune the non-linear term because only one parameter (β) needs to be tuned. Figure 2.10 shows the non-linear function Ψ that was used to tune the damping ratio of the closed-loop system. It can be seen that Ψ has decreased while the tracking error magnitude
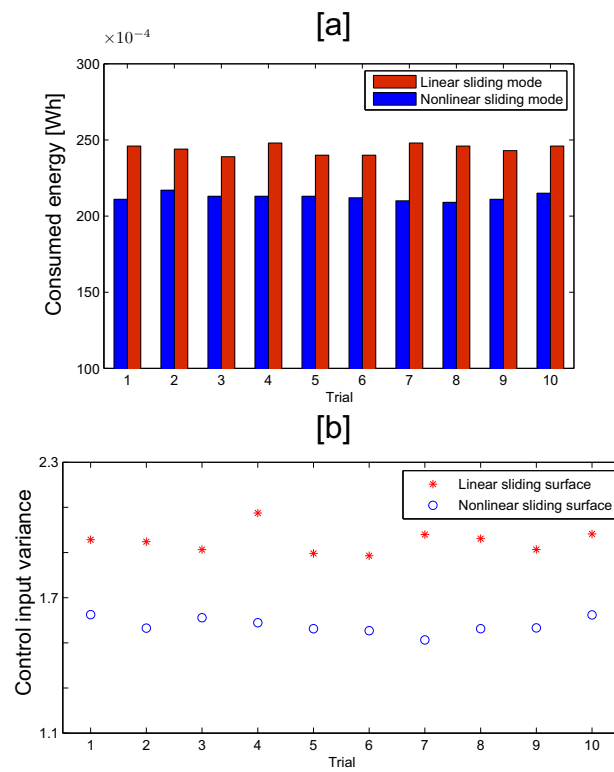
FIGURE 2.9: Experimental results for *Case No.* 2; (a) Consumed energy and (b) Control input variation
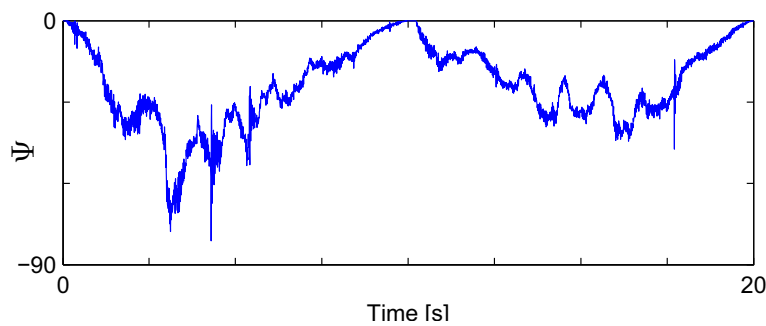
FIGURE 2.10: Non-linear function Ψ

decreased resulting in an increase of the damping ratio. Here, when the magnitude of $z_{1ref}(i) - z_1(i-1)$ is very small, we employ the linear sliding surface (i.e., $\Psi=0$) (this occurs around the time 10s of the experiments).

2.5 Conclusions

A sliding-mode controller with a non-linear sliding surface is proposed for ball-screw feed drive systems, and its effectiveness is verified experimentally in this chapter. Two cases were considered: the first case showed the effectiveness of the proposed non-linear sliding surface at reducing the tracking error, while the second one verified the ability of the proposed approach to reduce the consumed energy and control input variation. For the first case, the mean of the tracking error magnitude was reduced by 35% without the need for additional electrical energy or control input variation, while in the second case, the consumed energy and control input variation were reduced by about 12.9% and 19.1%, respectively.

Chapter 3

Model Predictive Contouring Controller for Biaxial Feed Drive systems

3.1 Introduction

Model predictive control (MPC) refers to a class of model-based controllers that uses an explicit process model to predict future responses of a plant. At each sampling instant, an optimization problem is solved on-line yielding optimal control, and only its first portion is applied until the next sampling instant. MPC was pioneered by Richalet, Rault, Testud and Papon, and Cutler and Ramaker [77]. Boucher *et al.* proposed using generalized predictive control (GPC) of the self synchronous motors in the machine tool field, which incorporates both reference preview action as well as disturbance rejection in the same control scheme [78]. This formulation is expandable to tracking error constraints. Zhe and Chen proposed a cross-coupled generalized predictive control algorithm. This provides a combined feedback-feedforward controller that results in zero-pole cancellation of poles that do not correspond to reference models [79]. They presented a new cost function in which synchronization errors are included. Dumur *et al.* proposed complete implementation of axis drives predictive controllers for an industrial machining center based on a generalized predictive control RST structure [80]. Susanu and Dumur proposed a hierarchical predictive control architecture, dedicated to feed drives of machining centers [81], in which the performance index is a weighted

FIGURE 3.1: Definitions of tracking and contour errors

sum of predicted tracking errors from a minimum prediction horizon to a maximum horizon and future control signal increments over the control horizon. However, motion control based only on the tracking ability of each axis in multi-axis feed drive system does not always guarantee high-precision machining.

To improve the contouring performance in machine tool feed drive systems, this chapter presents a model predictive contouring controller design based on a coordinate transformation approach. The main advantage of the proposed approach is that it allows easy adjustment of controller parameters by including transformed error and input signals in the performance index of MPC. The control law based on real-time optimization of the performance index is analytically derived so that the resulting control system provides improved performance in terms of tracking and contour errors. In addition, the proposed approach takes into account the modeling errors of the dynamics, the cutting forces and disturbances such as friction.

3.2   Problem Formulation

3.2.1   Definition of contour error

Contour error is defined as the shortest distance between the actual contour and the desired contour. The relationships between the contour and tracking errors in each feed drive axis is shown in Fig. 3.1. Two coordinate frames are used. The first is Σ_w, whose axes X and Y correspond to feed-drive axes and is the fixed frame. The curve c is the desired contour curve of the point of a machined part driven by the feed drive system. The desired position of the point of the machined part at time t, and defined in Σ_w, is $r = [r_x, r_y]^T$. The actual position of the feed drive system is represented by $x = [q_x, q_y]^T$, which is also defined in the fixed frame. The second coordinate frame Σ_l is attached at r and its axes are T and N. The axis T is in the tangential direction to c at r, and the direction of N is perpendicular to T. The tracking error in each feed drive axis is defined as

$$e_w = [e_x, e_y]^T = x - r. \tag{3.1}$$

This error vector can be expressed with respect to Σ_l as

$$e_l = [e_t, \ e_n]^T = R^T e_w, R = \begin{bmatrix} \cos\theta & -\sin\theta \\ \sin\theta & \cos\theta \end{bmatrix}. \tag{3.2}$$

where θ is the inclination of Σ_l to Σ_w. Because calculating the actual contour error in real time for complex contour is an intensive computational task, we regard the error component e_n as an approximation of the contour error e_c, which is the distance between the actual position x and the nearest point on the desired curve c [17, 82, 83].

For machining, error components orthogonal to the desired contour curve are more important than tracking errors with respect to feed drive axes. Contouring controller design gives the designer an opportunity to assign controller gain to reduce the error along N to a level below that along T by transforming the error e_w into e_l and using the error e_l as the feedback signal.

3.2.2   Modeling of biaxial feed drive system

This study considers a typical biaxial feed drive system, as shown in Fig. 3.2. Two servo motors, commonly used in industrial applications, are used to drive the feed drive system. The feed drive system is generally represented by the following decoupled second order system:

$$
\begin{aligned}
& M\ddot{x} + C\dot{x} = f, \\
& M = \mathrm{diag}\{m_i\}, \ C = \mathrm{diag}\{c_i\}, \ i = x, y, \\
& f = [f_x, \ f_y]^T.
\end{aligned}
\tag{3.3}
$$

where $m_i(> 0)$, $c_i(\geq 0)$ and f_i are the mass of load, viscous friction coefficient and driving force along the drive axis i, respectively. The notation $\mathrm{diag}\{a_i\}$ denotes a diagonal matrix with the elements a_i at the ith diagonal position.

Two ball screws are used to convert angular motion of the motors to linear motion of the table. The motor dynamics for driving the feed drive system is described as follows:

$$
\begin{aligned}
& N\ddot{\theta}_{mi} + Z\dot{\theta}_{mi} + \tau = Ku, \\
& \theta_{mi} = [\theta_{mx}, \theta_{my}]^T, \\
& N = \mathrm{diag}\{n_i\}, \ Z = \mathrm{diag}\{z_i\}, \\
& K = \mathrm{diag}\{k_i\}, \ i = x, y, \\
& \tau = [\tau_x, \ \tau_y]^T, \ u = [u_x, \ u_y]^T.
\end{aligned}
\tag{3.4}
$$

where θ_{mi}, $n_i(> 0)$, $z_i(\geq 0)$, $k_i(> 0)$, τ_i and u_i are the rotational angle of the motor, motor inertia, motor viscous friction coefficient, torque-voltage conversion ratio, torque needed to drive the feed drive system [represented by Eq.(3.3)] and the motor input voltage of the ith axis, respectively. The relationships between the force f_i and torque τ_i, and position q_i and angle θ_{mi} are

$$
f_i = \frac{2\pi\tau_i}{p_i}, \ q_i = \frac{p_i\theta_{mi}}{2\pi}.
\tag{3.5}
$$

where p_i is the pitch of the ball screw.
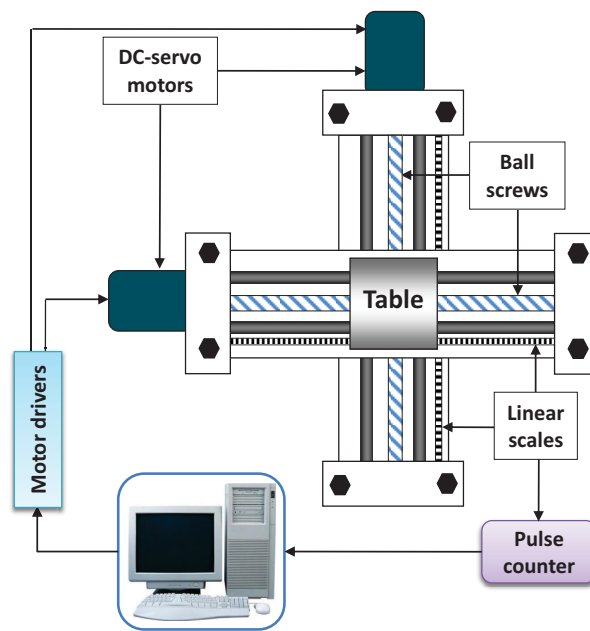
FIGURE 3.2: A typical biaxial feed drive system

The equivalent dynamics of the system can be estimated by combining Eq. (3.3), (3.4) and (3.5) as follows:

$$(N + \frac{p_i^2}{4\pi^2}M)\ddot{\theta}_{mi} + (Z + \frac{p_i^2}{4\pi^2}C)\dot{\theta}_{mi} = Ku. \tag{3.6}$$

Hence, the equivalent friction coefficients are a combination of the linear and rotary friction coefficients. The linear and rotary friction coefficients for the system are given in Table 3.1. The linear friction is coming from ball guide friction and air damping, and it is very small compared to the rotary friction. In addition, the linear friction coefficients are multiplied by a very small value ($p_i^2/4\pi^2 = 6.33 \times 10^{-7}$) due to the high reduction gears used in the system.

3.3 Model Predictive Contouring Controller (MPCC) Design

3.3.1 Model predictive control

Since the discrete-time model is suitable for implementing controllers with digital computers, we convert the continuous-time model Eqs. (3.3) and (3.4) into a

discrete-time model. The following transfer function model is used to describe the biaxial feed drive system:

$$y_i(k) = \frac{q^{-d}B_i(q^{-1})}{A_i(q^{-1})}u_i(k-1) + \frac{C_i(q^{-1})}{T_i(q^{-1})}v_i(k),$$
$$v_i(k) = \Delta\zeta_i(k), \Delta = 1 - q^{-1}, i = x, y. \tag{3.7}$$

where k is the sampling instant, $y_i(k)$ and $u_i(k)$ are the output and the control input of each feed drive axis, d is the time delay, $\zeta_i(k)$ represents a random disturbance, and $A_i(k), B_i(k), C_i(k)$ and $T_i(k)$ are polynomials for each feed drive axis in the delay operator q^{-1} . The predicted output of the plant is

$$\hat{y}_i(k+i) = \frac{q^{-\hat{d}}\hat{B}_i(q^{-1})}{\hat{A}_i(q^{-1})}u_i(k+i-1) + \frac{F_i}{\hat{C}_i}(y_i(k) - \hat{y}_i(k)). \tag{3.8}$$

The symbol "^" denotes estimates, F_i is a polynomial that satisfies the Diophantine equation

$$\frac{C_i}{T_i} = E_i + q^{-1}\frac{F_i}{T_i}. \tag{3.9}$$

where E_i is a polynomial. The purpose of this controller is to allow the feed drive to follow the reference trajectory as closely as possible. In addition, the following performance index has been presented [84]:

$$J_i = (\hat{y}_i^* - w_i^*)^T(\hat{y}_i^* - w_i^*) + \rho_i u_i^{*T}u_i^*,$$
$$\hat{y}_i^* = [P_i\hat{y}_i(k + H_m), ..., P_i\hat{y}_i(k + H_P)]^T,$$
$$w_i^* = [P_i(1)w_i(k + H_m), ..., P_i(1)w_i(k + H_P)]^T,$$
$$u_i^* = [u_i^*(k), ..., u_i^*(k + H_P - \hat{d} - 1)]^T,$$
$$u_i^*(k) = \frac{Q_{ni}}{Q_{di}}u_i(k). \tag{3.10}$$

where P_i is a polynomial used to tune the servo behavior of the control system, H_m and H_p are the minimum cost horizon and prediction horizon, respectively, w_i^* is the reference signal, ρ_i is a non-negative weighting factor to adjust the control input, and Q_{ni} and Q_{di} are monic polynomials with no common factors and can be used to obtain the weighting factor for $u_i(k)$.

3.3.2 Proposed model predictive contouring control

In the previous performance index (3.10), as well as in Ref. [81], only tracking errors with respect to each feed drive axis are included. The error components orthogonal to the desired contour curves are more important than tracking errors, and hence, the orthogonal error component is included in the proposed performance index with control inputs in the normal and tangential directions as follows:

$$
J = \rho_{cn} \sum_{j=H_m}^{H_P} e_{n_j}{}^2 + \rho_{ct} \sum_{j=H_m}^{H_P} e_{t_j}{}^2 + \rho_n \sum_{j=H_m}^{H_P} u_{n_j}{}^2 + \rho_t \sum_{j=H_m}^{H_P} u_{t_j}{}^2,
$$
$$
[e_{t_j}, e_{n_j}]^T = R^T(k)[e_{x_j}, e_{y_j}]^T,
$$
$$
[u_{t_j}, u_{n_j}]^T = R^T(k)[u_{x_j}, u_{y_j}]^T. \tag{3.11}
$$

where ρ_{cn} and ρ_{ct} are weighting factors to adjust the importance of the error component in the orthogonal and tangential directions, respectively, ρ_n and ρ_t are weighting factors used to adjust the control inputs in the normal and tangential directions, respectively, and u_{x_j}, u_{y_j}, u_{n_j} and u_{t_j} are the jth control inputs in the X, Y, N and T directions, respectively. As described in Appendix A, minimization of the performance index (3.11) gives:

$$
\begin{bmatrix} u_{xj} \\ u_{yj} \end{bmatrix} = \begin{bmatrix} \Pi_{xx} & \Pi_{xy} \\ \Pi_{yx} & \Pi_{yy} \end{bmatrix}^{-1} \begin{bmatrix} \Gamma_{xx} \\ \Gamma_{yy} \end{bmatrix},
$$
$$
\Pi_{xx} = \mathbf{M}^T[(\rho_{cn}S^2 + \rho_{ct}C^2)\mathbf{G}_x^T\mathbf{G}_x + (\rho_n S^2 + \rho_t C^2)\mathbf{\Phi}^T\mathbf{\Phi}]\mathbf{M},
$$
$$
\Pi_{xy} = \mathbf{M}^T S^2 C^2[(\rho_{ct} - \rho_{cn})\mathbf{G}_x^T\mathbf{G}_y + (\rho_t - \rho_n)\mathbf{\Phi}^T\mathbf{\Phi}]\mathbf{M},
$$
$$
\Pi_{yx} = \mathbf{M}^T S^2 C^2[(\rho_{ct} - \rho_{cn})\mathbf{G}_y^T\mathbf{G}_x + (\rho_t - \rho_n)\mathbf{\Phi}^T\mathbf{\Phi}]\mathbf{M},
$$
$$
\Pi_{yy} = \mathbf{M}^T[(\rho_{cn}C^2 + \rho_{ct}S^2)\mathbf{G}_y^T\mathbf{G}_y + (\rho_n C^2 + \rho_t S^2)\mathbf{\Phi}^T\mathbf{\Phi}]\mathbf{M},
$$
$$
\Gamma_{xx} = -\mathbf{M}^T[\mathbf{\Phi}^T((\rho_n S^2 + \rho_t C^2)(\mathbf{\Omega}\tilde{u}_x + \mathbf{\Phi}\mathbf{N}\breve{u}_x) + SC(\rho_t - \rho_n)(\mathbf{\Omega}\tilde{u}_y + \mathbf{\Phi}\mathbf{N}\breve{u}_y))
$$
$$
+ \mathbf{G}_x((\rho_{cn}S^2 + \rho_{ct}C^2)(\mathbf{H}_x\breve{u}_x + \mathbf{F}_x c_x + \zeta_x + \mathbf{G}_x\mathbf{N}\breve{u}_x - x^*) + (\rho_{cn} - \rho_{cn})(\mathbf{H}_y\breve{u}_y
$$
$$
+ \mathbf{F}_y c_y + \zeta_y + \mathbf{G}_y\mathbf{N}\breve{u}_y - y^*))],
$$
$$
\Gamma_{yy} = -\mathbf{M}^T[\mathbf{\Phi}^T((\rho_n C^2 + \rho_t S^2)(\mathbf{\Omega}\tilde{u}_y + \mathbf{\Phi}\mathbf{N}\breve{u}_y) + SC(\rho_t - \rho_n)(\mathbf{\Omega}\tilde{u}_x + \mathbf{\Phi}\mathbf{N}\breve{u}_x))
$$
$$
+ \mathbf{G}_y((\rho_{cn}C^2 + \rho_{ct}S^2)(\mathbf{H}_y\breve{u}_y + \mathbf{F}_y c_y + \zeta_y + \mathbf{G}_y\mathbf{N}\breve{u}_y - y^*) + (\rho_{ct} - \rho_{cn})(\mathbf{H}_y\breve{u}_x
$$
$$
+ \mathbf{F}_x c_x + \zeta_x + \mathbf{G}_x\mathbf{N}\breve{u}_x - x^*))],
$$
$$
S = \sin\theta(k), C = \cos\theta(k), \tag{3.12}
$$
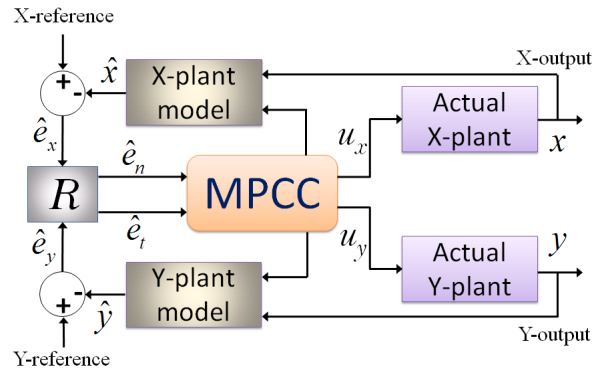
FIGURE 3.3: Model predictive contouring controller block diagram

where x and y refer to the corresponding feed drive axis, $\mathbf{G}_i$, $\mathbf{H}_i$ and $\mathbf{F}_i$ are the matrices

$$
\mathbf{G} = \begin{bmatrix} g_{i0} & 0 & \cdots & 0 \\ g_{i1} & g_{i0} & \ddots & \vdots \\ \vdots & & \ddots & 0 \\ g_{i(H_P - \hat{d} - 1)} & \cdots & \cdots & g_{i0} \end{bmatrix}, \mathbf{H} = \begin{bmatrix} H_{i(\hat{d}+1)} \\ \vdots \\ H_{ij} \\ \vdots \\ H_{iH_P} \end{bmatrix}, \mathbf{F} = \begin{bmatrix} F_{i(\hat{d}+1)} \\ \vdots \\ F_{ij} \\ \vdots \\ F_{iH_P} \end{bmatrix}. \quad (3.13)
$$

that consist of the elements of the polynomials G_{im}, H_{im} and F_{im}, respectively, that satisfy the Diophantine equations

$$
\frac{\hat{B}_i}{\hat{A}_i} = G_{im} + q^{-im+\hat{d}} \frac{H_{im}}{\hat{A}_i}. \quad (3.14)
$$

$$
\frac{1}{\hat{A}_i} = E_{im} + q^{-j} \frac{F_{im}}{\hat{A}_i}, m = [\hat{d}+1, \cdots, H_P]. \quad (3.15)
$$

$\mathbf{M}$ and $\mathbf{N}$ are matrices that consist of plant parameters with dimensions $H_P - \hat{d} \times H_c$ and $H_P - \hat{d} \times n_\phi + n_{P_i} - H_c$, respectively, and H_c is the control horizon. The matrices $\mathbf{M}$ and $\mathbf{N}$ are

TABLE 3.1: Parameter values of the experimental system

Parameter	X-axis	Y-axis
$m_i[\text{kg}]$	8.0	2.5
$n_i[\text{kgm}^2]$	0.05	0.05
$z_i[\text{Nm/(rad/s)}]]$	0.31	0.31
$k_i[\text{Nm/V}]$	1.42	1.42
$c_i[[\text{Ns/m}]]$	0.0	0.0
$p_i[\text{m}]$	0.005	0.005
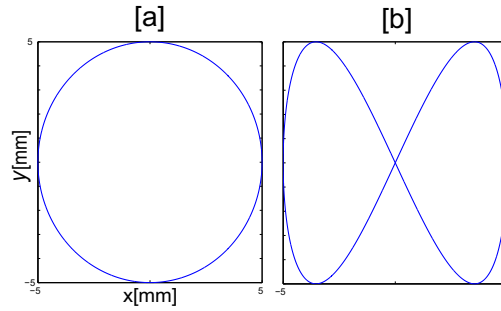
FIGURE 3.4: Reference trajectories. (a) Circular and (b) non circular

$$\mathbf{M} = \left[\begin{array}{cccccc} 1 & 0 & & \cdots & & 0 \\ 0 & 1 & & & & \\ & & & & & \vdots \\ \vdots & & \ddots & \ddots & \ddots & \\ & & & & & 0 \\ 0 & & \cdots & & 0 & 1 \\ \hline 0 & \cdots & 0 & g_{1,n_G} & \cdots & g_{1,0} \\ \vdots & & \vdots & \vdots & & \vdots \\ 0 & \cdots & 0 & g_{j,n_G} & \cdots & g_{j,0} \end{array}\right]. \tag{3.16}$$

$$\mathbf{N} = \left[\begin{array}{ccc} 0 & \cdots & 0 \\ \vdots & & \vdots \\ 0 & \cdots & 0 \\ \hline h_{1,0} & \cdots & h_{1,n_H} \\ \vdots & & \vdots \\ h_{j,0} & \cdots & h_{j,n_H} \end{array}\right]. \tag{3.17}$$

where $j = H_P - H_c - \hat{d}$, $\mathbf{\Phi}$ is a lower triangular matrix of dimension $(H_P - \hat{d}) \times (H_P - \hat{d})$, $\mathbf{\Omega}$ is a matrix of dimension $(H_P - \hat{d}) \times n_\Omega$, with $n_\Omega = \max(n_{Q_{ni}}, n_{Q_{di}})$, and $\mathbf{\Phi}$ and $\mathbf{\Omega}$ contain the elements of the polynomials Φ and Ω, respectively, which satisfy the Diophantine equation

$$\frac{Q_{ni}}{Q_{di}} = \Phi + q^{-1}\frac{\Omega}{Q_{di}}. \tag{3.18}$$

The quantities x^* and y^* are

$$x^* = P(1)[r_x(k + H_m), \cdots, r_x(k + H_P)]. \tag{3.19}$$

$$y^* = P(1)[r_y(k + H_m), \cdots, r_y(k + H_P)]. \tag{3.20}$$

where r_x and r_y are the reference trajectories in X and Y directions respectively, and $\tilde{u}$, $\check{u}$, $\breve{u}$ and c are given by:

$$\tilde{u} = \left[\begin{array}{ccc} \frac{u(k-1)}{Q_{di}}, & \cdots, & \frac{u(k-n_\Omega)}{Q_{di}} \end{array} \right]^T. \tag{3.21}$$

$$\check{u} = [u(k-1), \cdots, u(k + H_c - n_\phi - n_P)]^T. \tag{3.22}$$

$$\breve{u} = \frac{u(k)}{\hat{A}_i}. \tag{3.23}$$

$$c = [c(k), c(k-1), \cdots]^T, c(k) = \frac{y_i(k) - \hat{y}_i(k)}{T_i}. \tag{3.24}$$

A problem that can occur when solving u_{xj} and u_{yj} from (3.12) is that the inverse matrix calculation suffers from singularity if the weighting factors for the control inputs are zeros. To avoid this problem the following conditions must at least be satisfied:

$$H_m \geq \hat{d} + 1,$$
$$H_c \leq H_P - H_m + 1.$$

The inverse matrix in (3.12) is of dimension $H_c \times H_c$. Hence, a small control horizon is preferable for numerical reasons and to save the computational time.

3.3.3   MPCC algorithm

MPC is a strategy that uses an explicit process model and tracking error dynamics to predict the future behaviour of a plant. The block diagram of the proposed

contouring control system is as shown in Fig. 3.3. The proposed algorithm can be
summarized as follows:

(1) At each sampling time k, the output of the biaxial feed drive system is
predicted over the prediction horizon H_P. This prediction depends on the
future values of the control actions u_x and u_y and the biaxial feed drive
model (3.7) within a control horizon H_c.

(2) Reference trajectories $r_x(t+k)$ and $r_y(t+k)$, $k=1,..,H_P$ are used to estimate
the future transformed errors $\hat{e}_t$ and $\hat{e}_n$ beyond the prediction horizon using
the predicted tracking errors $\hat{e}_x$ and $\hat{e}_y$ and transformation matrix $R(k)$.

(3) The future control inputs $u_x(t+k)$ and $u_y(t+k)$, $k = H_c$ are calculated by
minimization of the proposed performance index (3.11).

(4) Once the minimization problem is solved, only the first optimized control
inputs [i.e. the first elements of u_x and u_y in (3.12)] are applied to the
system.

(5) The actual outputs of the system (q_x and q_y) are used as the initial states of
the model to perform the next iteration.

(6) Shift the horizon and repeat steps 1 to 5 at each sampling instant.

3.4 Experiments

To verify the effectiveness of the proposed controller, the control law given in Eq.
(3.12) was implemented with C^{++} language by a personal computer (OS: Windows
XP). The control input signal has been applied to a biaxial feed drive system,
that is driven by two DC servo motors via DA board (CONTEC DA12-8(PCI)).
The motors are coupled to, and drive, two ball screws through a high-reduction
gearbox to provide the required high torque. In addition, a linear encoder accurate
to 0.1μm is attached to each feed drive axis to measure the actual position of the
biaxial feed drive system. A pulse counter board (CONTEC CNT24-4D(PCIH))
is used to count the encoder pulses. The nominal parameter values of the biaxial
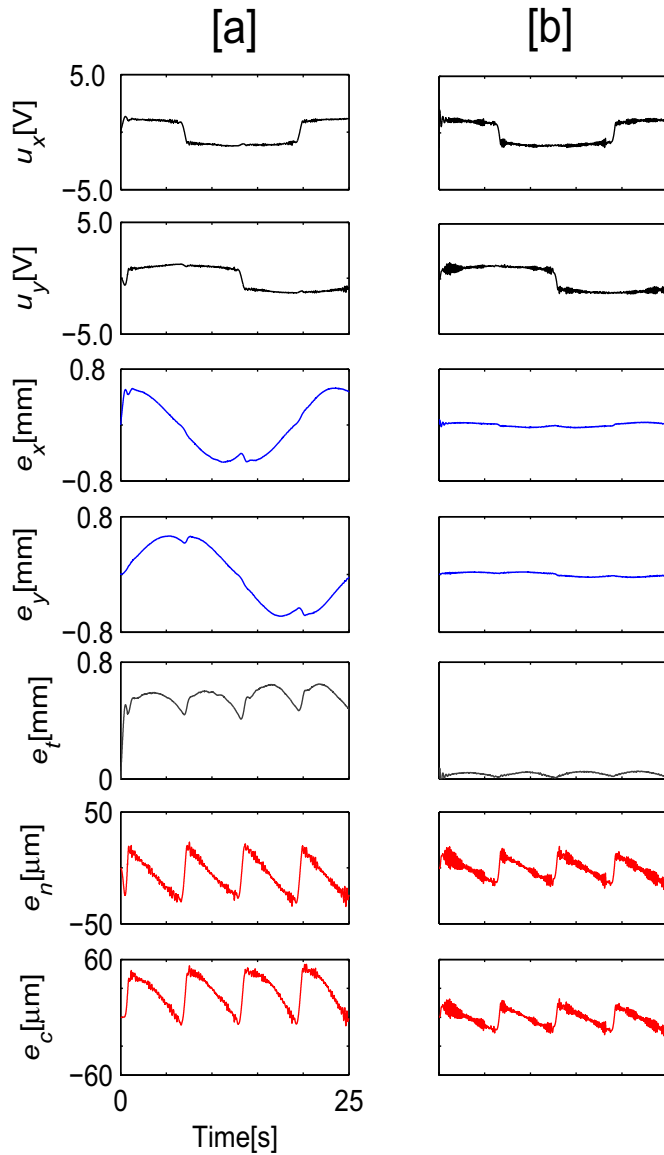
FIGURE 3.5: Experimental results (circular trajectory, ρ_{cn}=300). (a) H_P=6 and (b) H_P=25

feed drive system are shown in Table 3.1. The corresponding discrete-time model for the biaxial feed drive system is represented by the following polynomials:

$$A_i(q^{-1}) = 1.00 - 1.97q^{-1} + 0.97q^{-2}. \tag{3.25}$$

$$B_i(q^{-1}) = 0.28 \times 10^{-6}q^{-1} + 0.28 \times 10^{-6}q^{-2}. \tag{3.26}$$

This model is obtained from continuous-time model using zero-order hold and sampling time $T = 5.0$ms. Two reference trajectories are used to evaluate the
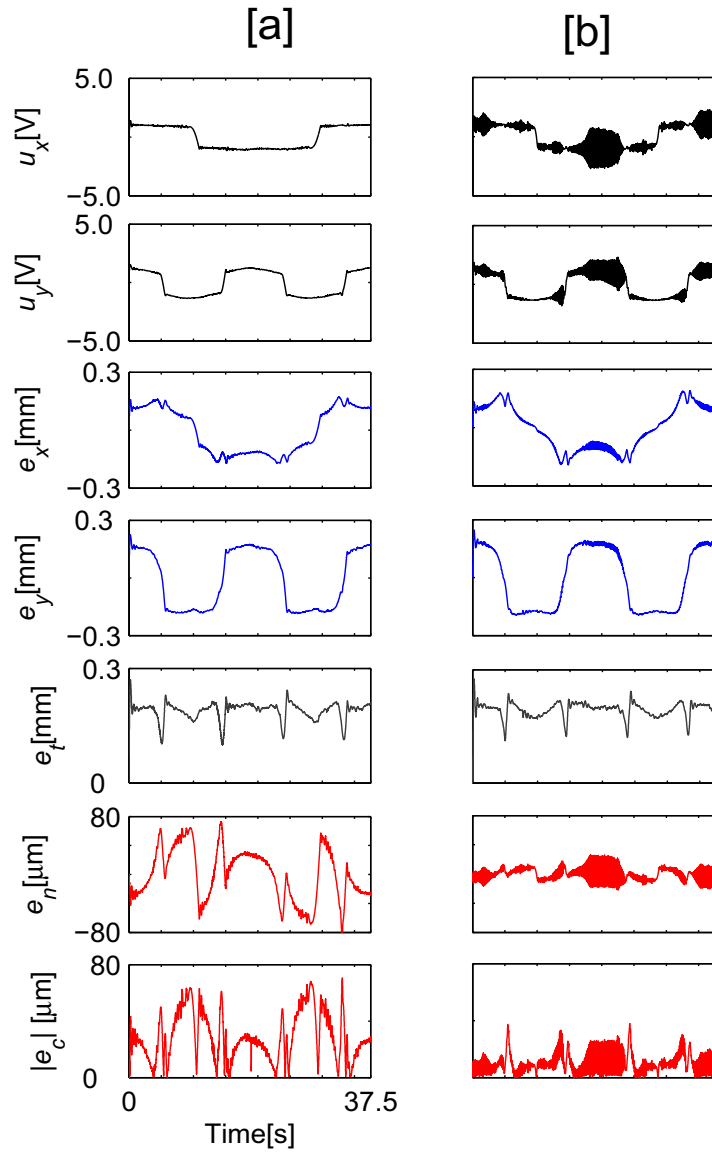
FIGURE 3.6: Experimental results (non-circular trajectory, $\rho_{cn}=300$). (a) $H_P=6$ and (b) $H_P=25$

proposed controller:

(1) Circular reference trajectory

$$x = 5.0\sin\left(\frac{t}{4}\right) \text{ [mm]},$$

$$y = 5.0\cos\left(\frac{t}{4}\right) \text{ [mm]}. \tag{3.27}$$
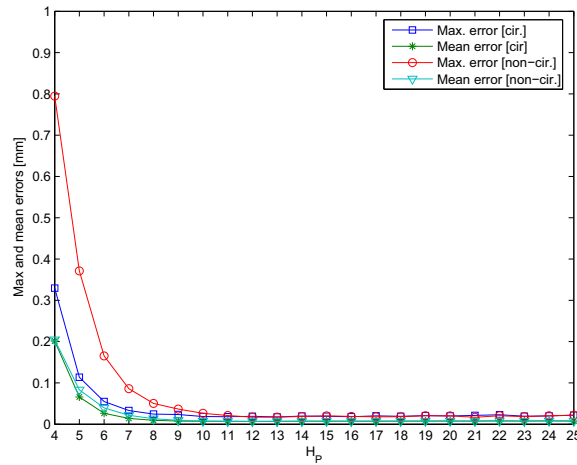
FIGURE 3.7: Contouring performance under different prediction horizons H_P

(2) Non-circular reference trajectory

$$x = 5.0\sin\left(\frac{t}{6}\right) \ [\text{mm}],$$

$$y = 5.0\sin\left(\frac{t}{3}\right) \ [\text{mm}]. \tag{3.28}$$

The circular and non-circular reference trajectories are shown in Figs. 3.4(a) and 3.4(b), respectively. For the first reference trajectory, the actual contour error can be easily calculated using the following equation (note that this equation is used for verification only and is not used to calculate the controller parameters):

$$e_c = 5 - \sqrt{x^2 + y^2}[\text{mm}]. \tag{3.29}$$

An essential advantage of the proposed contouring control strategy is that it takes into account not only the current values but the future values of the control input as well as the reference trajectories. Consequently, the prediction horizon H_P is an essential tuning parameter that gives the designer a more optimized control of performance. To demonstrate the effectiveness of the prediction horizon as tuning parameter in the proposed controller, experimental results for the cases of H_p=6[30 ms] and 15[75 ms] for the circular reference trajectory are shown in Figs. 3.5(a) and 3.5(b), respectively. The weighting factor $\rho_{cn} = 300$, and the other wighting factors in the performance index are set as given in Table 3.2. Better control performance is obtained, and maximum and mean magnitudes of the contour error are reduced in Fig. 3.5(b).
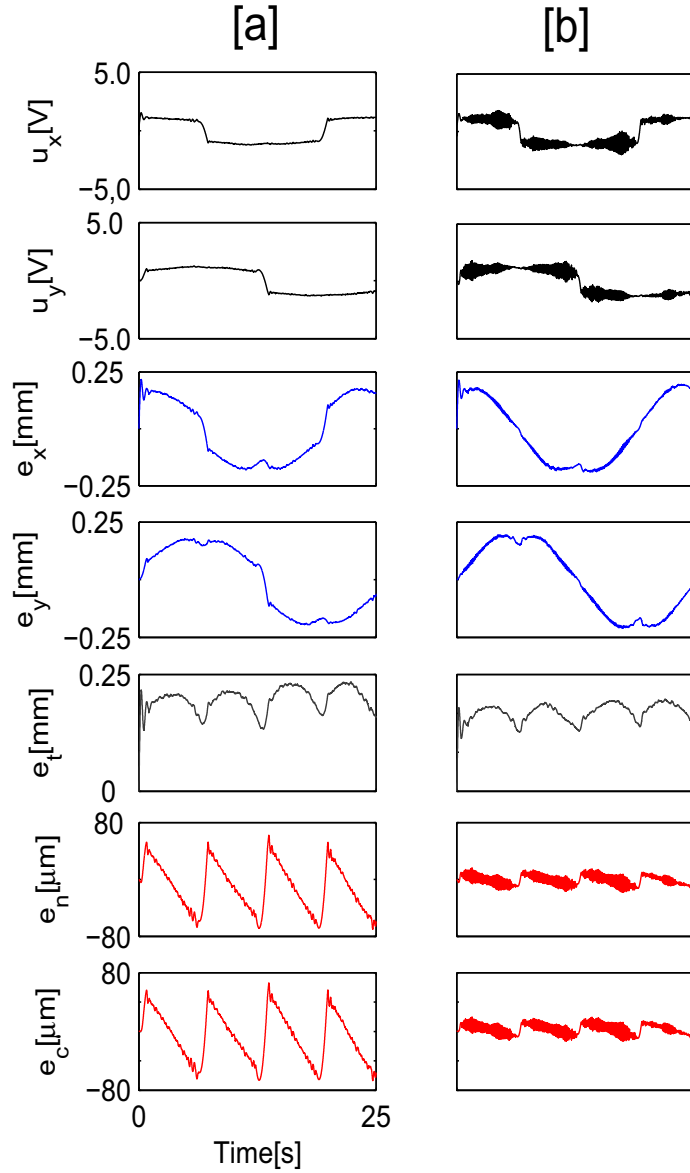
FIGURE 3.8: Experimental results (circular trajectory, H_P=9). (a) ρ_{cn}=50 and (b)ρ_{cn}=650

To verify the effectiveness of the proposed controller to follow non-circular trajectories, the same controllers are applied to the trajectory in Fig 3.4(b). Because it is difficult to calculate the actual contour error on-line for the non-circular trajectory, the following minimization problem is solved off-line to calculate the magnitude of the actual contour error at time t_k:

$$|e_c(t_k)| = \min_{t} \sqrt{\{(r_x(t_k) - q_x)^2 + (r_y(t_k) - q_x)^2\}}. \tag{3.30}$$

Note that this error magnitude is used only for verification purposes. Figure 3.6
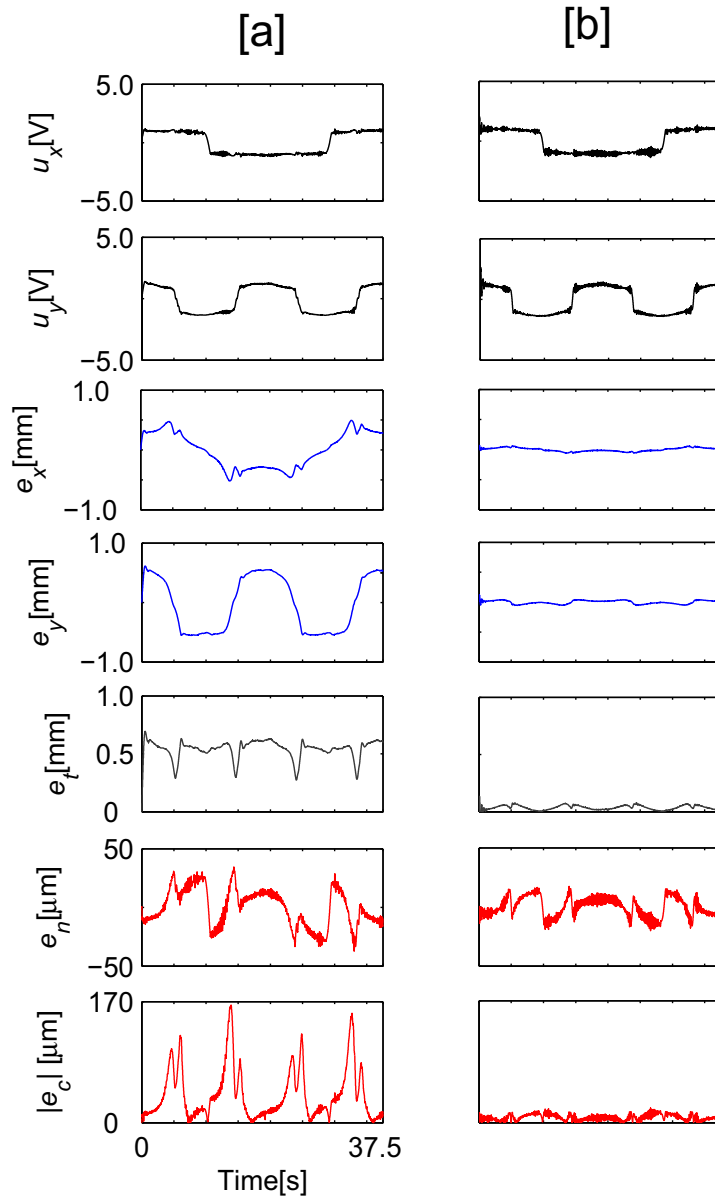
FIGURE 3.9: Experimental results (non-circular trajectory, H_P=9). (a) ρ_{cn}=50 and (b)ρ_{cn}=650

shows the experimental results for the non-circular trajectory, where the prediction horizon is set to same values as those used in the experiment shown in Fig. 3.5. Figure 3.7 summarizes the maximum and mean magnitudes of the contour errors for circular and non-circular trajectories, where the prediction horizon is changed from 4 to 25. The weighting factor for error components orthogonal to the desired contour curve ρ_{cn} is set to 300 in the experiments shown in Fig. 3.6.

Weighting factors ρ_{cn}, ρ_{ct}, ρ_n and ρ_t are tuning parameters for the proposed contouring controllers that allow importance of the performance index terms to be
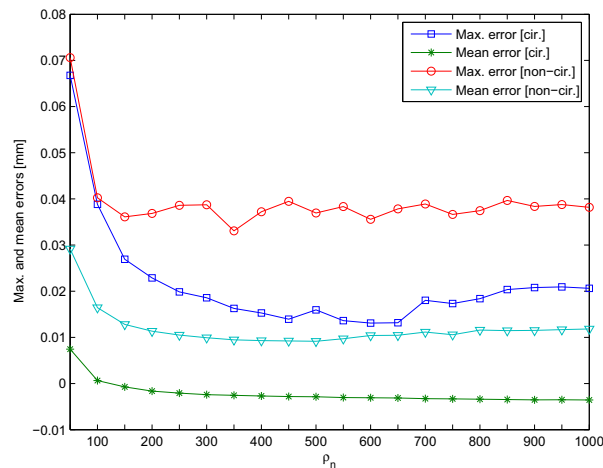
Fig. 10 Contouring performance under different weighting factors ρ_{cn}

FIGURE 3.10: Contouring performance under different weighting factors ρ_{cn}

TABLE 3.2: Values of the performance index wighting factors

Parameter	Value
ρ_{ct}	1.00
ρ_n	6.0×10^{-8}
ρ_t	3.0×10^{-9}

adjusted. Experimental results for the circular reference trajectory, where the weighting factor for error components orthogonal to the desired contour curve ρ_{cn} is set to 50, are shown in Fig. 3.8(a). The prediction horizon H_P is set to 9 from the result in Fig. 3.7. Because the error components orthogonal to the desired contour curve are more important than tracking errors with respect to each feed drive axis, a better contouring performance is obtained by increasing the weighting factor for error components orthogonal to the desired contour curve. Figure 3.8(b) shows the experimental results for the case of circular trajectory with $\rho_{cn}= 650$.

Since the model predictive controller has more tuning parameters than the traditional controllers, it requires more tuning effort. However, a reasonable control performance can be obtained by simply choosing weighting factors for the performance index items. Generally speaking, all weighting factors should be positive. Since the normal direction error to the desired contour error is more important than the tangential one, the weighting factors in Eq. (3.11) can be easily adjusted compared to the conventional X-Y axis independent control approach. In addition, as shown in our experimental results we can used fixed values for all ρ_{ct}, ρ_n and

ρ_t, and only ρ_{cn} are changed to improve the contouring performance. Figure 3.9 shows the experimental results for the non-circular trajectory, where the weighting factor ρ_{cn} is set to same values as those in the results in Fig. 3.8. It is apparent that the weighting factor ρ_{cn} is essential in the proposed contouring controller. To demonstrate the effect of ρ_{cn}, Fig. 3.10 summarizes the maximum and mean magnitudes of the contour errors, where ρ_{cn} varies from 50 to 1000.

Chapter 4

Sliding Mode Contouring Control Design Using Nonlinear Sliding Surface for biaxial feed drive systems

4.1 Introduction

The goal of NC/CNC contouring systems is to control the positions of the cutting tool and workpiece to follow a predetermined path with minimum error with small energy consumption. Contour error that is defined as the shortest distance between the actual tool position and desired trajectory gives a better indication of machining accuracy. In machining, two main control approaches are used to improve contouring performance: the tracking control approach and the contouring control approach. Although many approaches for reducing tracking errors in multi-axis feed drive systems have been developed to date [12, 53, 78, 85–89], the most significant factor in the performance of contouring systems is the accuracy of the overall system or the contour error of the system [6, 90].

To reduce the contour error, researchers have developed a variety of alternative control approaches. By calculating the contour error from the tracking errors in biaxial contour-following tasks, Koren proposed the CCC [15], and Ho *et al.* decomposed the contour error into the normal tracking error and the advancing

tangential error [17]. A dynamic decoupling procedure is then applied to the system dynamics. Yeh and Hsu estimate the contour error as the vector from the actual position to the tangential line at the reference position [91]. Chen et. al proposed a contour-tracking controller based on the polar coordinates [92]. One disadvantage of the CCC methods is that both contour and tracking errors along the feed drive axes are used to calculate control inputs. This causes degradation in the contour tracking performance.

To address this problem, Lo and Chung proposed a contouring control method for biaxial feed drive systems based on a coordinate transformation [21], in which tracking errors are transformed into errors with components that are orthogonal and tangential to the desired contour curves. Cheng and Lee proposed a real-time contour error estimation algorithm and employed an integrated motion control scheme to improve the machining accuracy for contour following tasks [22]. Uchiyama *et al.* verified that the contouring controller is effective, in that it can achieve contouring performance comparable to that of a non-contouring controller with less control input variance[93]. In order to synthesize high contouring performance for high-speed machines driven by linear motors, adaptive robust controller design strategies have been applied to compensate for the effect of parametric uncertainties and uncertain nonlinearities [94]. Among these strategies, Hu *et al.* proposed a discontinuous-projection-based adaptive robust controller for the high-performance contouring controls of a linear motor [90]. The proposed algorithm takes into account the dynamic coupling effect and parametric uncertainties and uncertain nonlinearities. They extended this approach to consider the specific characteristics of cogging forces in the controller designs and employed a task coordinate formulation for coordinated motion control [95].

Sliding mode control (SMC) provides a viable and effective method with a strong robustness property and fast error convergence characteristics for non-linear systems subjected to external disturbances and parameter variations by emulating a prescribed reduced-order system [63, 96, 97]. In the conventional sliding mode controller design, a linear sliding surface is utilized which gives a constant damping ratio. In control systems, the most important requirements are fast response and small overshoot. However, quick response produces high overshoot, which causes contour errors and also increases the consumed energy. On the other hand, low overshoot means slow response, which leads to significant contour errors. Thus, it

is very difficult to achieve small overshoot with a fast response using the conventional linear SMC method. This particular problem can be solved by employing the composite nonlinear feedback (CNF) technique [44]. The nonlinear sliding surface consists of a linear term and a nonlinear term. The linear term comprises a gain matrix that has a very low damping ratio value, thereby facilitating a fast response [45]. The nonlinear term is introduced to provide a variable damping ratio in order to achieve a small overshoot and settling time of the closed loop system as the contour error converges to zero.

In our previous work [98], where a single axis case is considered only, we have verified that increase of the linear gain of the sliding surface results in a reasonable performance. However, saturation of the control input precludes the designer to increase the linear gain to achieve smaller error. To improve the contouring performance in machine tool feed drive systems, we extend our previous approach to a biaxial feed drive systems. In the current study, a nonlinear sliding mode contouring controller for biaxial feed drive systems is designed based on a coordinate transformation approach. The aim of the proposed controller is to guarantee stability and enhance the contouring performance of biaxial feed drive systems. The main advantage of the proposed approach is that it achieves a quick response and a small overshoot, thereby providing improved performance in terms of contour errors and consumed energy saving. To verify the effectiveness of the proposed approach, experiments have been conducted for a biaxial feed drive system. The experimental results show that by using of the nonlinear term, a significant reduction in the consumed energy and control input variance is achieved.

4.2 Contour error and Dynamics Modeling

4.2.1 Definition of contour error

Contour error is defined as the shortest distance between the actual contour and the desired contour. Figure 4.1 shows the relationships between the contour and tracking errors in each feed drive axis. The coordinate frame Σ_w is a fixed coordinate frame and its axes x and y correspond to feed-drive axes. The desired position of the point of the machined part at time t, and defined in Σ_w, is $r = [r_x, r_y]^T$. The actual position of the feed drive system is represented by $q = [q_x, q_y]^T$, which
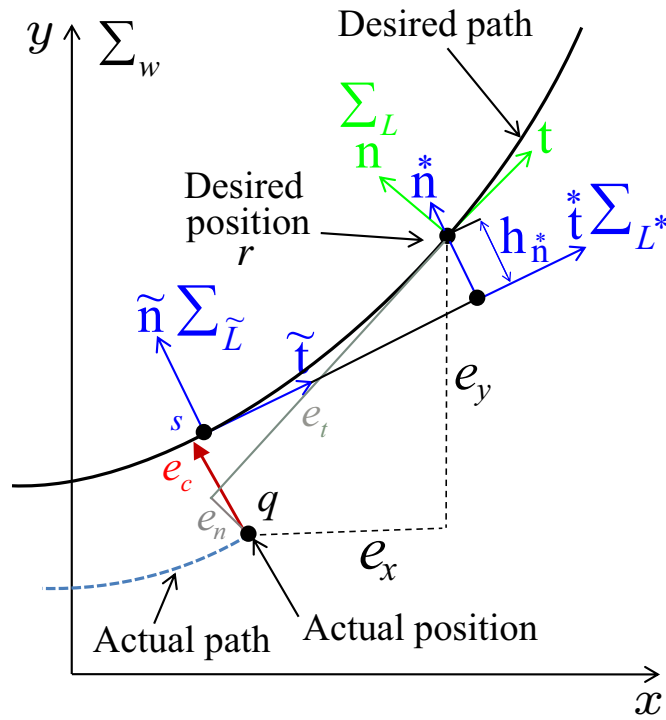
FIGURE 4.1: Contour error definition and estimation

is also defined in the fixed frame. The tracking error in each feed drive axis is defined as

$$e_w = [e_x, \ e_y]^T = q - r. \tag{4.1}$$

The coordinate frame Σ_L is attached at r and its axis directional vectors are t and n. The axis t is in the tangential direction of the desired trajectory at r, and the direction of n is perpendicular to t. For the parametric trajectory, vectors t and n are calculated at a time t as follows:

$$t = [t_x, t_y]^T = \frac{\dot{r}}{\| \dot{r} \|}, \dot{r} \neq 0. \tag{4.2}$$

$$n = [n_x, n_y]^T = \frac{\dot{t}}{\| t \|}, \ddot{r} \neq 0. \tag{4.3}$$

This tracking error vector can be expressed with respect to Σ_L as

$$e_L = [e_t, e_n]^T = L^T e_w,$$
$$L = \begin{bmatrix} t_x & n_x \\ t_y & n_y \end{bmatrix}. \tag{4.4}$$

The normal component e_n, can be considered as an approximate value of the actual

contour error. However, this estimation may be inaccurate when the curvature of the desired trajectory is not small. To avoid this estimation error, we assume that the distance between the desired position r and the point s on the desired trajectory is approximately equal to the tangential error e_t. In addition, the desired velocity along this segment is nearly constant and equals to the desired velocity at r. The required time to traverse this segment t_d is calculated as follows:

$$t_d = \frac{e_t}{\| \dot{r} \|}, \dot{r} \neq 0. \tag{4.5}$$

A new coordinate frame $\Sigma_{\tilde{L}}$ corresponding to the instantaneous time $\tilde{t} = t - t_d$ is defined by two unit vectors as follows:

$$\tilde{t} = \left[\tilde{t}_x, \tilde{t}_y \right]^T = t(\tilde{t}). \tag{4.6}$$

$$\tilde{n} = \left[\tilde{n}_x, \tilde{n}_y \right]^T = n(\tilde{t}). \tag{4.7}$$

The corresponding error vector $e_{\tilde{L}}(t) = [\tilde{e}_t, \tilde{e}_n]^T$ is calculated with respect to the transformed frame $\Sigma_{\tilde{L}}$ having two axes $\tilde{t}$ and $\tilde{n}$ as follows:

$$e_{\tilde{L}} = [e_{\tilde{t}}, \ e_{\tilde{n}}]^T = \tilde{L}^T e_w,$$
$$\tilde{L} = L(\tilde{t}). \tag{4.8}$$

The error vector $e_{\tilde{L}}$ is transformed into a new coordinate frame Σ_{L^*} as shown in Fig. 4.1. The transformed error vector can be expressed as follows:

$$e_{L^*} = [e_{t^*}, \ e_{n^*}]^T = \tilde{L}^T e_w + h^*,$$
$$h^* = [0, \ h_n^*] = J\tilde{h},$$
$$\tilde{h} = \tilde{L}^T \left[\ r(\tilde{t}) - r(t) \ \right]. \tag{4.9}$$

where $J \in R^{2 \times 2}$ is a diagonal matrix diag$\{0,1\}$ and $r(\tilde{t})$ is the desired position at the instantaneous time $\tilde{t}$.

Because calculating the actual contouring error in real time for complex contour is an intensive computational task, we regard the error component e_n^* as an approximation of the contouring error e_c, which is the distance between the actual position x and the nearest point on the desired curve.

4.2.2   Feed drive dynamics modeling

This study considers a typical biaxial feed drive system, as shown in Fig. 4.2. Two servo motors, commonly used in industrial applications, are used to drive the feed drive system. The feed drive system is generally represented by the following decoupled second order system:

$$
\begin{aligned}
& M\ddot{x} + C\dot{x} = f - d, \\
& M = \text{diag}\{m_i\},\ \ C = \text{diag}\{c_i\},\ \ i = x, y, \\
& f = [f_x, f_y]^T, \\
& d = [d_x, d_y]^T.
\end{aligned}
\tag{4.10}
$$

where $m_i(> 0)$, $c_i(\geq 0)$, d_i and f_i are the mass of load, viscous friction coefficient, external disturbance and driving force along the ith drive axis, respectively. The notation $\text{diag}\{a_i\}$ denotes a diagonal matrix with the elements a_i at the ith diagonal position.

Two ball screws are used to convert angular motion of the motors to linear motion of the table. The motor dynamics for driving the feed drive system is described as follows:

$$
\begin{aligned}
& N\ddot{\theta}_{mi} + Z\dot{\theta}_{mi} + \tau = Ku, \\
& \theta_{mi} = [\theta_{mx}, \theta_{my}]^T, \\
& N = \text{diag}\{n_i\},\ \ Z = \text{diag}\{z_i\}, \\
& K = \text{diag}\{k_i\},\ \ i = x, y, \\
& \tau = [\tau_x,\ \tau_y]^T,\ \ u = [u_x,\ u_y]^T.
\end{aligned}
\tag{4.11}
$$

where θ_{mi}, $n_i(> 0)$, $z_i(\geq 0)$, $k_i(> 0)$, τ_i and u_i are the rotational angle of the motor, motor inertia, motor viscous friction coefficient, torque-voltage conversion ratio, torque needed to drive the feed drive system in Eq.(4.10), and the motor input voltage of the ith axis, respectively. The relationships between the force f_i and torque τ_i, and position q_i and angle θ_{mi} are

$$
f_i = \frac{2\pi\tau_i}{p_i},\ \ q_i = \frac{p_i\theta_{mi}}{2\pi}.
\tag{4.12}
$$

where p_i is the pitch of the ith ball screw.
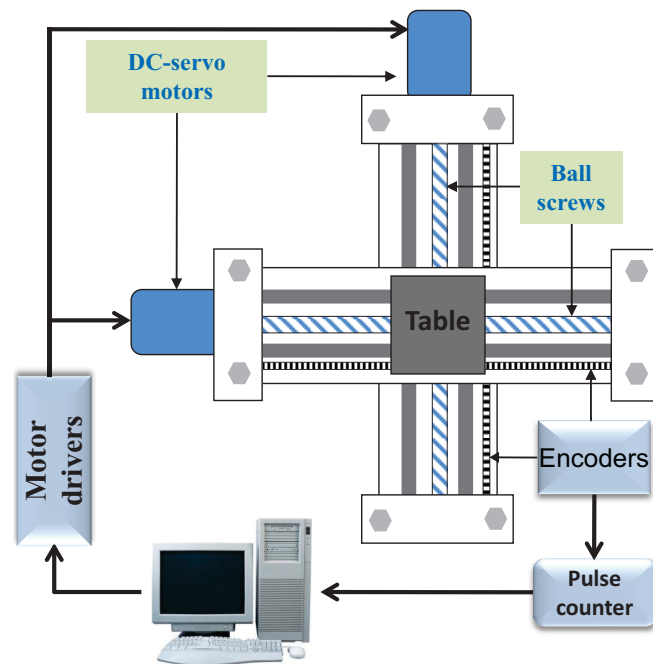
FIGURE 4.2: A typical biaxial feed drive system
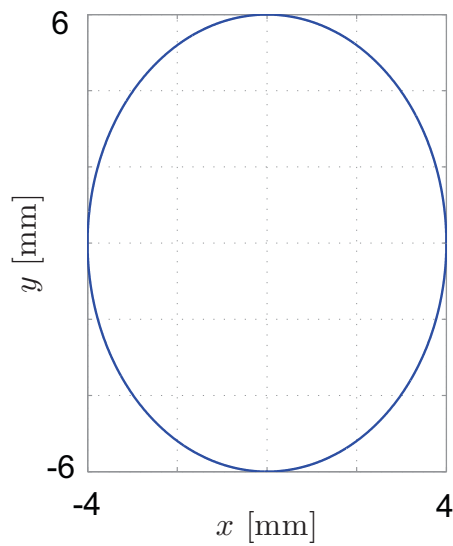
FIGURE 4.3: The reference trajectory used in the experiments

4.3   Contouring Controller Design and Stability Analysis

4.3.1   Controller design

In the conventional sliding mode control with a linear sliding surface, the damping ratio of the system remains constant regardless of the error value. Thus the designer has to consider the trade-off between two important characteristics; fast response (low damping ratio) and small overshoot (high damping ratio). In order to handle this trade-off, the sliding surface should be designed in such a way that the damping ratio may be changed according to the error. Using a nonlinear sliding surface, the damping ratio of the closed loop system can be changed from its initial low value to a final high value. The initial low value of the damping ratio results in a quick response and the later high damping avoids overshoot to save energy consumption. Based on the the dynamics of the feed drive system (4.10), (4.11) and (4.12), we propose the following nonlinear sliding surface:

$$S = \begin{bmatrix} F - \Psi P & I \end{bmatrix} \begin{bmatrix} e_{L^*} \\ \dot{e}_{L^*} \end{bmatrix}, S \in R^{2 \times 1}. \tag{4.13}$$

Here, $F \in R^{2 \times 2}$ is the linear term of the sliding surface, which is chosen such that the dominant poles have small damping ratios to achieve a fast response. $P \in R^{2 \times 2}$ is a positive definite matrix to adjust the final damping ratio. $\Psi \in R^{2 \times 2}$ is a diagonal matrix with non-positive nonlinear entries depending on the transformed errors and is used to change the damping ratio of the system. The choice of Ψ is not unique, and one possible choice is as follows [99]:

$$\Psi = \text{diag} \left\{ -\beta_i \frac{\bar{k}_i \exp(-\tilde{e}_i) + \bar{k}_i \exp(\tilde{e}_i)}{2} \right\},$$

$$\tilde{e}_i = \begin{cases} e_i & \text{if } |e_i| \leq e_{imax} \\ e_i \text{sgn}(e_i) & \text{if } |e_i| > e_{imax}, i = t^*, n^* \end{cases} \tag{4.14}$$

where e_{imax}, β_i and $\bar{k}_i$ are positive tunning parameters used to adjust the maximum bound, minimum bound and variation rate of the nonlinear function magnitude $|\Psi|$, respectively. $\text{sgn}(e_i)$ represents the sign function of the error signal e_i. By applying some control law, which will be presented later, the system can be forced

to the sliding surface. During the ideal sliding surface $S = 0$, we have

$$\dot{e}_{L^*} = (-F + \Psi P)e_{L^*}. \tag{4.15}$$

The above equation includes the time variant parameter Ψ. In order to show the stability of the proposed sliding dynamics, we consider a Lyapunov function candidate for the system in Eq. (4.15) as follows:

$$V_1 = \frac{1}{2}e_{L^*}^T e_{L^*}. \tag{4.16}$$

Using Eq. (4.15), the time derivative of the Lyapunov function candidate becomes

$$\dot{V}_1 = (-F + \Psi P)e_{L^*}^T e_{L^*}. \tag{4.17}$$

Since $\Psi < 0$, $F > 0$ and $P > 0$, we have

$$\dot{V}_1 \leq 0. \tag{4.18}$$

and this ensure the system stability during the ideal sliding mode.

From the definition of the tracking error e_w and system dynamics (Eqs. (4.10),(4.11) and (4.12)), the tracking error dynamics of the feed drive system in the fixed coordinate frame Σ_W are expressed as:

$$
\begin{aligned}
\ddot{e}_w &= H^{-1}\left[-E\dot{x} - \tilde{d} + u\right] - \ddot{r}, \\
H &= \text{diag}\left\{\frac{m_i + n_i\left(\frac{2}{p_i}\right)^2}{k_i\left(\frac{2\pi}{p_i}\right)}\right\}, \\
E &= \text{diag}\left\{\frac{c_i + z_i\left(\frac{2}{p_i}\right)^2}{k_i\left(\frac{2\pi}{p_i}\right)}\right\}, i = x, y, \\
\tilde{d} &= \left[\tilde{d}_x, \tilde{d}_y\right]^T = \left[\frac{d_x}{k_x}, \frac{d_y}{k_y}\right]^T.
\end{aligned}
\tag{4.19}
$$

The transformed error dynamics can be estimated by differentiating Eq. (4.9) twice with respect to time as follows:

$$\ddot{e}_{L^*} = \tilde{L}^T\ddot{e}_w + 2\dot{\tilde{L}}^T\dot{e}_w + \ddot{\tilde{L}}^T e_w + \ddot{h}^*. \tag{4.20}$$

Based on the proposed nonlinear sliding surface (4.13), assuming that the reference velocity and acceleration are given, substituting Eq.(4.19) into (4.20), and considering feed drive dynamics, we design the following controller:

$$
\begin{aligned}
u \;=\; & H\Bigg\{ \ddot{r} - \tilde{L}\Big[(F - \Psi P)\dot{e}_{L^*} + \ddot{\tilde{L}}^T e_w + 2\dot{\tilde{L}}^T \dot{e}_w + \ddot{h}^* - \frac{d\Psi}{dt} P e_{L^*} \Big] \\
& - K_c S - Q\,\mathrm{sgn}(S) \Bigg\} + E\dot{x}.
\end{aligned}
\tag{4.21}
$$

Here, $K_c \in R^{2\times 2}$ is a diagonal gain matrix, $\mathrm{sgn}(S)$ contains the signs of the sliding surface vector S and $Q \in R^{2\times 2}$ is a diagonal matrix with diagonal elements chosen from the maximum bound of the uncertainty as follows:

$$
Q_i \geq \max(\hat{d}_i), i = x, y.
\tag{4.22}
$$

where $\hat{d}_i$ represents the diagonal elements of $\tilde{L}^T H^{-1} \tilde{d}$.

4.3.2   Stability analysis

In order to analyze the stability of the proposed controller and insure that the controller forces the transformed errors onto the desired nonlinear sliding surface as $t \to \infty$, the time derivative of the following Lyapunov function must be negative:

$$
V = \frac{1}{2} S^T S.
\tag{4.23}
$$

The time derivative of the Lyapunov function is

$$
\dot{V} = S^T \left\{ \ddot{e}_{L^*} + (F - \Psi P)\dot{e}_{L^*} - \frac{d\Psi}{dt} P e_{L^*} \right\}.
\tag{4.24}
$$

Substituting Eq. (4.20) into (4.24) leads to

$$
\begin{aligned}
\dot{V} \;=\; & S^T \Bigg\{ \tilde{L}^T \Big\{ H^{-1}(-E\dot{x} - \tilde{d} + u) - \ddot{r} \Big\} + 2\dot{\tilde{L}}^T \dot{e}_w + \ddot{\tilde{L}}^T e_w + \ddot{h}^* + (F - \Psi P)\dot{e}_{L^*} \\
& - \frac{d\Psi}{dt} P e_{L^*} \Bigg\}.
\end{aligned}
\tag{4.25}
$$
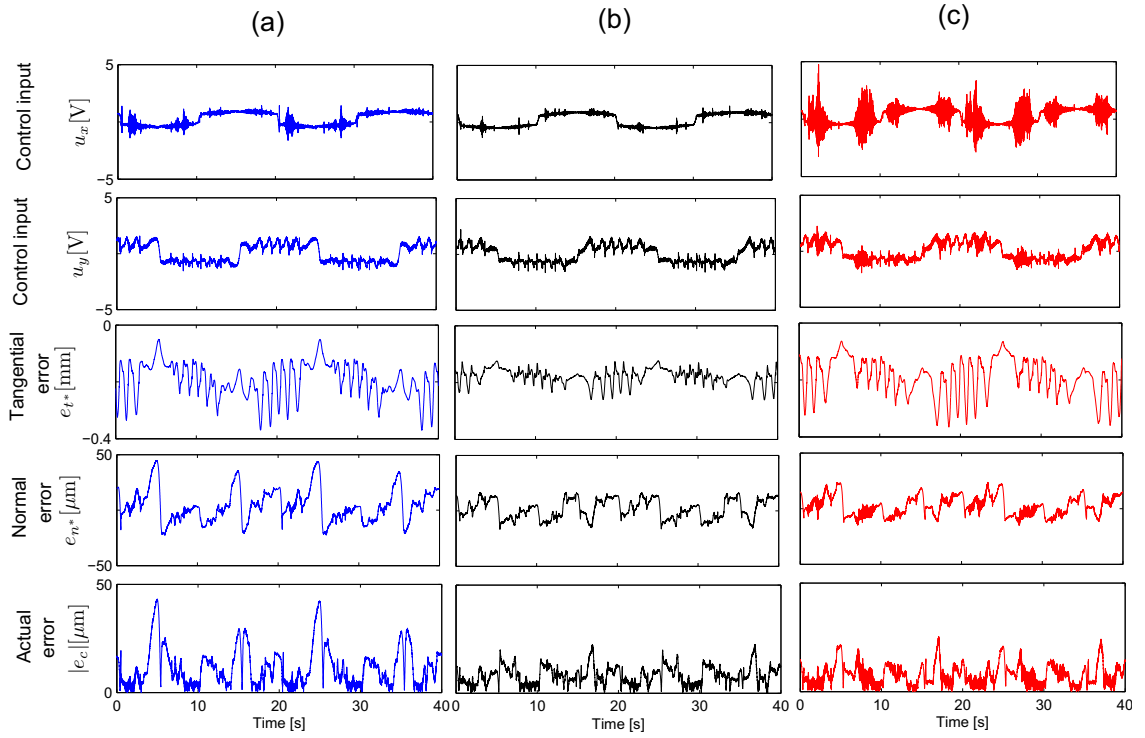
FIGURE 4.4: Experimental results:(a) Linear sliding surface with F=diag$\{110, 165\}$, (b) Nonlinear sliding surface with F=diag$\{10, 50\}$(Proposed) and (c) Liner sliding surface with with F=diag$\{170, 240\}$

Using control law (4.21), we have

$$\dot{V} = S^T \left\{ -KS - Q\text{sgn}(S) - \tilde{L}^T H^{-1} \tilde{d} \right\} \tag{4.26}$$

Thus, with (4.22), it is easy to show that

$$\dot{V} \leq -KS^T S. \tag{4.27}$$

Considering Eq. (4.18), the system stability is guaranteed.

4.4 Experimental Results

For verifying the advantage of the nonlinear sliding surface, the following three controllers have been implemented on a desk-top biaxial feed drive system:

TABLE 4.1: Parameter values of the experimental system

Parameter	Value
H[kgV/N]	diag$\{16.0, 4.6\}$
E[Vs/m]	diag$\{180, 48\}$

1. The conventional sliding mode controller with linear sliding surface (i.e., $\Psi=0$ in Eq. (4.14)) with a small damping ratio.

2. The proposed controller with nonlinear sliding surface (i.e., Eq.(4.17)).

3. The conventional sliding mode controller with linear sliding surface (i.e., $\Psi=0$ in Eq. (4.14)) with a high damping ratio.

The above controllers were implemented on a biaxial feed drive system using the C++ language on a personal computer (OS: Windows XP, CPU: 2 GHz) with sampling time of 5 ms. The biaxial feed drive system used in the experiments consists of two axes driven by DC servo motors that are coupled to and drive two ball screws. In addition, a linear encoder whose resolution is 0.1 μm is attached to each feed drive axis to measure the actual position of the feed drive system. The nominal parameter values of the machine are given in Table 4.1. In order to provide a fixed sampling period in Widows XP environment, we employ a timer on a counter board (CONTEC CNT24-4(PCI)H) with four channels of 24-bit up/down counters. The following elliptical reference trajectory (Fig. 4.3) is used in the experiments:

$$
\begin{aligned}
x &= 4 \cos\left(\frac{\pi}{10}t\right) \text{mm}, \\
y &= 6 \sin\left(\frac{\pi}{10}t\right) \text{mm}.
\end{aligned}
\tag{4.28}
$$

The actual contour error magnitude at each sampling time t_k is calculated through an iterative search for the shortest distance between the feed drive position and the desired path by solving the following off-line optimization problem:

$$
|e_c(t_k)| = \min_t \ \sqrt{(r_i(t_k) - q_i(t_k))^2}, i = x, y
\tag{4.29}
$$

First, we have verified the effectiveness of the proposed approach to reduce the contour error by comparing the performance of the controllers (a) and (b). In

TABLE 4.2: Parameter values of the controllers (a), (b) and (c)

Parameter	Controller (a)	Controller (b)	Controller (c)
$K_c[\text{s}^{-1}]$	diag{10,50}	diag{10,50}	diag{10,50}
$F[\text{s}^{-1}]$	diag{110,165}	diag{10,50}	diag{170,240}
$P[\text{-}]$	diag{1.5,1.7}	diag{1.5,1.7}	diag{1.5,1.7}
$\beta_t[\text{s}^{-1}]$	-	10	-
$\beta_n[\text{s}^{-1}]$	-	10	-
$k_{ot}[\text{mm}^{-1}]$	-	35	-
$k_{on}[\text{mm}^{-1}]$	-	300	-

this comparison, the controller gain matrix K_c and the positive definite matrix P are set to the same values in both controllers to conduct fare comparison. In this experiment, the controller gain matrix K_c, positive definite matrix P and the linear term of the sliding surface F have been adjusted as given in Table 4.2. In the nonlinear sliding surface, the matrix F is selected to have a small values compared with the linear sliding surface to insure a high damping ratio of the system to avoid overshoot. The nonlinear tunning parameters β_{t*}, β_{n*}, $\bar{k}_{t*}$ and $\bar{k}_{n*}$ are selected to be 10s^{-1}, 10s^{-1}, 35mm^{-1}, 300mm^{-1}, respectively (explanations on the selection of these parameters will be given later). In addition, because the normal error component is more important than the tangential one, we increase the controller gains for the normal error component. Fig. 4.4(a) shows the experimental results for the controller (a) with a linear sliding surface, where the control input of the feed drive axis, transformed error components and actual contour error (Eq. (4.29)) are plotted. In addition, it can be seen that when the contour error becomes very small (such as at the times 0-2.2s, 8-12.2s, 18-22.2s, 28-32.2s and 38-40s), the control input magnitude starts to increase because the effect of damping ratio is instantaneously small. The smaller damping ratio leads to significant overshoot that increases the control input magnitude. On the other hand, when the contour error increases (such as around the times 5s, 15s, 25s and 35s), the conventional controller could not reduce the error because the effect of damping ratio is instantaneously relatively larger than expected. This leads to increase the contour error. This disadvantage of the linear sliding surface hinders the designer to increase the gain of the system to achieve a better performance. This problem can be avoided by reducing the damping ratio instantaneously when the error converges to a small value using a nonlinear sliding surface. The results for the proposed nonlinear sliding surface (controller (b)) is shown in Fig. 4.4(b).
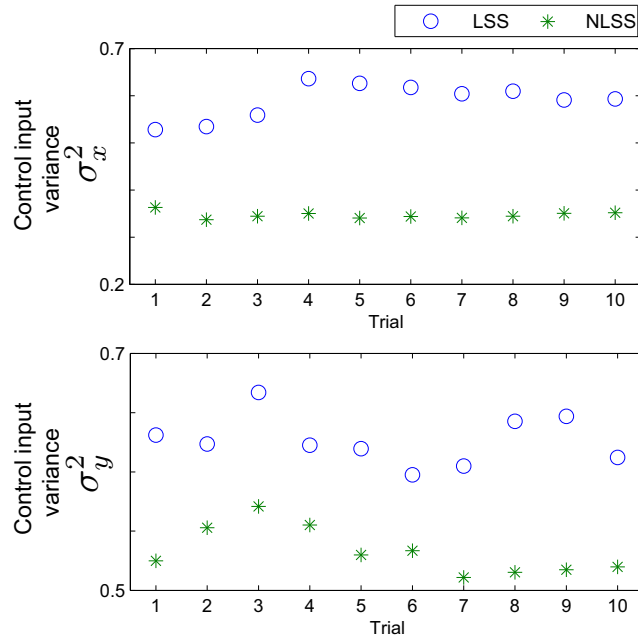
FIGURE 4.5: The control input variance

It can be confirmed that the proposed sliding surface achieves better performance in terms of the contour error without any increase of the electrical energy or control input variation. The nonlinear sliding surface allows the damping ratio to be changed to a high value when the contour error is small (to prevent overshot or saturation) or to a small value when the error is increased (to achieve fast response). In many researches, for example [95, 100–103], comparisons of the conventional and enhanced methods are usually based on contour error perspective only and do not consider the control input. A similar contour error profile to that shown in Fig. 4.4(b) can be obtained by increasing the damping ratio in the conventional design. In the controller (c), the values of F's components of linear sliding surface is increased to achieve a performance roughly similar to the controller (b). From the viewpoint of the consumed energy it appears fair to compare the controllers (b) and (c) for similar contouring performance. The results of this case are shown in Fig. 4.4(c) where the linear term F is adjusted to be diag$\{170, 240\}$s^{-1}. However, achieving similar contouring performance using the linear sliding surface increased the control input as shown in Fig. 4.4(c).

The same experiments with Figs. 4.4(b) and (c) were repeated 10 times. Note that, to avoid inaccuracies in the comparison, the running time in Fig. 4.4(b) and (c) was increased to 120 s, and the energy consumption and the control input variance were verified. The consumed energy was measured by a power Hi-tester
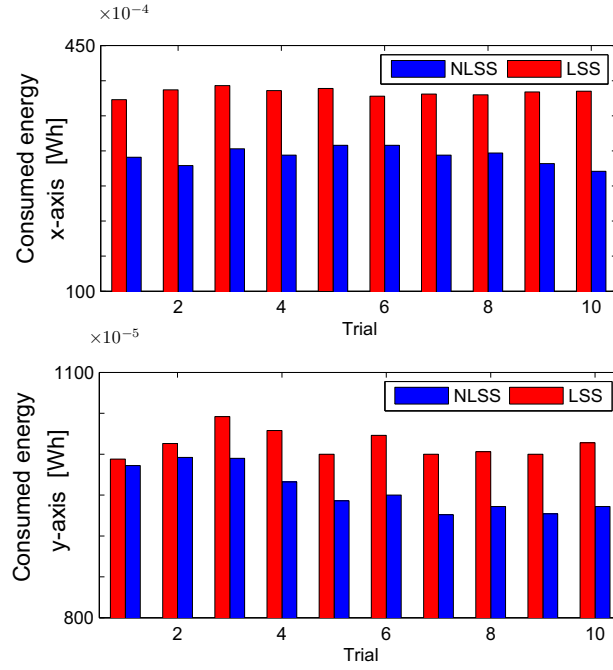
FIGURE 4.6: The consumed energy

(HIOKI 3334 AC/DC), and the control input variance was calculated as follows:

$$\sigma_j = \sqrt{\frac{\sum\limits_{i=1}^{I}(u_{ji} - \mu_j)^2}{I}}, j = x, y. \tag{4.30}$$

where u_{ji} denotes the control input value at the ith sampling instant of the jth axis, I is the total number of sampling instants ($i = 1, ..., I$), and μ_j is the mean of all of the control input values of the jth axis. As shown in Fig. 4.5, the proposed approach provided a control input variance that was about 45.7% and 18.9% smaller for x and y-axis, respectively. Figure 4.6 shows the consumed electrical energy by the feed drive axes x and y for the controllers (b) and (c). It is confirmed that the proposed controller with nonlinear sliding surface reduced the consumed energy by 29% and 12.5% for x and y-axis, respectively.

In addition, the proposed approach is easy to tune the non-linear term because only the function (Ψ) needs to be tuned. The choice of tunning parameters β_{t*} and β_{n*} to be small (10s^{-1} and 10s^{-1}, respectively) is to ensure a small initial value of the nonlinear function Ψ. Because the range of the normal error is very small compared to the tangential error as shown in Fig. 4.4, the tunning parameters $\bar{k}_{t*}$ and $\bar{k}_{n*}$ are selected to be 35mm^{-1} and 300mm^{-1}, respectively. The above two
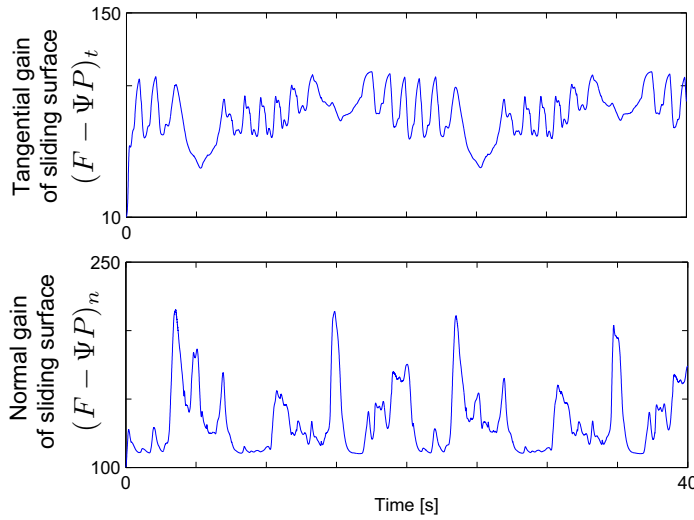
FIGURE 4.7: Diagonal elements of the matrix $F - \Psi P$

points allow the nonlinear function to have a small initial value and decrease when the error values increase to provide sufficient total gain of the sliding surface as shown in Fig. 4.7.

In order to improve the steady state performance, the proposed sliding surface can be extended to include integral action. The nonlinear term Ψ is very effective to achieve high performance with saturated actuators and the integral action is to ensure invariance against disturbances. The proposed sliding surface (4.13) can be extended without loss of stability as follows:

$$
S = \left[\begin{array}{ccc} F - \Psi P & I & K_i \end{array} \right] \left[\begin{array}{c} e_{L^*} \\ \dot{e}_{L^*} \\ \int_0^t e_{L^*}(t)\, dt \end{array} \right], S \in R^{2 \times 1}. \tag{4.31}
$$

where $K_i \in R^{2 \times 2}$ is an integral gain diagonal matrix with positive constant entires. In order to verify the effectiveness of the proposed nonlinear sliding surface with integral action, a sliding mode contouring controller based on (4.31) is designed and compared to the sliding mode controller with a proportional-integral-derivative (PID) sliding surface presented in [104]. In addition, for fare comparison, the integral gain matrices are set to the same value for both controllers. The gain matrices for the velocity error e_{L^*} are unity matrices for both controller. The positional gain matrix for the proposed sliding surface varies nonlinearly according to the function Ψ, and the parameters F, $\bar{k}_{t^*}$ and $\bar{k}_{n^*}$ are set to $\mathrm{diag}\{20,50\}s^{-1}$,
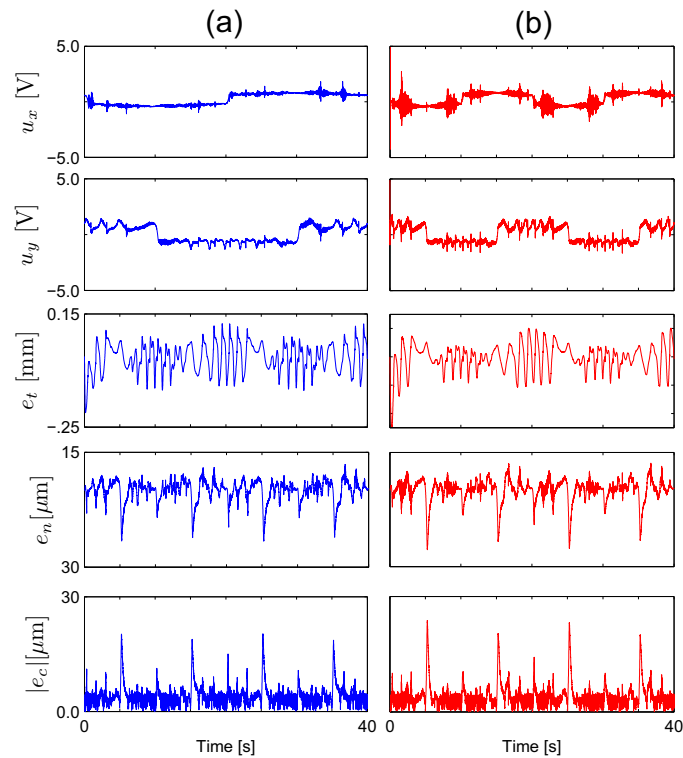
FIGURE 4.8: Experimental results: (a) Controller with the proposed NLSS with integral action Eq. (4.31) and (b) Controller with PID sliding surface presented in [104]

35mm^{-1} and 600mm^{-1}, respectively. On the other hand, the positional gain matrix for the sliding surface in [104] is constant and set to diag$\{80,120\}s^{-1}$ to achieve similar contouring performance with the proposed sliding surface. As shown in Fig. 4.8, the proposed sliding surface reduces the contour error with small control input because of employing the nonlinear function that increases the system damping ratio when the contour error converges to a small magnitude to prevent energy consumption. However, the controller in (b) is based on a constant damping ratio that is smaller than the optimal damping ratio when the contour error magnitude is small and vice versa.

4.5 Conclusions

A sliding mode contouring controller with a nonlinear sliding surface for biaxial feed drive systems based on coordinate transformation is presented in this study. The advantage of the proposed approach is that the sliding surface varies due to the contour error so that the damping ratio of the system changes from its

initial low value to its final high value as the contour error changes from high value to small value and vice versa so that the system simultaneously achieves low overshoot and a small settling time, resulting in a smaller error. To verify the effectiveness of the proposed control approach, we conducted experiments for elliptical reference trajectories. The results indicated that the proposed controller can significantly improve the contouring accuracy for smooth contour by adjusting the tunning parameters of the nonlinear function without any additional electrical energy. In addition, the proposed approach reduced the control input variance and consumed energy on average by about 41.2% and 14.9% (for x and y-axis, respectively) and 23.6% and 5.5% (for x and y-axis, respectively), respectively.

Chapter 5

Sliding Mode Contouring Control Design Using Nonlinear Sliding Surface for Three-Dimensional Machining

5.1   Introduction

High-precision machining and saving of the consumed energy are essential requirements for modern computerized numerical control (CNC) machines. For machining, error components orthogonal to the desired contour curve are called contour errors and represent good indicators of the machining precision. Tracking and contour errors are important aspects that significantly affect machining accuracy. Two main control approaches are used to improve contouring performance: the tracking control approach and the contouring control approach. Many existing approaches for reducing tracking errors in multi-axis feed drive systems have been developed to date [12, 53, 78, 85–87, 89].

The most significant factor in the performance of contouring systems is the accuracy of the overall system or the contour error of the system [6]. To reduce the contour error, researchers have developed a variety of alternative control approaches as presented in the previous chapter. However, in all of the previous contouring algorithms, the case of three-dimensional contouring control is not considered. To

69

reduce the contour error in three-axis machines, Lo proposed a three-axis contouring controller that operated in a trajectory coordinate basis that is moving along the tool path trajectory [105]. Other researchers such as Chiu and Tomizuka introduced transforming machine tool feed drive dynamics into a moving task coordinate frame attached to the desired contour, i.e., the task coordinate frame at the desired position of the feed drive system. The control system dynamics are then reformulated with respect to the new coordinate frame [18]. Uchiyama *et al.* established a contouring controller for three-dimensional machining based on a coordinate transformation [93]. In addition, they proposed a method to reduce the inherent contour error resulting from the coordinate transformation approach. Recently, Khalick and Uchiyama introduced a contouring controller for three-dimensional machining based on iterative contour error estimation and a coordinate transformation approach [106].

To improve the contouring performance in machine tool feed drive systems, a nonlinear sliding mode contouring controller is presented in this chapter based on iterative contour error estimation and a coordinate transformation approach. We propose a novel sliding surface, in which the normal and bi-normal error components are given more importance than the tangential component, to reduce the contour error. The aim of the proposed controller is to guarantee stability and enhance the contouring performance of three-axis feed drive systems. The main advantage of the proposed approach is that it achieves a quick response and a small overshoot, thereby providing improved performance in terms of contouring errors and consumed energy savings. To verify the effectiveness of the proposed approach, experiments have been conducted for a three-axis CNC machine. The experimental results show that by adjusting the parameters of the nonlinear term, the contour error can be significantly reduced.

5.2 Three-Dimensional Contour Error Estimation

This section briefly explains the iterative estimation method for contour errors in three-dimensional machining, presented by the first two authors [106]. The contour error is defined as the shortest distance between the actual contour and the desired one. The relationship between the contour error and the tracking error
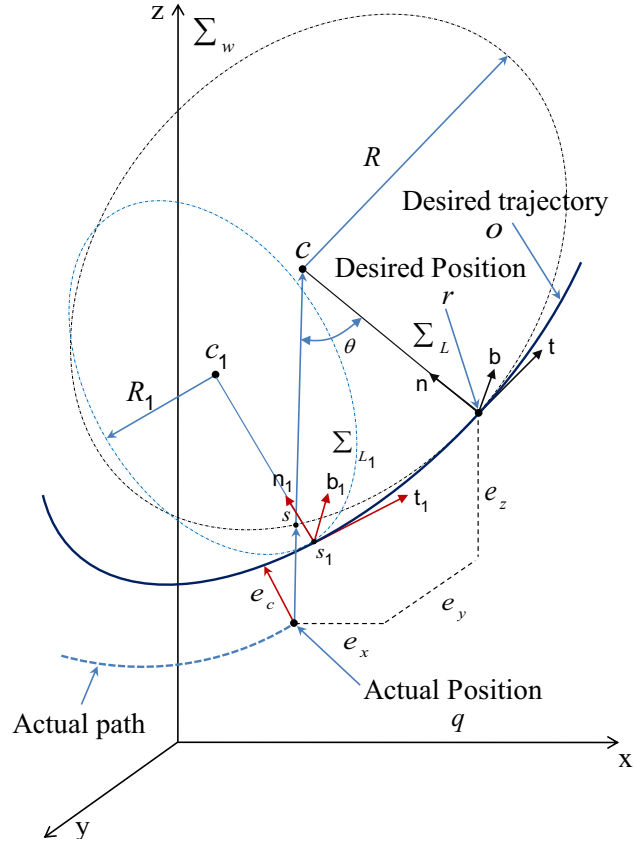
FIGURE 5.1: Iterative approach for three-dimensional contour error estimation

in each feed drive axis is shown in Fig. 5.1. The curve o is the desired contour curve of the point of a machined part driven by the feed drive system. The variable $r = [r_x, r_y, r_z]^T$ is the desired position of the point of the machined part at time t, and is defined in a fixed frame Σ_w, whose axes x, y, and z correspond to the feed drive axes. In addition, we assume that the first and second time derivatives, $\dot{r}$ and $\ddot{r}$, of the reference signal r are available. The actual position of the feed drive system is assumed to be $q = [q_x, q_y, q_z]^T$, which is also defined in the fixed frame Σ_w. The tracking error in each feed drive axis, $e_w = [\ e_x,\ e_y,\ e_z]^T$, are defined as follows:

$$e_w = [e_x, e_y, e_z]^T = q - r. \tag{5.1}$$

The above errors are defined in the coordinate frame Σ_w. For a parametrically defined curve, the curvature at the desired position r is calculated as follows [107]:

$$\frac{1}{R} = \frac{||\dot{r} \times \ddot{r}||}{||\dot{r}||^3}, \dot{r} \neq 0. \tag{5.2}$$

The iterative algorithm can be summarized as follows:

(1) A local coordinate frame Σ_L is defined with origin at r and axes t, n, and b, as shown in Fig. 5.1. The t-axis is in the tangential direction of o at r, the n-axis is in the normal direction of o at r, and the b-axis is the bi-normal component normal to t and n. For the parametric trajectory, the tangential, normal, and bi-normal vectors, denoted as t, n, and b, respectively, are calculated at a time t as follows:

$$\text{t} = \frac{\dot{r}}{\| \dot{r} \|}. \tag{5.3}$$

$$\text{n} = \frac{\dot{\text{t}}}{\| \dot{\text{t}} \|}. \tag{5.4}$$

$$\text{b} = \text{t} \times \text{n}. \tag{5.5}$$

(2) The circle of curvature is located in the t - n plane and perpendicular to b. The center of the circle c can be estimated using a coordinate transformation between the fixed and the local coordinate frames:

$$c = [c_x, c_y, c_z]^T = r + L \begin{bmatrix} 0 & R & 0 \end{bmatrix}^T,$$
$$L = \begin{bmatrix} \text{t} & \text{n} & \text{b} \end{bmatrix}. \tag{5.6}$$

(3) The angle θ can be estimated as follows:

$$\theta = \cos^{-1} \frac{a \cdot \text{n}}{||a|| \, ||\text{n}||},$$
$$a = \frac{c - q}{||c - q||}. \tag{5.7}$$

(4) A new local coordinate frame Σ_{L_1} is defined at point $s_1 = r(t_1)$, where the time t_1 can be estimated by assuming a constant velocity throughout the segment r - s equaling to the desired velocity at r. The time required to pass the segment r - s is the same as that required to pass the segment r - s_1 on the desired trajectory. The delayed time t_1 is calculated as follows:

$$t_1 = t - t_d.$$
$$t_d = \frac{R\theta}{||\dot{r}||}, \dot{r} \neq 0. \tag{5.8}$$
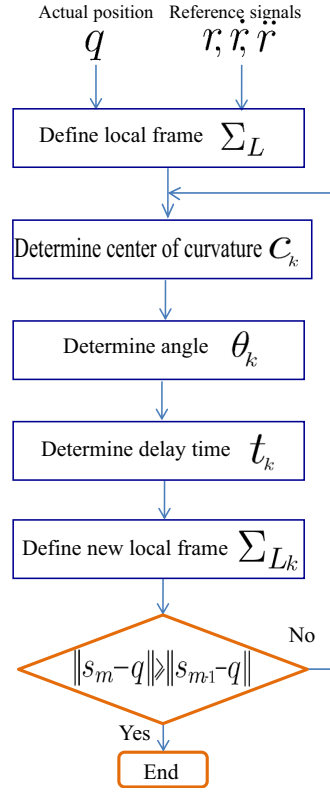
FIGURE 5.2: Flow chart of the iterative approach for contour error estimation

(5) The three unit vector for the coordinate system Σ_{L_1} corresponding to the instantaneous reference position, s_1, are calculated as follows:

$$t_1 = t(t_1). \tag{5.9}$$

$$n_1 = n(t_1). \tag{5.10}$$

$$b_1 = b(t_1). \tag{5.11}$$

(6) Execute the above approximation procedure by circular curves to obtain $e_k, k = 1, 2, ..., m$. If the error magnitude $||e_m|| = ||s_m - q||$ increases during the iterative process, we quit this procedure. We can also define the maximum number of repeat times for quiting this procedure. The flow chart of this iterative approximation procedure is shown in Fig. 5.2. Executing the iteration two times seems to yield sufficient results and saves computational effort.

Since the tangential vector t_m is not in the direction of reference point r, the following approach is intended to adjust the tangential vector. Let us consider a

vector $\hat{t}$ in the direction from s_m to the desired position r

$$\hat{t} = \frac{r - s_m}{||r - s_m||}. \tag{5.12}$$

In addition, $\hat{n}$ is in the plane t_m - n_m and perpendicular to $\hat{t}$, and hence, perpendicular to b_m. This vector $\hat{n}$ is therefore equal to the cross product of the vectors $\hat{t}$ and b_m:

$$\hat{n} = \hat{t} \times b_m. \tag{5.13}$$

Consequently, the third vector of the local coordinate frame $\Sigma_{\hat{L}}$ is

$$\hat{b} = \hat{t} \times \hat{n}. \tag{5.14}$$

The corresponding error vector with respect to the transformed frame $\Sigma_{\hat{L}}$, $e_{\hat{L}}(t)$ = $[\hat{e}_t, \hat{e}_n, \hat{e}_b]^T$, is calculated as

$$e_{\hat{L}} = \hat{L}^T e_w,$$
$$\hat{L} = \begin{bmatrix} \hat{t} & \hat{n} & \hat{b} \end{bmatrix}. \tag{5.15}$$

The above error components will be used to design a sliding mode contouring controller with nonlinear sliding surface in order to improve the contouring performance in three-dimensional machining.

5.3   Modeling of the System and Controller Design

5.3.1   Modeling of three-axis machine

This study considers a three-axis machine with three servo motors which commonly used in industrial applications to drive the feed drive systems. The feed drive
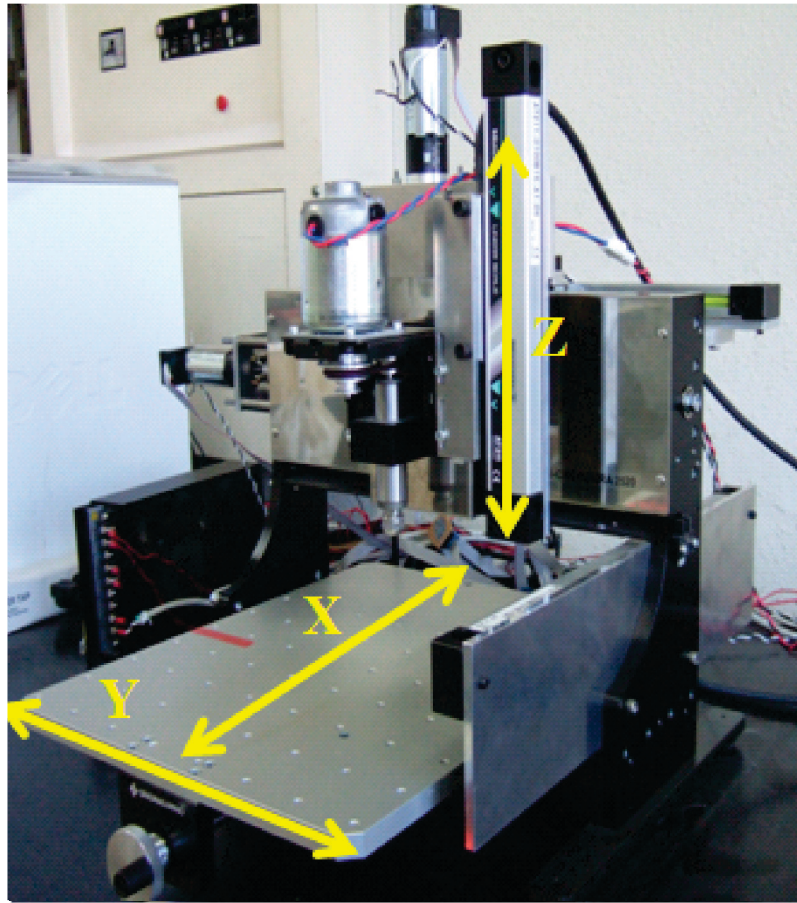
FIGURE 5.3: Experimental three-axis CNC machine

system is generally represented as follows:

$$\dot{z}_1 = A_{11}z_1 + A_{12}z_2,$$

$$\dot{z}_2 = A_{21}z_1 + A_{22}z_2 + Bu + \rho,$$

$$z_1 = \begin{bmatrix} q_x & q_y & q_z \end{bmatrix}^T, z_2 = \begin{bmatrix} \dot{q}_x & \dot{q}_y & \dot{q}_z \end{bmatrix}^T,$$

$$u = \begin{bmatrix} u_x & u_y & u_z \end{bmatrix}^T, \rho = \begin{bmatrix} \rho_x & \rho_y & \rho_z \end{bmatrix}^T. \tag{5.16}$$

where $(\dot{\ })$ denotes time derivative, $A_{11} = 0$, $A_{12} = I$, $A_{21} = 0$, $A_{22} = \text{diag}(-c_i/m_i)$, and $B = \text{diag}(k_i/m_i)$ are all 3×3 matrices; c_i, m_i, and k_i are the viscous friction coefficient, mass, and force-voltage conversion ratio of the feed drive axis i ($i = x, y, z$), respectively; and p, u, and ρ are the feed drive position, control input, and disturbance, respectively.

5.3.2   Contouring controller design with nonlinear sliding surface

In this section, the design of the contouring controller with nonlinear sliding surface for three-dimensional machining will be considered. Using a nonlinear sliding surface, the damping ratio of the closed loop system can be changed from its initial low value to a final high value. The initial low value of the damping ratio results in a quick response and the later high damping avoids overshoot to save energy consumption. Based on the regular form in (5.16), we propose the following nonlinear sliding surface:

$$
S = \begin{bmatrix} F - \Psi A_{12}^T P & I \end{bmatrix} \begin{bmatrix} e_{f1} \\ e_{f2} \end{bmatrix}, S \in R^3,
$$
$$
e_{f1} = \hat{L}^T e_w,
$$
$$
e_{f2} = \dot{\hat{L}}^T e_w + \hat{L}^T \dot{e}_w. \tag{5.17}
$$

Here, $P \in R^{3\times3}$ is a positive-definite matrix that can be found by solving the Lyapunov equation given by

$$
(A_{11} - A_{12}F)^T P + (A_{11} - A_{12}F)P = -W, W \in R^{3\times3} \tag{5.18}
$$

where W is a positive-definite matrix. I is a 3×3 identity matrix, F is chosen such that $(A_{11} - A_{12}F)$ has stable eigenvalues and the dominant poles have small damping ratios to achieve a fast response. Ψ is a 3×3 diagonal matrix with non-positive nonlinear entries depending on the output and is used to change the damping ratio of the system. One possible choice of Ψ is

$$
\Psi = \text{diag}(-\beta_i \exp(-e_i{}^2)), i = \hat{t}, \hat{n}, \hat{b}. \tag{5.19}
$$

In this section, the following sliding mode controller is proposed

$$u = -[\hat{L}^T B]^{-1}[-C^T H \dot{z}_d + C^T H A_{reg} z + C^T \dot{H}(z - z_d) - \frac{d\Psi}{dt} A_{12}^T P \hat{L}^T e_w$$

$$+ Q\text{sgn}(S) + K_c S], Q \in R^{3\times 3}, \text{sgn}(S) \in R^3, K_c \in R^{3\times 3},$$

$$z = \begin{bmatrix} z_1^T & z_2^T \end{bmatrix}^T,$$

$$C = \begin{bmatrix} F - \Psi A_{12}^T P & I \end{bmatrix}, C^T \in R^{3\times 6},$$

$$H = \begin{bmatrix} \hat{L}^T & 0 \\ \dot{\hat{L}}^T & \hat{L}^T \end{bmatrix}, H \in R^{6\times 6},$$

$$A_{reg} = \begin{bmatrix} A_{11} & A_{12} \\ A_{21} & A_{22} \end{bmatrix}, A_{reg} \in R^{6\times 6}. \tag{5.20}$$

Here, $\dot{z}_d = [\dot{r}^T \ \ddot{r}^T]^T$ consists of the desired velocity and acceleration of the feed drive axis and sgn(S) contains the signs of the sliding surface vector S. K_c is the gain matrix. $Q = \text{diag}(Q_i)$ is a diagonal matrix with diagonal elements chosen from the maximum bound of the uncertainty as follows:

$$Q_i \geq \max(\rho_i), i = x, y, z. \tag{5.21}$$

For asymptotic stability and to force the transformed tracking errors onto the desired sliding surface, the time derivative of the following Lyapunov function must be negative:

$$V = \frac{1}{2} S^T S. \tag{5.22}$$

The time derivative of the Lyapunov function is

$$\dot{V} = S^T[(F - \Psi A_{12}^T P)\dot{e}_{f1} - \frac{d\Psi}{dt} A_{12}^T P e_{f1} + \dot{e}_{f2}]. \tag{5.23}$$

Equations (5.16), (5.20), and (5.23) lead to

$$\dot{V} = S^T[-C^T H \dot{z}_d + C^T H A_{reg} z + C^T \dot{H}(z - z_d) - \frac{d\Psi}{dt} A_{12}^T P \hat{L}^T e_w + Bu + \rho_d] \tag{5.24}$$

By using control law (5.20), it can be seen that

$$\dot{V} = S^T[-K_c S - Q\text{sgn}(S) + \rho_d] \tag{5.25}$$

TABLE 5.1: Three-axis machine parameter values

Parameter	m		c	
$X - \text{axis}$	16.0	Vs^2/m	180	Vs/m
$Y - \text{axis}$	4.6	Vs^2/m	48	Vs/m
$Z - \text{axis}$	5.7	Vs^2/m	100	Vs/m
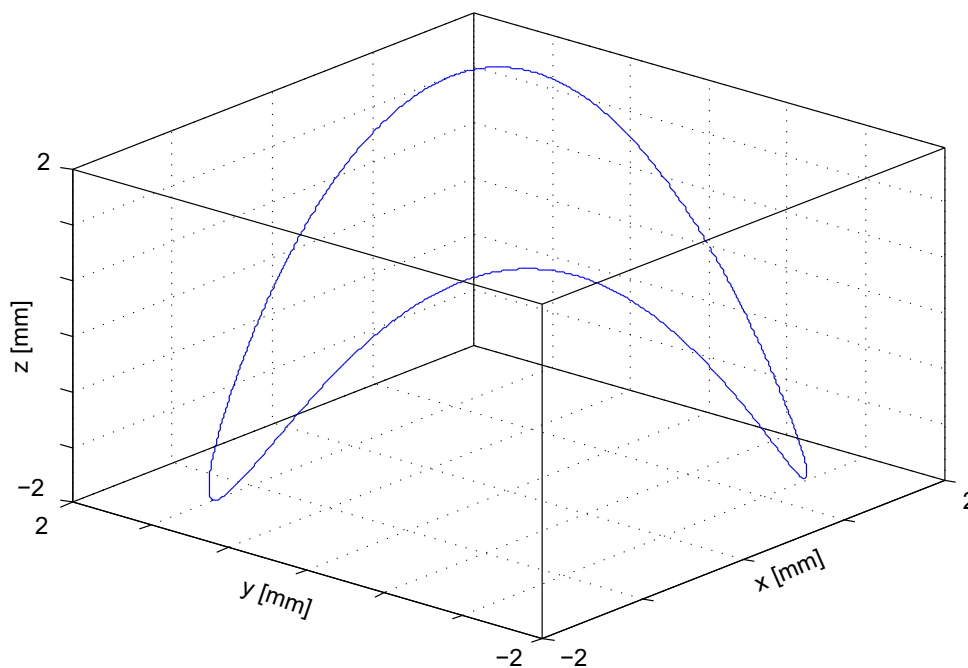
FIGURE 5.4: Three-dimensional reference trajectory used for simulation and experiments

Thus, with (5.21), it is easy to show that

$$\dot{V} < 0 \qquad (5.26)$$

5.4   Simulation and Experimental Results

We used a desk-top three-dimensional CNC machine to demonstrate the effectiveness of the proposed approach. This machine consists of three axes driven by DC servo motors that are coupled to and drive, three ball screws. In addition, a linear
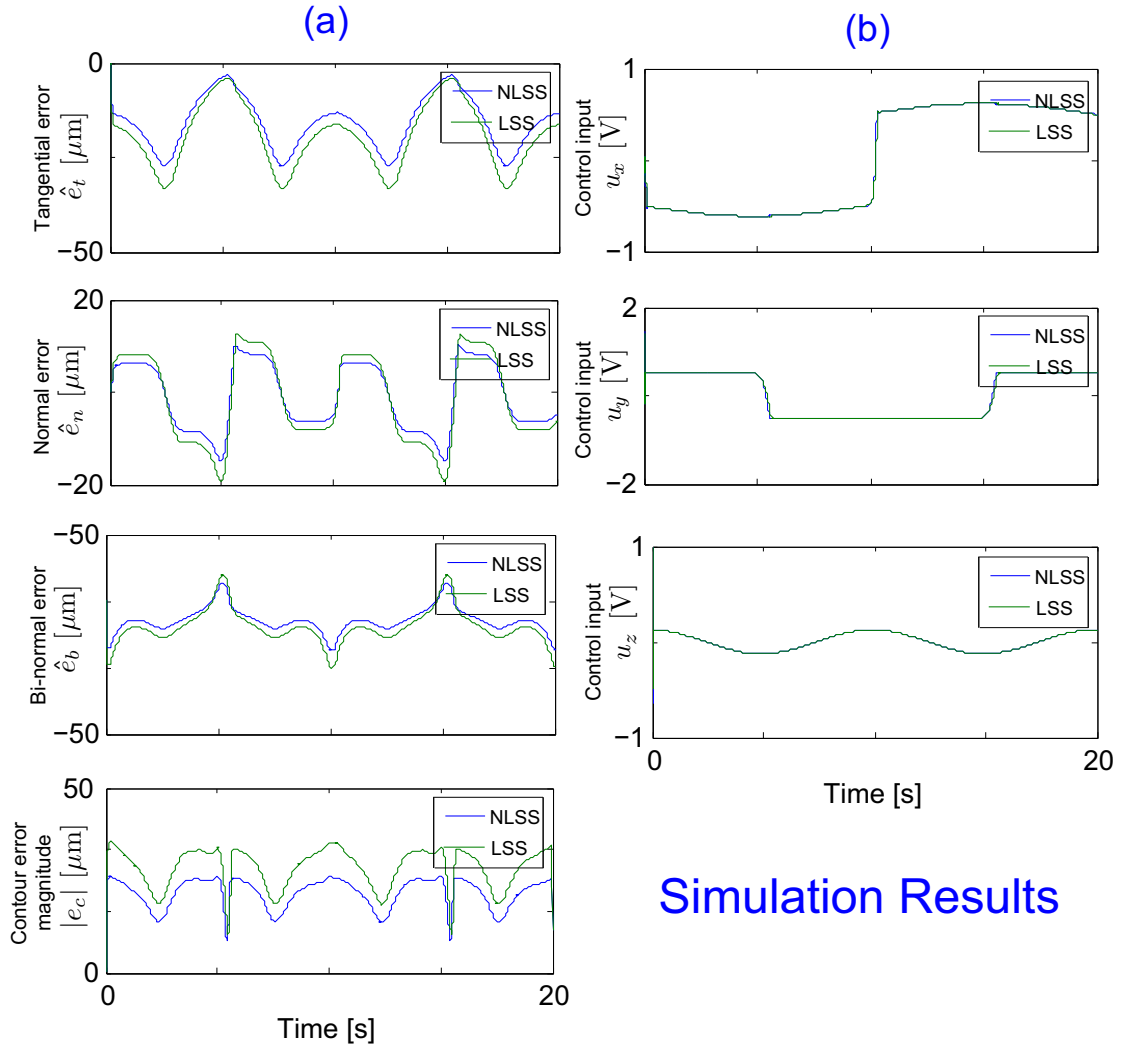
FIGURE 5.5: Simulation results of Exp. No. 1; comparison of linear and nonlinear sliding surfaces, (a) Transformed errors (tangential, normal and binormal) and actual contour error and (b) Control inputs in x,y and z directions

encoder whose resolution is 0.1 μm is attached to each feed drive axis to measure the actual position of the feed drive system. The nominal parameter values of the machine are given in Table 5.1. The following three-dimensional reference trajectory is used in the experiment:

$$x = 2\cos\left(\frac{\pi}{10}t\right) \qquad \text{mm,}$$
$$y = 2\sin\left(\frac{\pi}{10}t\right) \qquad \text{mm,}$$
$$z = 2\sin\left(\frac{2\pi}{10}t\right) \qquad \text{mm.} \qquad (5.27)$$
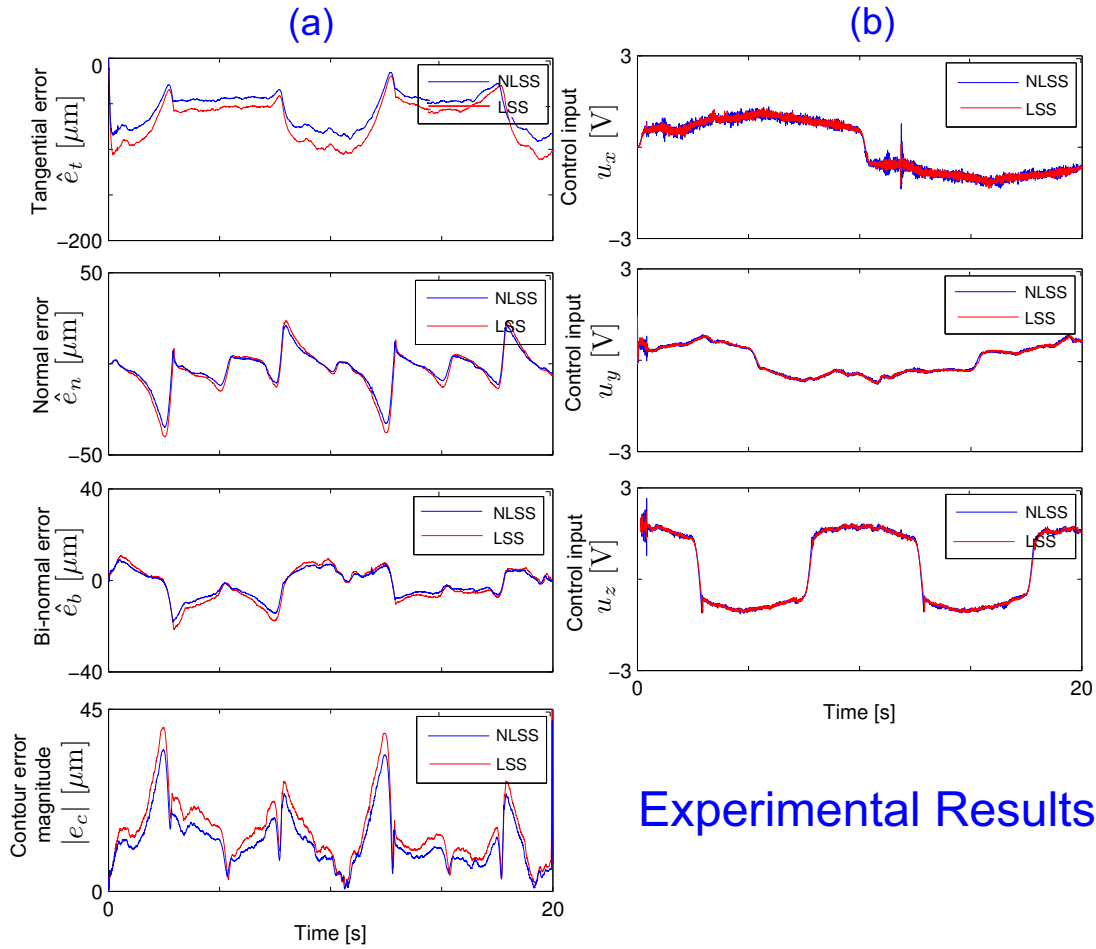
FIGURE 5.6: Experimental results of Exp. No. 1; comparison of linear and nonlinear sliding surfaces, (a) Transformed errors (tangential, normal and bi-normal) and actual contour error and (b) Control inputs in x,y and z directions

The control law given in Eq. (5.20) was implemented using the C++ language on a personal computer (OS: Windows XP, CPU: 2 GHz) with sampling time of 5 ms. In order to provide a fixed sampling period in Widows XP environment, we employ a timer on a counter board (CONTEC CNT24-4(PCI)H) with four channels of 24-bit up/down counters. To demonstrate the effectiveness of the proposed approach, the following two experiments were conducted:

(1) *Exp. No. 1: The effectiveness of the nonlinear sliding surface*

In this experiment, we compared the contouring controller with nonlinear sliding surface (i.e., Eq. (5.20)) and contouring controller with linear sliding surface (i.e., $\Psi=0$ in Eq. (5.19)). To provide a fair comparison between both controllers, controller gains K_c as well as the linear term of the sliding
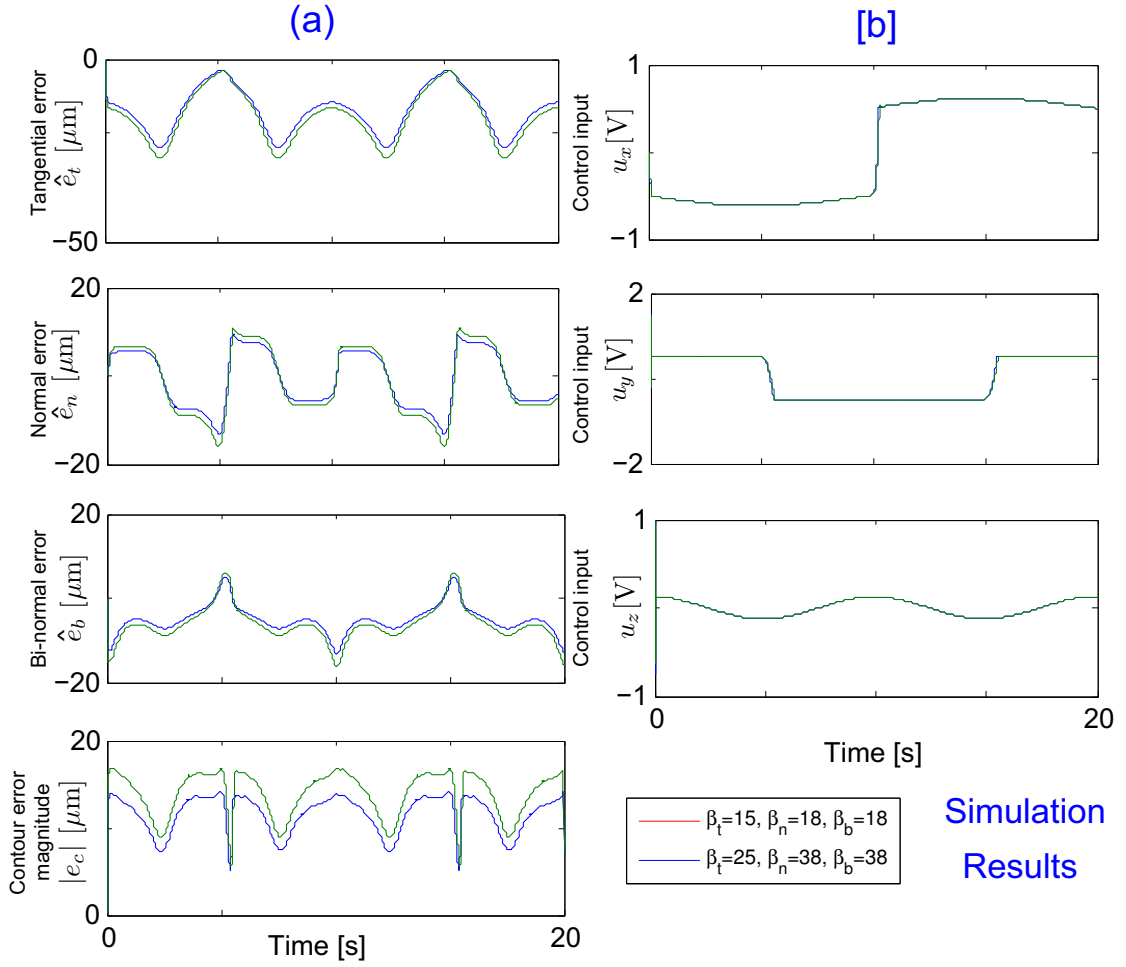
FIGURE 5.7: Simulation results of Exp. No. 2; contouring performance with different β_i, (a) Transformed errors (tangential, normal and bi-normal) and actual contour error and (b) Control inputs in x,y and z directions

surface F are set to the same values in both controllers. In addition, because the normal and bi-normal error components are more important than the tangential one, we have selected the gains in such a way that the normal and bi-normal components declined faster than the tangential one. The controller gain K_c and matrix F are selected to be diag(30 40 40) and diag(100 140 120), respectively. In these experiments, we set the maximum number of repeat times, m, to 2 for quitting the iterative procedure. The main concern of the proposed approach is achieving low overshoot and settling time, resulting in a smaller error, by changing of the systems damping ratio from its initial low value to its final high value. Hence, elimination of the control input chattering was not considered in the experiments

Simulations and experiments are conducted with the same parameters to
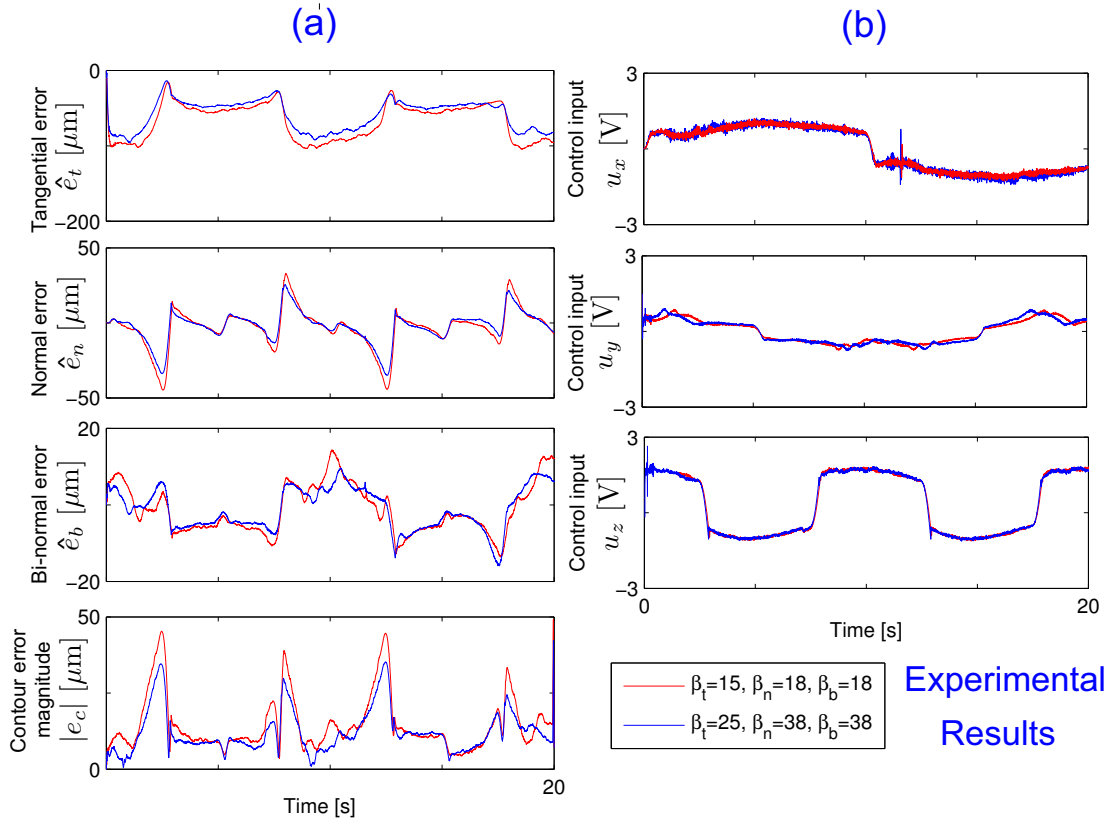
FIGURE 5.8: Experimental results of Exp. No. 2; contouring performance with different β_i, (a) Transformed errors (tangential, normal and bi-normal) and actual contour error and (b) Control inputs in x,y and z directions

verify the effectiveness of the nonlinear term of the proposed controller. Figures 5.5 and 5.6 show the simulation and experimental results, respectively, where, the control inputs u_x, u_y, and u_z; the tangential, normal, and bi-normal error components denoted as $\hat{e}_t$, $\hat{e}_n$, and $\hat{e}_b$, respectively; and the actual magnitude of the contour error $|e_c|$ for both controllers are plotted. Simulation and experimental results show that the proposed approach gives a better performance in terms of contour error without any increase of the required electrical energy as shown in Figs. 5.5 and 5.6.

The actual contour error is calculated through an iterative search for the shortest distance between the tool position and the actual path by solving the following off-line optimization problem:

$$|e_c(t)| = \min_t \ \sqrt{(r_i(t) - q_i)^2}, i = x, y, z \qquad (5.28)$$

Note that this error is used for verification and not to design the controller.

(2) *Exp. No. 2: The effectiveness of parameter β_i*

β_i is a tuning parameter for the proposed contouring controller that allows the importance of the nonlinear term to be adjusted by changing the system's closed loop damping ratio. Simulation and experimental results for the same reference trajectory used in Exp. No. 1, where the controller gain K_c and matrix F are selected to be diag(20 30 30) and diag(80 90 90), respectively, are shown in Figs. 5.7 and 5.8, respectively.

Two cases of β_i were selected and their performance can be compared as follows:

  (a) $\beta_1 = [\beta_t \ \beta_n \ \beta_b] = [15 \ 18 \ 18]$.
  (b) $\beta_2 = [\beta_t \ \beta_n \ \beta_b] = [25 \ 38 \ 38]$.

It is apparent that the weighting factor β_i is essential in the proposed nonlinear sliding surface and the contouring performance significantly improves by adjusting β_i.

To verify the repeatability of the proposed approach, the same experiment as in Figs. 3 and 4 were repeated 10 times and the mean values of $|e_c|$ were compared. Figure 5.9(a) shows a comparison between the proposed nonlinear sliding surface and the linear sliding surface. It is can be seen that the proposed approach reduced the mean value of the contour error by about 30%. In addition, adjusting the tuning parameter β_i gives a better contouring performance in terms of the mean value of the actual contour error as shown in Fig. 5.9(b).

5.5   Conclusions

A sliding mode contouring controller with nonlinear sliding surface for three-dimensional machining based on iterative contour error approximation and a co-ordinate transformation approach is presented in this chapter. The effectiveness of the proposed control approach is demonstrated through experiments and simulation involving a three-dimensional reference trajectory. Two cases of simulation and experiments are conducted; the first experiment is to show the effectiveness of the proposed nonlinear sliding surface a against the linear sliding surface, while the second one is to show the effect of the tuning parameter of the nonlinear term.
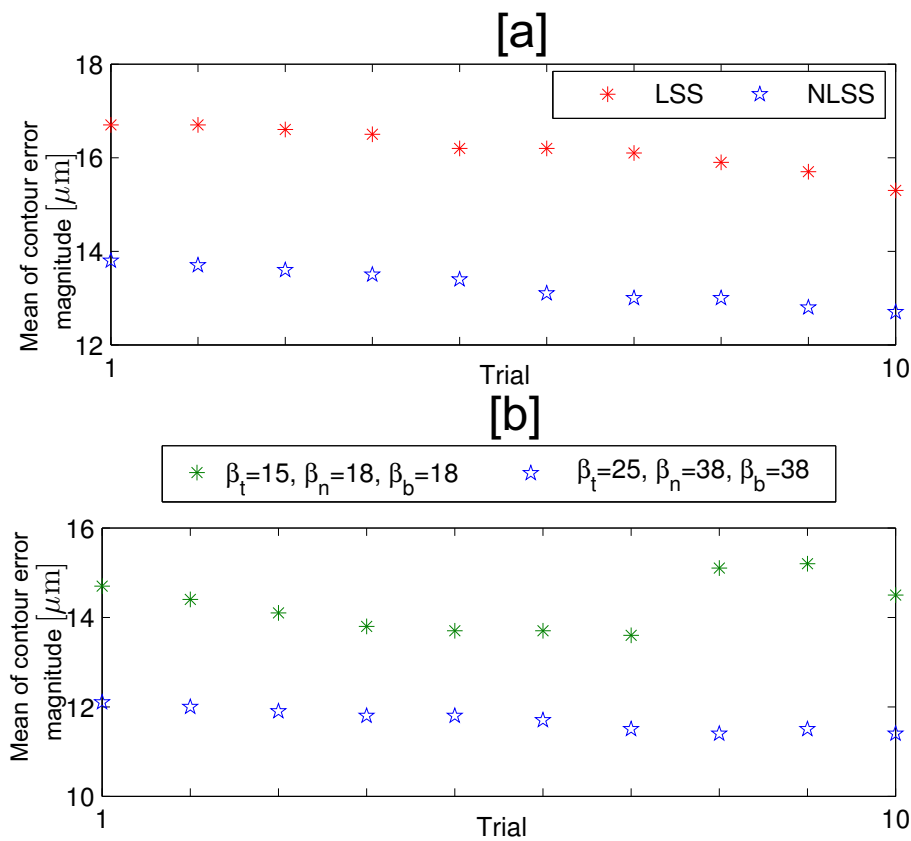
FIGURE 5.9: (a) Mean value of the actual contour error with linear and nonlinear sliding surfaces and (b) Mean value of the actual contour error with different β_i

The results indicated that the proposed sliding surface achieve a good performance compared to linear sliding surface. In addition, contouring performance can be significantly improved by adjusting the tuning parameter of the nonlinear term. Extension of the proposed method to a five-axis machine for considering tool tip and orientation contour errors are left for future work.

Chapter 6

Estimation of Tool Orientation Contour Errors for Five-Axis Machining

6.1 Introduction

Five-axis computer numerically controlled (CNC) machines are widely used for high-precision machining of complex sculptured surfaces in aerospace, automotive and die/mould industries. Free-form surface machining with machines that offer more than three degrees of freedom requires synchronization of the tool position and orientation to avoid overcut and undercut during machining.

Five-axis machines generally employ a control scheme that attempts to minimize tracking errors along all five driving axes independently. Using the conventional servo controller results in unavoidable tracking errors between the commanded and actual positions in each feed drive axis. To reduce these tracking errors, various advanced control techniques such as sliding mode controllers [12], zero phase error tracking control [85] and a feed-forward friction compensator [108] have been developed. Although many effective controllers have been applied to individual axis control loops, eliminating the tracking errors of each individual axis does not guarantee the desired contouring accuracy.

As mentioned in the previous chapters, from the viewpoint of machining, eliminating the contour error, which is defined as the deviation in the normal direction of

the tool from the desired tool path, is more important than eliminating the tracking error in each driving axis. One of the approaches that used to eliminate the contour error is employing a cross coupled controller. In this method, both contour error and tracking error along each driving axis are considered in the design of the controller. As a result, it is difficult to determine which controller dominates the contour error; hence, some difficulties in adjusting controller parameters appear.

To address this problem, Chiu and Tomizuka formulated the contour tracking problem in a task coordinate frame attached to the desired contour [18]. By transforming the machine tool feed drive dynamics to this task coordinate frame, a control law can be formulated to assign different dynamics to the normal and tangential directions relative to the desired contour. Lo and Chung proposed a tangential contour controller for biaxial motion based on the coordinate transformation between a fixed frame and a tangential contour frame that is defined along the contour [21]. Lo proposed three-axis contouring control which operates in a trajectory coordinate basis that is moving along the tool path trajectory [105]. Uchiyama *et al.* proposed a contouring controller for three-dimensional machining based on coordinate transformation [93]. In addition, they proposed a method to reduce the inherent contour error resulting from the coordinate transformation approach. However, in the above contouring algorithms, five-axis contouring control is not considered.

In five-axis machining, the challenges are more difficult than two/three-axis cases because of non-Cartesian kinematics, geometrical structure and high flexibility of the five-axis machines. Lo proposed real-time transformation between the machine coordinate and workpiece coordinate frames and employed a coupled proportional integral derivative (PID) controllers [109]. He reduced the deviation and orientation errors by minimizing the tracking error of each individual axis in the workpiece coordinates frame instead of minimizing it in the machine coordinates frame. Bohez defined the closed loop volumetric error as the difference between the cutter contact point on the tool side and the corresponding point on the reference surface and used this definition to compensate the systematic errors in five-axis machines [110].

Recently, Sencer *et al.* proposed an estimation model for tool tip and tool orientation contour errors for five-axis machines [111]. They transformed the tool tip tracking error using a moving Frenet frame into tangential, normal and bi-normal

error components. In addition, they applied a sliding mode controller to each individual driving axis to verify the proposed estimation models. Sencer and Altintas utilized the model presented in [111] and proposed a sliding mode tool tip contour controller and tool orientation contour controller [104]. They showed that the proposed approach reduced the tool tip and orientation contour errors compared to independent controller. However, there are two shortages in the above two literatures; first, the two controllers run simultaneously and individually consider only kinematic transformations; second, because it is assumed that the gain assigned to the error component in the tangential direction is relatively small compared to the normal and bi-normal error components, a relatively larger tangential error component is obtained. As a result, reduction in the tool orientation error based on the definition given in [111] does not guarantee contouring control performance between the tool tip position and orientation. In other words, even if the tool tip and tool orientation contour errors are very small, any mismatch between the tool position and tool orientation will cause an overcut or undercut when these errors are treated independently.

To address the above problem in [111], this chapter presents a new definition of the actual tool orientation contour error. In addition, we propose an estimation model for the tool orientation contour error. The elimination of the proposed error guarantees synchronization between the tool tip and tool orientation to avoid any overcut or undercut in a machined surface.

6.2 Kinematics and Contour Error Modeling in Five-Axis Machines

6.2.1 Kinematics of five-axis machine

The five-axis machine is similar to two cooperating robots, one robot carrying the cutting tool and one robot carrying the workpiece [112]. In this chapter we consider the widely used five-axis machines with three translational motions, X, Y, and Z (represents the robot carrying the cutting tool), combined with two rotations A and C around X and Z axes, respectively (represents the robot carrying the workpiece). Generally, the tool position and orientation are represented in the tool frame coordinate system Σ_W as shown in Fig. 6.1. Here, the desired tool tip
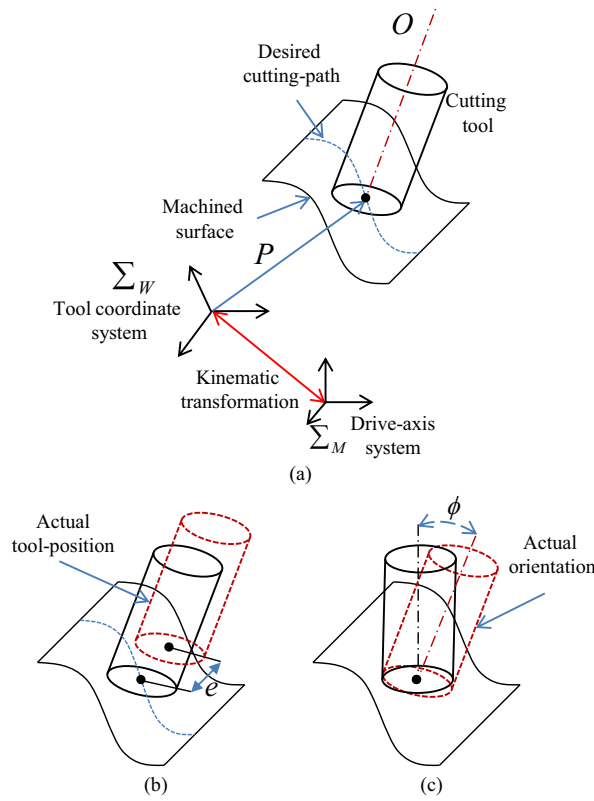
FIGURE 6.1: (a) Cutting tool configuration in Σ_W and Σ_M frames, (b) tool-tip contour error, and (c) tool-orientation contour error

position and tool orientation, defined in the tool coordinate frame Σ_W, are $P = [P_x\ P_y\ P_z]^T$ and $O = [O_i\ O_j\ Ok]^T$, respectively. The orientation results from the rotation of the rotary drives A and C are with angles of θ_a and θ_c, respectively. The desired tool position and orientation vector P, in the tool coordinate frame Σ_W, is transformed to a position and rotation commands to the physical actuators. The position and rotation command vector, represented in the machine coordinate frame Σ_Q which is regarded as fixed to the global coordinate system, is given by $q = [q_x\ q_y\ q_z\ q_a\ q_c]^T$. A kinematics transformation from the machine coordinate frame Σ_M to the tool coordinate frame Σ_W is carried out by the transformation matrix T as follows:

$$
\begin{bmatrix} P_x \\ P_y \\ P_z \end{bmatrix} = \begin{bmatrix} -C_c & -S_cC_a & S_aS_c \\ S_c & -C_cC_a & S_aC_c \\ 0 & S_a & C_a \end{bmatrix} \begin{bmatrix} q_x \\ q_y \\ q_z \end{bmatrix} + \begin{bmatrix} 0 & -S_cS_a \\ 0 & -C_cS_a \\ -1 & -C_a \end{bmatrix} \begin{bmatrix} d_4 \\ a_2 \end{bmatrix}.
$$

$$(6.1)$$

where S_i and C_i represent $\sin(q_i)$ and $\cos(q_i)$, respectively, $i \in (a, c)$. d_4 and a_2 are the offset between the rotary drive axes. The tool orientation in the spherical coordinate frame is obtained from the angular motion of the rotary axes as follows:

$$
\begin{bmatrix} O_i \\ O_j \\ O_k \end{bmatrix} = \begin{bmatrix} \cos q_a \sin q_c \\ \cos q_a \cos q_c \\ -\sin q_a \end{bmatrix}. \tag{6.2}
$$

We define a vector $w = [w_x \; w_y \; w_z \; w_a \; w_c]^T$, with $w_a = \theta_a$ and $w_c = \theta_c$, represents the actual position and rotation of the feed drive axes in the tool coordinate frame Σ_W and it will be used in the controller design later. In order to obtain the velocity transformation, a partial derivative of Eq. (6.1) is carried out with respect to the axis position as follows:

$$
J_{ij} = \frac{\partial P_i}{\partial q_j}, i \in (x, y, z), j \in (x, y, z, a, c). \tag{6.3}
$$

and by adding two unity elements on the diagonal for the rotational drive positions, the following square Jacobian matrix is formed [111]:

$$
J = \begin{bmatrix}
J_{xx} & J_{xy} & J_{xz} & J_{xa} & J_{xc} \\
J_{yx} & J_{yy} & J_{yz} & J_{ya} & J_{yc} \\
J_{zx} & J_{zy} & J_{zz} & J_{za} & J_{zc} \\
0 & 0 & 0 & 1 & 0 \\
0 & 0 & 0 & 0 & 1
\end{bmatrix}. \tag{6.4}
$$

The velocity and acceleration vectors of the cutting tool with respect coordinate frame Σ_W

$$
\dot{w} = J\dot{q}. \tag{6.5}
$$
$$
\ddot{w} = J\ddot{q} + \dot{J}\dot{q}. \tag{6.6}
$$

6.2.2 Estimation of tool tip contour error

During five-axis machining, the cutting tool deviates from the desired trajectory due to undesired disturbances such as cutting force, friction and measurement

FIGURE 6.2: Definitions of five-axis contour errors (a) tool tip contour error,
and (b) tool orientation contour error

errors. This deviation results in a tool tip contour error (Fig. 6.1(b)) and tool
orientation contour error (Fig 6.1(c)). The tool tip contour error is defined as
the deviation in the normal direction of the tool from the desired tool path. In
the following, we briefly explain estimation model for the tool tip contour error
presented in [111]. In Fig. 6.2, c is the desired trajectory of the cutting tool and
P is the tool tip desired position, with respect the tool coordinate frame Σ_W. The
tracking errors with respect to each feed drive axis $e_w = w_{ref} - w = [e_x\ e_y\ e_z\ e_a\ e_c]^T$.
At the desired position P, the tangent t, normal n, and bi-normal b vectors for
the parametric trajectory c are calculated at time t as follows:

$$\mathrm{t} = [\mathrm{t}_x, \mathrm{t}_y, \mathrm{t}_z]^T = \frac{\dot{P}}{\parallel \dot{P} \parallel}. \tag{6.7}$$

$$\mathrm{n} = [\mathrm{n}_x, \mathrm{n}_y, \mathrm{n}_z]^T = \frac{\ddot{\mathrm{t}}}{\parallel \ddot{\mathrm{t}} \parallel}. \tag{6.8}$$

$$\mathrm{b} = [\mathrm{b}_x, \mathrm{b}_y, \mathrm{b}_z]^T = \mathrm{t} \times \mathrm{n}. \tag{6.9}$$

The tracking error e_w is transformed to the moving Frenet frame Σ_F, whose axes are t, n, and b, by the transformation matrix F as follows:

$$e_F = F^T e_w,$$

$$F = \begin{bmatrix} t_x & n_x & b_x & 0 & 0 \\ t_y & n_y & b_y & 0 & 0 \\ t_z & n_z & b_z & 0 & 0 \\ 0 & 0 & 0 & 1 & 0 \\ 0 & 0 & 0 & 0 & 1 \end{bmatrix}. \tag{6.10}$$

We assume that the distance between the desired position P and nearest point on the desired trajectory (the dashed segment of the desired trajectory shown in Fig. 6.2) is approximately equal to the length of the tangential error e_t. In addition, the desired velocity along this segment is nearly constant and equal to the desired velocity at P. The required time to traverse this segment t_d is calculated as follows:

$$t_d = \frac{e_t}{\parallel \dot{P} \parallel}. \tag{6.11}$$

A new coordinate frame $\Sigma_{\tilde{F}}$ corresponding to the delayed time $\tilde{t} = t - t_d$ is defined by three unit vectors as follows:

$$\tilde{t} = t(\tilde{t}). \tag{6.12}$$

$$\tilde{n} = n(\tilde{t}). \tag{6.13}$$

$$\tilde{b} = b(\tilde{t}). \tag{6.14}$$

The corresponding error vector $e_{\tilde{F}} = [\tilde{e}_t, \tilde{e}_n, \tilde{e}_b, \tilde{e}_a, \tilde{e}_c]^T$ is calculated with respect to the transformed frame $\Sigma_{\tilde{F}}$ having three axes $\tilde{t}$, $\tilde{n}$ and $\tilde{b}$ as follows:

$$e_{\tilde{F}} = \tilde{F}^T e_w,$$

$$\tilde{F} = F(\tilde{t}). \tag{6.15}$$

As shown in Fig. 6.2, the vector between the current and the delayed reference positions is expressed as

$$h = \begin{bmatrix} P - P(\tilde{t}) \\ 0 \\ 0 \end{bmatrix} \tag{6.16}$$
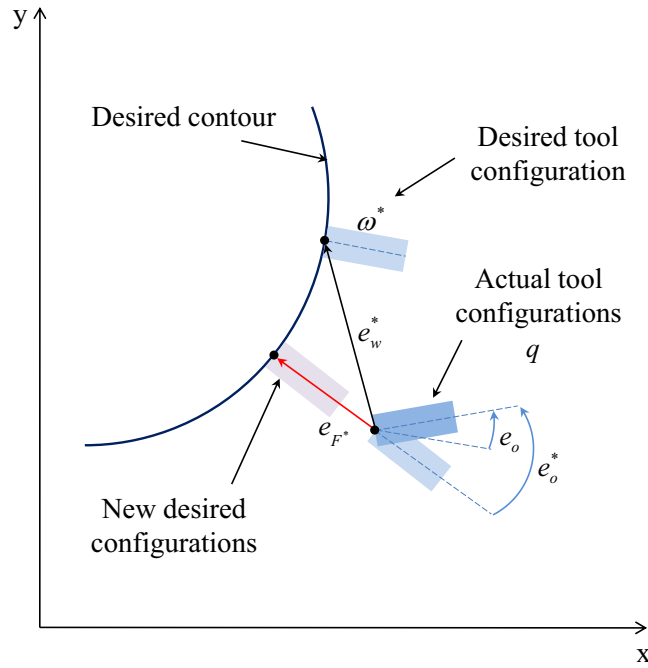
FIGURE 6.3: Tool orientation contour error in 2-dimensional case

where $P(\tilde{t})$ is the desired position at the time $\tilde{t}$ and it can be represented in the moving frame $\tilde{F}$ as follows:

$$h_F = \tilde{F}^T h. \tag{6.17}$$

The normal and bi-normal components are adjusted according to the new coordinate frame $\Sigma_{\tilde{F}}$ as shown in Fig. 6.2. Because only the normal and bi-normal components are considered as contour errors, the tangential component is excluded by multiplying with $W = \mathrm{diag}(0, 1, 1, 0, 0)$ [111]:

$$\tilde{h}_F = W h_F \tag{6.18}$$

The tracking errors on the moving frame $\Sigma_{\tilde{F}}$ become

$$\tilde{e}_F = \tilde{F}^T e_w + \tilde{h}_F, \tag{6.19}$$

6.2.3 Tool orientation contour error

As shown in Fig. 6.2(b), similar to Cartesian contour error approximation, the orientation contour error vector is predicted by transforming the tracking error to obtain the vector normal to the reference trajectory as follows [111]:

$$\varepsilon_o = \begin{bmatrix} \varepsilon_{oi} \\ \varepsilon_{oj} \\ \varepsilon_{ok} \end{bmatrix} = e_o - \frac{\omega}{|\omega|} \frac{e_o \cdot \omega}{|\omega|}. \tag{6.20}$$

where $\omega = [\omega_i, \omega_j, \omega_k]^T$ is the desired angular velocity, $e_o = O(t)\text{-}O_{act}(t)$ is the tool orientation tracking errors represented in the spherical coordinates, and $O_{act}(t)$ is the actual tool orientation. By using normalized angular velocity of the rotary axis, $\bar{\omega} = \omega/|\omega|$, we can rewrite Eq. (6.20) as:

$$\varepsilon_o = e_o - \bar{\omega}(e_o \cdot \bar{\omega}). \tag{6.21}$$

6.2.4 Proposed definition of tool orientation contour error

A disadvantage of the previous definition of the tool orientation contour error is that it does not give a true representation of machining precision because it does not take into account the tool tip contour error. In other words, tool tip contour error and tool orientation contour error control loops run independently.

To address this problem, we propose a new definition of the tool orientation contour error to consider the synchronization between the tool position and orientation. Figure 6.3 is a two-dimensional representation that shows the disadvantage of the definition of the tool orientation contour error presented in [111]. The desired tool configuration at the same instant time is ω^* and q is the actual tool configuration with some tracking error e_w^*. In this two dimensional case, e_{F^*} as defined in Eq. (6.19) is regarded as the position contour error. Although e_o is generally regarded as the tool orientation error, e_o^* is preferable as the tool orientation contour error, to avoid the undercut or overcut in machining. The tool orientation contour error in Eq. (6.20) can not be used to represent this error because $\omega/|\omega|$ in Eq. (6.20) is always equal to ± 1 and provides $\varepsilon_o = 0$ in this two dimensional case.
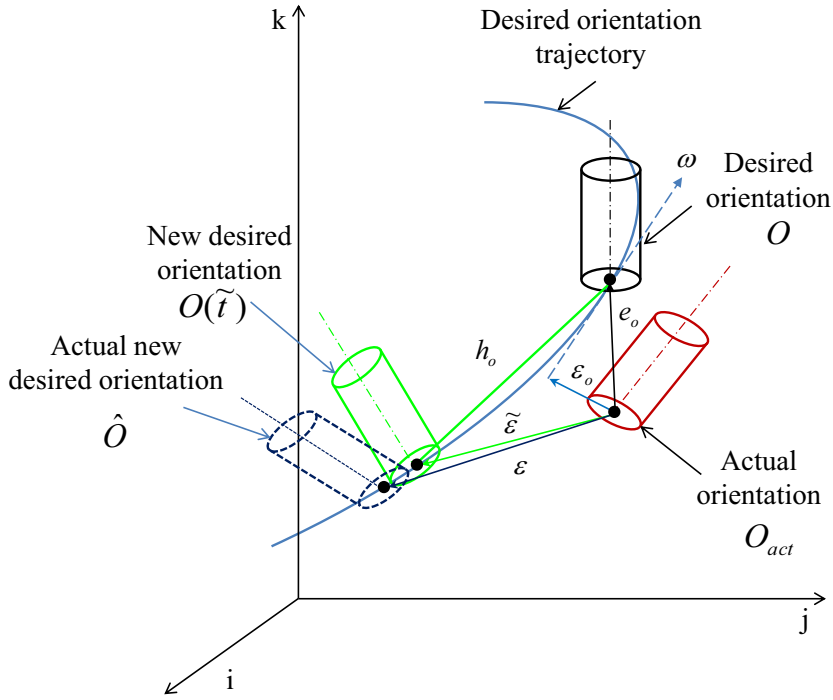
FIGURE 6.4: Proposed definition of five-axis tool orientation contour errors

6.2.5 Estimation of new tool orientation contour error

In previous approaches to the five-axis tool tip contour control, the tangential error component is larger than the normal and bi-normal components. On the other hand, the rotary drives in the five-axis machines attempt to eliminate the tool orientation tracking error e_o and deviation in the normal direction ε_o from the desired orientation trajectory, as shown in Fig. 6.2(b). A mismatch between the desired tool orientation O and the delayed desired orientation $\hat{O}$, which corresponds to a point on the reference trajectory c nearest to the actual tool tip position (Fig. 6.4), causes an overcut or undercut. In order to avoid this mismatch, the rotary drive axis must use a control scheme to reduce the actual tool orientation contour error ε, which is defined as the difference between the actual orientation O_{act} and the delayed desired orientation $\hat{O}$. Because it is an intensive task to calculate the actual tool orientation contour error $\varepsilon = [\varepsilon_i,\ \varepsilon_j,\ \varepsilon_k]^T$ in real time, an approximation of ε can be estimated by the error vector $\tilde{\varepsilon} = [\tilde{\varepsilon}_i,\ \tilde{\varepsilon}_j,\ \tilde{\varepsilon}_k]^T$, defined as follows:

$$\tilde{\varepsilon} = O(\tilde{t}) - O_{act}(t), \tilde{t} = t - t_d. \qquad (6.22)$$
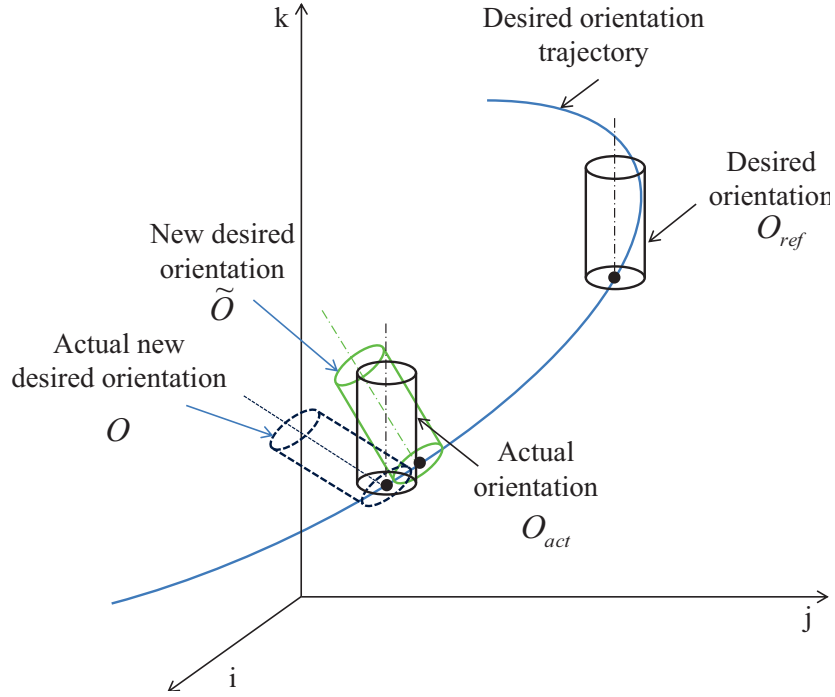
FIGURE 6.5: An example of machining for showing the advantage of the proposed approach

where $O(\tilde{t})$ is the new desired tool orientations. By differentiating Eq. (6.2) with respect to time and assuming that the orientation errors are compensated by a controller within the control sampling interval, the actual, proposed and conventional tool orientation contour errors can be estimated from the corresponding errors in the tool-coordinate frame Σ_W as follows [111]:

$$\varepsilon \approx J_o \bar{e}, \bar{e} = \begin{bmatrix} \bar{e}_a & \bar{e}_c \end{bmatrix}^T. \tag{6.23}$$

$$\tilde{\varepsilon} \approx J_o \tilde{e}, \tilde{e} = \begin{bmatrix} \tilde{e}_a & \tilde{e}_c \end{bmatrix}^T. \tag{6.24}$$

$$\varepsilon_o \approx J_o e_R, e_R = \begin{bmatrix} e_{Ra} & e_{Rc} \end{bmatrix}^T. \tag{6.25}$$

$$J_o = \begin{bmatrix} -\sin\theta_a \sin\theta_c & \cos\theta_a \cos\theta_c \\ -\sin\theta_a \cos\theta_c & -\cos\theta_a \sin\theta_c \\ -\cos\theta_a & 0 \end{bmatrix}. \tag{6.26}$$

In order to explain the advantage of the proposed estimation model over the conventional method, we consider the case in Fig. 6.5 under the following conditions:

(1) The tangential error exists.
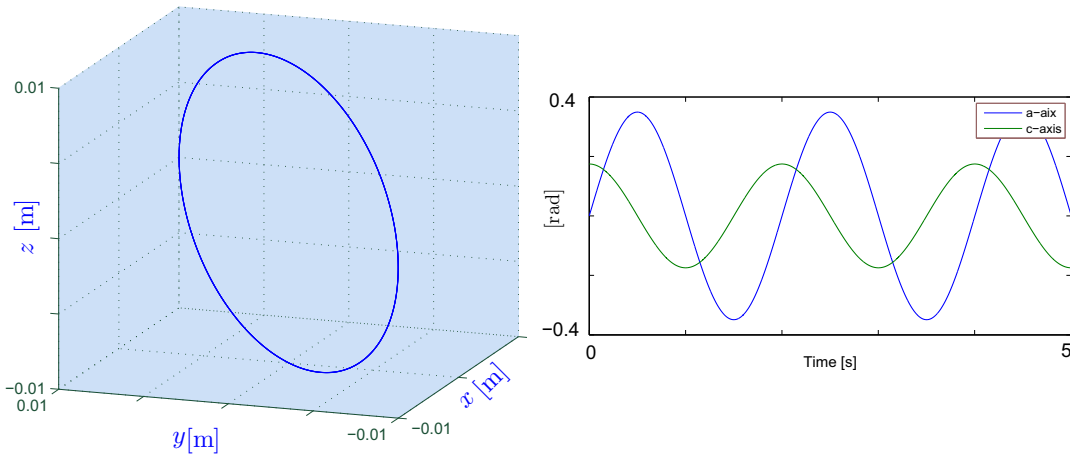
FIGURE 6.6: Reference trajectory used in the experiments

TABLE 6.1: Five-axis machine parameter values

Parameter	m		c	
$X -$ axis	5.33	Vs^2/m	25.175	Vs/m
$Y -$ axis	4.545	Vs^2/m	24.202	Vs/m
$Z -$ axis	1.72	Vs^2/m	71.647	Vs/m
$A -$ axis	0.0023	Vs^2/rad	0.022	Vs/rad
$C -$ axis	0.01489	Vs^2/rad	0.100	Vs/rad

(2) The tool orientation tracking error is equal to zero or has a very small magnitude.

(3) The tool tip contour error is equal to zero or has a very small magnitude.

Based on the conventional definition, the tool orientation contour error is equal to zero or has a very small magnitude (from Eq. (6.20)). However, as shown in Fig. 6.5, there is an orientation contour error between the actual orientation (O_{ref} is the same or very close to O_{act} in this case) and the orientation O that corresponds to the nearest position on the desired trajectory. In other words, the cutting tool should have the same orientation as that corresponding to the nearest position. Otherwise, overcut or undercut may occur during machining by five-axis machines. On the other hand, the proposed definition (Eqs. (6.22)) gives a better indication of the tool orientation contour error because the the new desired orientation $\tilde{O}$ and the actual new desired orientation O are approximately equal when the actual tool tip contour error is estimated accurately.
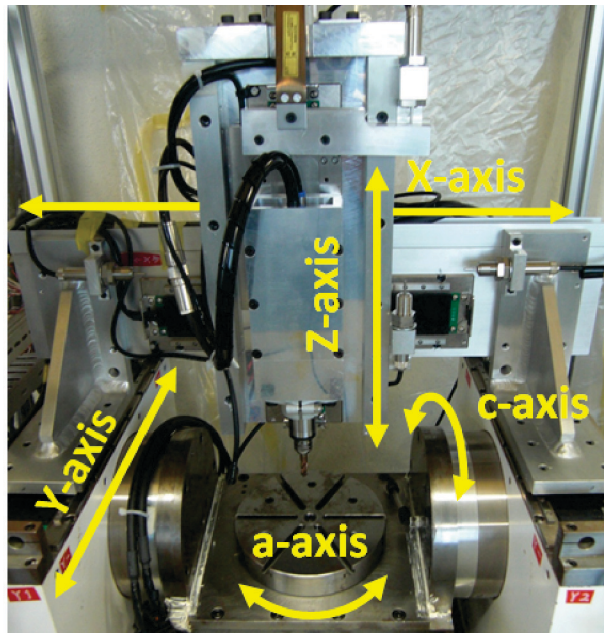
FIGURE 6.7: Five-axis machine

TABLE 6.2: Controller parameter values

Parameter	K_p		K_v	
Tangential	900	m/s^2	60	m/s
Normal	20164	m/s^2	280	m/s
Bi-normal	20164	m/s^2	280	m/s
$A-$axis	14400	rad/s^2	240	rad/s
$C-$axis	14400	rad/s^2	240	rad/s

6.3 Five-Axis Contouring Controller Design

Generally, five-axis machines are represented in the drive-axis coordinate frame Σ_M by the following differential equations:

$$
\begin{aligned}
& M\ddot{q}(t) + C\dot{q}(t) = v(t), \\
& M = \mathrm{diag}\{m_i\}, \ \ C = \mathrm{diag}\{c_i\}, \ \ i = (x, y, z, a, c), \\
& v(t) = [v_x, v_y, v_z, v_a, v_c]^T.
\end{aligned}
\tag{6.27}
$$

where $m_i(> 0)$, $c_i(\geq 0)$, and v_i are the equivalent inertia, equivalent viscous friction coefficient, and the control input in the drive axis i, respectively. The symbol diag$\{a_i\}$ denotes a diagonal matrix with elements a_i at the ith diagonal positions. The acceleration of the feed drive system in the drive-axis coordinate

frame Σ_M, $\ddot{q}(t)$, can be calculated by differentiating Eq. (6.3) as follows:

$$\ddot{q}(t) = J^{-1}[\ddot{w}(t) - \dot{J}(t)\dot{q}(t)]. \tag{6.28}$$

From the definition of the tracking error e_w and Eq. (6.27), the tracking error dynamics of the cutting tool in the fixed coordinate frame Σ_W are expressed as:

$$\ddot{e}_w = \ddot{P} - M^{-1}\left[v - C\dot{q}\right]. \tag{6.29}$$

where $\ddot{P}$ is the desired acceleration of the tool tip with respect to the tool coordinate frame Σ_W. The transformed error dynamics can be estimated by differentiating Eq. (6.19) twice with respect to time as follows:

$$\ddot{\tilde{e}}_F = \tilde{F}^T \ddot{e}_w + 2\dot{\tilde{F}}^T \dot{e}_w + \ddot{\tilde{F}}^T e_w + \ddot{\tilde{h}}_F. \tag{6.30}$$

Considering Eq. (6.30), assuming that the reference velocity and acceleration are given, substituting Eq.(6.28) into Eq. (6.27), and considering feed drive dynamics, we design the following controller:

$$\begin{aligned} v = MJ^{-1}[\ddot{P} + \tilde{F}^{-1}(K_v \dot{e}_{\tilde{F}} + K_p e_{\tilde{F}} \\ +2\dot{\tilde{F}}\dot{e}_w + \ddot{\tilde{F}}e_w + \ddot{\tilde{h}}_F) - \dot{J}\dot{q}] + C\dot{q}, \end{aligned} \tag{6.31}$$

where $v = [v_x, v_y, v_z, v_a, v_c]^T$ is the control input vector in the drive-axis coordinate frame Σ_M, $K_v = \text{diag}(k_{vt}, k_{vn}, k_{vb}, k_{va}, k_{vc})$ and $K_p = \text{diag}(k_{pt}, k_{pn}, k_{pb}, k_{pa}, k_{pc})$ are the velocity and position feed back gain matrices, respectively. Note that in the above controller, minimization of the tool orientation contour error is not considered to conduct a fare comparison as shown in the Experimental section. Then, we have the following closed-loop dynamics:

$$\ddot{e}_{\tilde{F}} + K_v \dot{e}_{\tilde{F}} + K_p e_{\tilde{F}} = 0. \tag{6.32}$$

Because the elimination of the normal and bi-normal error components is more important than that of the tangential error component, the design of the controller is expected to set the velocity and position gains in such a way that the normal and bi-normal components can be reduced faster than the tangential component.
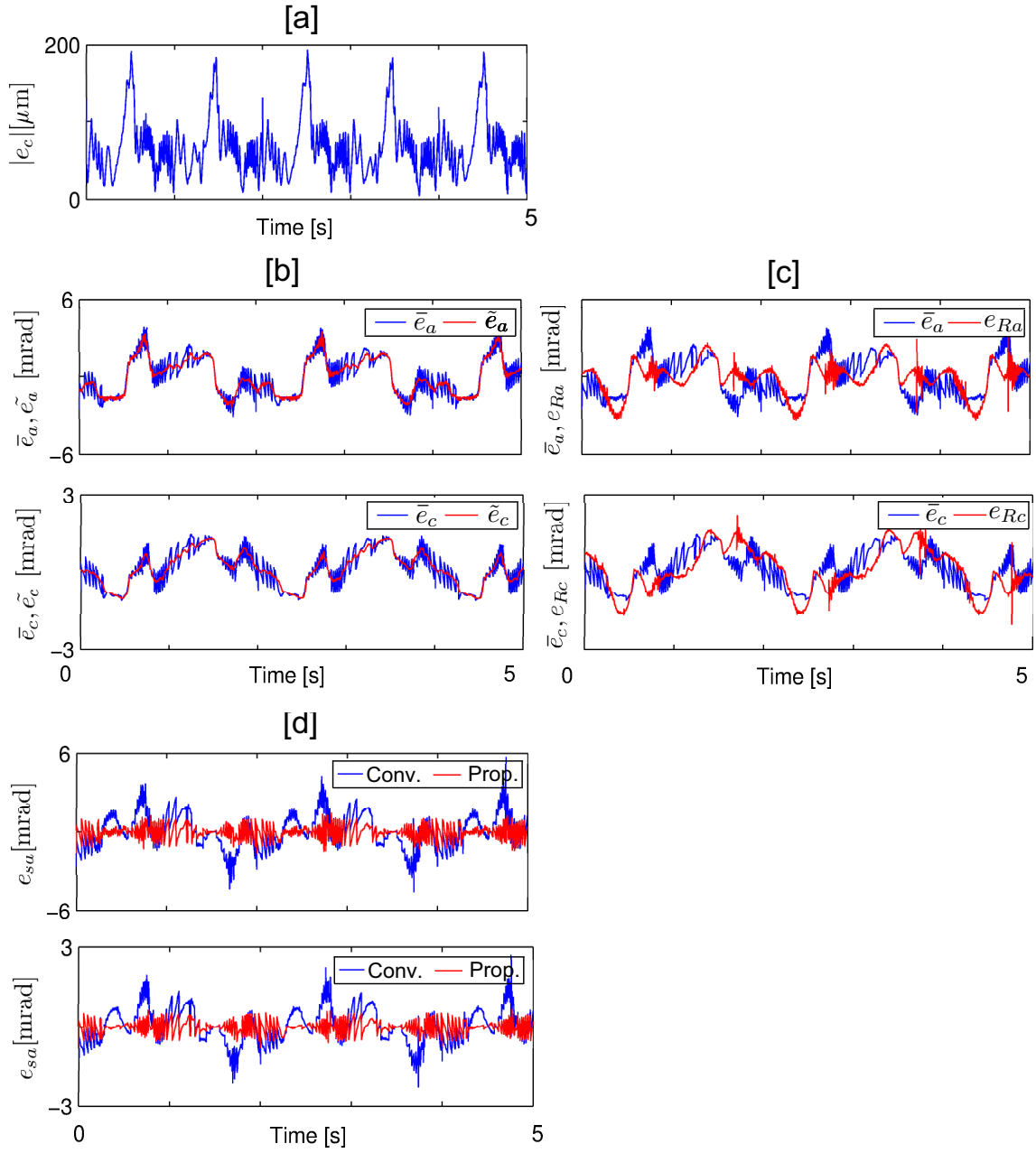
FIGURE 6.8: Experimental results. (a) Actual tool-tip contour error, (b) Actual and estimated tool orientation contour error in Σ_W, (c) Actual and conventional tool orientation contour error in Σ_W, and (d) Discrepancy of the actual tool orientation contour error in Σ_W
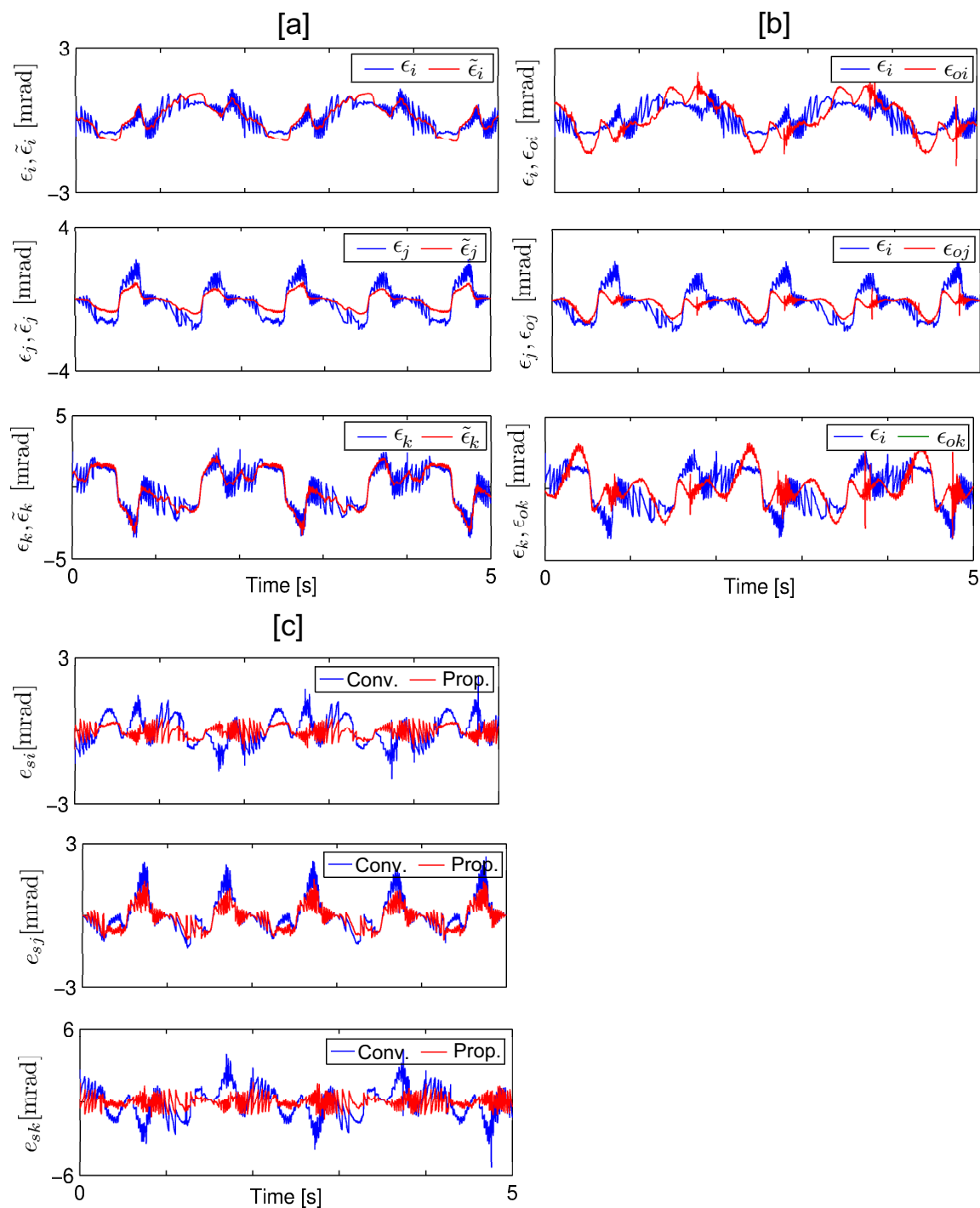
FIGURE 6.9: Experimental results. (a) Actual and estimated tool orientation contour error in spherical coordinate, (b) Actual and conventional tool orientation contour error in spherical coordinate, and (c) Discrepancy of the actual tool orientation contour error in spherical coordinate

6.4   Experimental Results

In order to demonstrate the validity of the proposed estimation model, a desk-top five-axis machine developed in our laboratory is used for the five-axis tool path and orientation shown in Fig. 6.6 and its representation in the tool-coordinate frame Σ_W is as follows:

$$x = 0.01 \sin(2\pi t)(\text{m}),$$
$$y = 0.01 \sin(2\pi t)(\text{m}),$$
$$z = -0.01 \cos(2\pi t)(\text{m}),$$
$$a = \frac{\pi}{9} \sin(\pi t)\,(\text{rad}),$$
$$c = \frac{\pi}{18} \cos(\pi t)\,(\text{rad}). \tag{6.33}$$

The machine consists of three-axis driven by four linear motors (Y-axis is driven by two linear motors) as shown in Fig. 6.7 equipped with 0.1 μm resolution linear encoders. Two rotary axis driven by two DC servo motors are used for the rotary table with 4.0212 μrad resolution. The dynamics parameters of the drivers are given in Table 6.1.

In the following discussion, we compare the performance between the proposed and conventional tool orientation estimation methods under the same contouring controller. For a fare comparison to the model presented in [111], the controller in Eq. (6.31) is implemented, which considers only tool tip contouring control and tracking control for the rotary axis (i.e. tool orientation contouring control is not applied). This controller forces the cutting tool to follow the desired trajectory shown in Fig. 6.6 with minimum tool tip contour error and to reduce the tool orientation tracking error. In addition, because the normal and bi-normal error components are more important than the tangential one, we have selected controller gains in such away that the normal and bi-normal error components are reduced faster than the tangential one. The closed loop gains of the system are set as given in Table 6.2.

Figure 6.8(a) shows the actual contour error calculated by solving a minimization problem off-line for calculating the shortest distance between the tool position and the actual tool path. A comparison between the actual tool orientation contour error $\bar{e}$ (Eq. (6.23)) in the tool coordinate frame Σ_W and the estimated error $\tilde{e}$ (Eq. (6.24)) is shown in Fig. 6.8(b). Figure 6.8(c) shows a comparison between
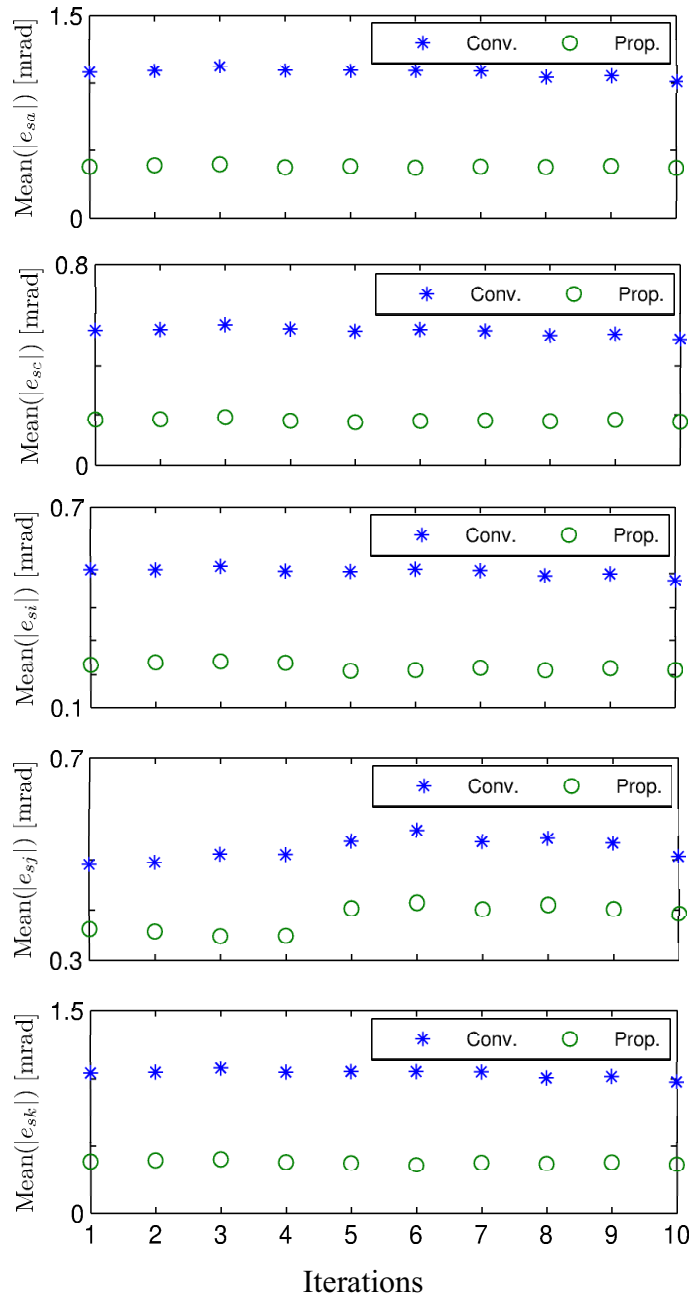
FIGURE 6.10: Mean of the absolute value of the discrepancy of the actual tool orientation contour error

actual tool orientation error $\bar{e}$ and the estimated tool orientation error e_R (Eq. (6.25)) presented in [111]. It can be seen that the proposed estimation gives a better indication of the actual error. The discrepancy from the actual tool orientation contour error is calculated for the proposed method and the model presented in [111] as e_s and the results are shown in Fig. 6.8(d). It is clear that the proposed model has a small estimation error than the conventional model. The

comparisons in Figs. 6.8(b), (c) and (d) are done for the tool orientation contour error in the spherical coordinate (Eqs. (6.23), (6.24), and (6.25), respectively) and the results are shown in Figs. 6.9(a), (b) and (c), respectively. The results show that the proposed estimation model estimates the actual tool orientation error more accurately than the conventional method. In addition, the conventional method shows not only significant discrepancy from the actual tool orientation contour error but also different shape of error profiles. The reason of this incorrect tracking is that the conventional method dose not take the tool tip contour error into account, and it leads to overcut or undercut during machining.

In order to show the repeatability of the proposed approach the above experiments are repeated ten times. The mean of the absolute value of the discrepancy of the actual tool orientation contour error e_s is calculated and compared for the proposed model and the model given in [111] as shown in Fig. 6.10. The proposed model gives smaller error than the conventional estimation method, and leads to a synchronization between the tool tip contour error and tool orientation contour error to avoid a mismatch between the observed tool tip position and orientation.

6.5 Conclusions

A new definition of tool orientation contour error for five-axis machining tasks is presented in this chapter. Unlike the conventional definition of the tool orientation contour error, the proposed model considers the synchronization between the tool tip contour error and tool orientation contour error to avoid a mismatch between the actual tool tip position and orientation. The proposed tool orientation estimation model is compared with the conventional one under the same tool tip contour error and tool tracking controller for a five-axis machine. The experimental results demonstrated the effectiveness of the proposed model to reduce the mismatch between the tool tip contour error and tool orientation contour error which causes overcut or undercut during machining.

Chapter 7

Sliding Mode Contouring Controller Design with Nonlinear Sliding Surface for Five-Axis CNC Machines

7.1 Introduction

The five-axis CNC (computer numerical control) machines are highly flexible compared to those with three-axis and this makes them a popular key factor in modern industries of valuable parts such as aerospace parts, dies and molds with sculptures surfaces. In addition, five-axis machines improve machining accuracy, increase industrial productivity, and increase material removal rate. However, five-axis machines are more susceptible to disturbance such as friction, cutting force, measurement noise and modeling errors due to the increased flexibility in their geometry. These disturbance result in a geometric errors of the machined surface if these disturbance are not well compensated in the servo controller.

Sliding mode control (SMC), a class of variable structure control, is widely accepted as a powerful and effective control method with a strong robustness property and fast error convergence characteristics for systems subjected to external disturbances and parameters uncertainties. In the resent few decades, the SMC with linear sliding surface technique for mechanical systems has been extensively

studied by many researchers [63, 64]. Although, electromechanical servo systems such as robotics and CNC machines should settle quickly without any overshoot to reduce the consumed energy and guarantee high performance, which can not be achieved with a linear sliding surface. Thus, employing of nonlinear sliding surfaces is presented by Rimarez and Bolnar [71], however the design algorithm was not provided in their study. In our previous work [98], we verified the effectiveness of employing nonlinear sliding surface for ball screw feed drive systems. In this study, we extend our previous work [98] to the five-axis machining to reduce the tool tip and tool orientation contour errors. The main advantage of the proposed sliding surface is that it varies according to the contour error vector and hence achieves a variable system closed-loop damping ratio. The variable system closed-loop damping ratio results in low energy consumption because it provides a fast response with small overshoot. In addition, the nonlinear sliding surface has a simple geometric interpretation and its parameters can be tuned easily.

Because the conventional sliding mode control design includes the *sign* function in the control action as a rigid switcher. It causes a discontinuous control action and hence chattering phenomena will take place when the system operates near the sliding surface which may lead the system performance to be unstable. One way to eliminate the chattering is to introduce a thin boundary layer neighboring the sliding surface [113]. The disadvantage of this method is finite steady state error will exist. Another way is to attenuate the amplitude of the switching control signal during the control system design [114]. However, the robustness properties of the control system are affected and the transient performance will become poor. Aghababa and Akbarithe proposed a different technique by replacing the discontinuous *sign* function by the continuous *tanh* function with the adaptive gain and steepness [115]. Zhihong and Habibi introduced an adaptive mechanism for rigid robotic control systems to estimate the upper bound of the norm of input disturbance vector and they employed it as an adaptive controller to guarantee that the effects of the arbitrary bounded input disturbances can be eliminated [116]. In this chapter, in addition to the contouring controller with nonlinear sliding surface, we design an adaptive sliding mode disturbance observer based on the concept of model following and sliding mode compensator. In the proposed approach, the gain matrix of the disturbance compensator are adapted in such a way that the error between the actual plant output and plant model output converges to zero.

7.2 Sliding Mode Contouring Controller Design

7.2.1 Dynamics of Five-Axis Machine

Generally, five-axis machines are represented in the drive-axis coordinate frame Σ_M by the following decoupled second order differential equations:

$$
\begin{aligned}
M\ddot{q} + C\dot{q} &= u - d, \\
M &= \text{diag}\{m_i\}, \ \ C = \text{diag}\{c_i\}, \ \ i = (x, y, z, a, c), \\
u &= [u_x, u_y, u_z, u_a, u_c]^T.
\end{aligned} \tag{7.1}
$$

where $m_i(> 0)$, $c_i(\geq 0)$, v_i and d_i are the equivalent inertia, equivalent viscous friction coefficient, the control input, and the equivalent disturbance in the drive axis i, respectively. The symbol $\text{diag}\{a_i\}$ denotes a diagonal matrix with elements a_i at the ith diagonal positions. The acceleration of the feed drive system in the drive-axis coordinate frame Σ_M, $\ddot{q}(t)$, can be calculated from Eq. (6.6) as follows:

$$
\ddot{q} = J^{-1}[\ddot{w} - \dot{J}\dot{q}]. \tag{7.2}
$$

From the definition of the tracking error e_w and Eq. (7.1), the tracking error dynamics of the cutting tool in the fixed coordinate frame Σ_W is expressed as:

$$
\ddot{e}_w = \ddot{w}_{ref} - M^{-1}\left[u - d - C\dot{q}\right]. \tag{7.3}
$$

where $\ddot{w}_{ref}$ is the desired acceleration of the tool tip with respect to the tool coordinate frame Σ_W. The transformed error dynamics can be obtained by differentiating Eq. (6.19) twice with respect to time as follows:

$$
\ddot{e}_F = \tilde{F}^T\ddot{e}_w + 2\dot{\tilde{F}}^T\dot{e}_w + \ddot{\tilde{F}}^T e_w + \ddot{\tilde{h}}_F. \tag{7.4}
$$

In addition, the dynamics for tool orientation tracking error is estimated by differentiating of Eq. (6.21) twice with respect to time as follows:

$$
\ddot{\tilde{\varepsilon}} = \ddot{\tilde{\theta}} - \ddot{\theta}. \tag{7.5}
$$

Hence, in Eq. (7.5), the last two elements of the reference acceleration should be replaced by the new desired reference acceleration $\ddot{\tilde{\theta}}$.

7.2.2   Sliding Mode Contouring Controller Design with Non-linear Sliding Surface

The most important step of sliding mode control design is the construction of the sliding surface that is expected to response the desired control specifications and performance. In this subsection, we present a design of sliding mode contouring control with a nonlinear sliding surface for five-axis machining tasks. The advantage of employing a nonlinear sliding surface is that it allows the damping ratio of the closed-loop system to be changed according to the tool tip contour error and tool orientation contour error nonlinearly. The low damping ratio is useful to speed up the system response when the error is large. Conversely, the high damping ratio prevents the overshoot when the error becomes smaller. Based on the dynamics of the feed drive system in Eq. (22), we propose the following nonlinear sliding surface:

$$
S = \begin{bmatrix} F_s - \Psi P_s & I \end{bmatrix} \begin{bmatrix} e_{\tilde{F}} \\ \dot{e}_{\tilde{F}} \end{bmatrix}, S \in \Re^{5\times5}.
$$

$$
S = \begin{bmatrix} F_s - \Psi P_s & I \end{bmatrix} \left\{ \begin{bmatrix} \tilde{F}^T & 0 \\ \dot{\tilde{F}}^T & \tilde{F}^T \end{bmatrix} \begin{bmatrix} e_w \\ \dot{e}_w \end{bmatrix} + \begin{bmatrix} \tilde{h}_F \\ \dot{\tilde{h}}_F \end{bmatrix} \right\}. \tag{7.6}
$$

Here, $F \in \Re^{5\times5}$ is the linear term of the sliding surface, which is chosen such that the dominant poles have small damping ratios to achieve fast response. $P_s \in \Re^{5\times5}$ is a positive definite matrix to adjust the final damping ratio. $\Psi \in \Re^{5\times5}$ is a diagonal matrix with non-positive nonlinear entries depending on the tool tip and tool orientation contour errors, and is used to change gain of the sliding surface. The choice of Ψ is not unique, and one possible choice is as follows:

$$
\Psi = \mathrm{diag} \left\{ -\beta_i \frac{\exp(-\bar{k}_i e_i) + \exp(\bar{k}_i e_i)}{2} \right\},
$$

$$
e_i = \begin{cases} e_i & \text{if } |e_i| \le e_i^u. \\ e_i^u \mathrm{sgn}(e_i) & \text{if } |e_i| > e_i^u, i = t, n, b, a, c. \end{cases}
$$

$$
\tag{7.7}
$$

where e_i^u, β_i and $\bar{k}_i$ are positive tunning parameters used to adjust the maximum bound, minimum bound and variation rate of the nonlinear function magnitude $|\Psi|$, respectively. $\mathrm{sgn}(e_i)$ represents the *sign* function of the error signal e_i.

The second step in the sliding mode control design procedure is to determine a control law that forces the system dynamics on the sliding surface within finite time and then remain on it for a subsequent time. We propose the following sliding mode contouring controller:

$$
\begin{aligned}
u \;=\; & MJ^{-1}F\Bigg\{ C^T H \begin{bmatrix} \dot{e}_w \\ \ddot{w}_{ref} - \dot{J}\dot{q} \end{bmatrix} + C^T \dot{H} \begin{bmatrix} e_w \\ \dot{e}_w \end{bmatrix} + C^T H \begin{bmatrix} \dot{\tilde{h}}_f \\ \ddot{\tilde{h}}_f \end{bmatrix} \\
& - \dot{\tilde{\Psi}} P_s (F^T e_w + \tilde{h}_f) + K_s S \Bigg\} + \hat{d} + C\dot{q}, \\
C^T \;=\; & \begin{bmatrix} F - \Psi P_s & I \end{bmatrix}, C^T \in \Re^{5\times10}, \\
H \;=\; & \begin{bmatrix} \tilde{F}^T & 0 \\ \dot{\tilde{F}}^T & \tilde{F}^T \end{bmatrix}, H \in \Re^{10\times10}.
\end{aligned}
\tag{7.8}
$$

where $K_s \in \Re^{5\times5}$ is a diagonal gain matrix with positive entries and $\hat{d}$ is the estimated disturbance by the disturbance observer discussed later.

7.2.3 Stability Analysis

In order to check the stability of the proposed design, the time derivative of the following Lyapunov function candidate must be negative definite:

$$
V = \frac{1}{2} S^T M S.
\tag{7.9}
$$

The time derivative of the Lyapunov function candidate is

$$
\begin{aligned}
\dot{V} \;=\; & S^T M \Bigg\{ C^T H \begin{bmatrix} \dot{e}_w \\ \ddot{e}_w \end{bmatrix} + C^T \dot{H} \begin{bmatrix} e_w \\ \dot{e}_w \end{bmatrix} + C^T H \begin{bmatrix} \dot{\tilde{h}}_f \\ \ddot{\tilde{h}}_f \end{bmatrix} - \dot{\tilde{\Psi}} P (F^T e_w \\
& + \tilde{h}_f) \Bigg\}.
\end{aligned}
\tag{7.10}
$$

Substituting Eq. (7.4) into (7.10), we have

$$
\begin{aligned}
\dot{V} \;=\; S^T M \Bigg\{ & C^T H \begin{bmatrix} \dot{e}_w \\ \ddot{w}_{ref} - JM^{-1}(u - d - C\dot{q}) - \dot{J}\dot{q} \end{bmatrix} + C^T \dot{H} \begin{bmatrix} e_w \\ \dot{e}_w \end{bmatrix} \\
& + \; C^T H \begin{bmatrix} \dot{\tilde{h}}_f \\ \ddot{\tilde{h}}_f \end{bmatrix} - \dot{\tilde{\Psi}} P(F^T e_w + \tilde{h}_f) \Bigg\}.
\end{aligned}
$$

$$(7.11)$$

using control law (7.8)

$$
\dot{V} = -S^T M K_s S + S^T \left[(d - \hat{d}) \right]. \tag{7.12}
$$

Thus, if the disturbance is well estimated by some disturbance observer, $\dot{V} < 0$ can be achieved.

7.2.4   Disturbance Observer Design

This subsection presents a disturbance observer to compensate for the model parameter variations and the external disturbance of the five-axis machine. The disturbance observer is constructed as follows:

$$
\begin{aligned}
\begin{bmatrix} \dot{\hat{d}} \\ \dot{\hat{v}} \end{bmatrix} \;=\; & - \begin{bmatrix} 0 & 0 \\ M^{-1} & M^{-1}C \end{bmatrix} \begin{bmatrix} \hat{d} \\ \hat{v} \end{bmatrix} + \begin{bmatrix} 0 \\ M^{-1} \end{bmatrix} u \\
& + \begin{bmatrix} K_d \\ K_v \end{bmatrix} (\hat{v} - v).
\end{aligned}
$$

$$(7.13)$$

where $v \in \Re^{5\times1}$ is the velocity vector of the feed drive axes in the machine coordinate frame Σ_M (i.e. $v = \dot{q}$ in Eq. (7.1)). $\hat{d} \in \Re^{5\times1}$ and $\hat{v} \in \Re^{5\times1}$ are the estimated values of the disturbance and velocity of the feed drive axes. $K_d \in \Re^{5\times5}$ and $K_v \in \Re^{5\times5}$ are positive correction gains for estimation. Define the observation errors as follows:

$$
\tilde{d} \;=\; \hat{d} - d. \tag{7.14}
$$

$$
\tilde{v} \;=\; \hat{v} - v. \tag{7.15}
$$

Substituting Eqs. (7.14) and (7.15) into (7.13) we have

$$\dot{\hat{d}} = K_d \tilde{v}. \tag{7.16}$$

$$\dot{\hat{v}} = K_v \tilde{v} + M^{-1}(u - C\hat{v} - \hat{d}). \tag{7.17}$$

In order to check the stability of the proposed disturbance observer, consider the a Lyapunov function candidate

$$V_1 = \frac{1}{2}\tilde{d}^T M^{-1} K_d^{-1} \tilde{d} + \frac{1}{2}\tilde{v}^T \tilde{v}. \tag{7.18}$$

The time derivative of V_1 is

$$\begin{aligned} \dot{V}_1 &= \tilde{d}^T M^{-1} K_d^{-1} \dot{\tilde{d}} + \tilde{v}^T \dot{\tilde{v}}. \\ &= \tilde{d}^T M^{-1} K_d^{-1} (\dot{\hat{d}} - \dot{d}) + \tilde{v}^T (\dot{\hat{v}} - \dot{v}). \end{aligned} \tag{7.19}$$

By substituting Eqs. (7.1) and (7.19), equation (7.17) can be rewritten as

$$\begin{aligned} \dot{V}_1 &= \tilde{d}^T M^{-1} K_d^{-1} (\dot{\hat{d}} - \dot{d}) + \tilde{v}^T \big[K_v \tilde{v} + M^{-1}(u - C\hat{v} - \hat{d}) \\ &\quad - M^{-1}(u - Cv - d) \big]. \\ &= \tilde{d}^T M^{-1} K_d^{-1} (\dot{\hat{d}} - \dot{d}) + \tilde{v}^T \big[K_v \tilde{v} + M^{-1}(-C\tilde{v} - \tilde{d}) \big]. \end{aligned} \tag{7.20}$$

Assuming that the disturbance change very slowly and considering Eq. (7.16), Equation (7.20) becomes

$$\begin{aligned} V_1 &= \tilde{d}^T M^{-1} \tilde{v} + \tilde{v}^T \left[K_v \tilde{v} + M^{-1}(-C\tilde{v} - \tilde{d}) \right] \\ &= -\tilde{v}^T M^{-1} C \tilde{v} + \tilde{v}^T K_v \tilde{v} \\ &= \tilde{v}^T (K_v - M^{-1}C) \tilde{v}. \end{aligned} \tag{7.21}$$

Choosing the gain matrix such that $K_v - M^{-1}C$ becomes negative definite, $V_1 < 0$ can be achieved.

7.3 Simulation Results

In order to demonstrate the effectiveness of the proposed approach, a computer simulation has been conducted for the following five-axis tool path represented in

TABLE 7.1: Five-axis machine parameter values

Parameter	m		c	
$X-$ axis	5.33	Vs^2/m	25.175	Vs/m
$Y-$ axis	4.545	Vs^2/m	24.202	Vs/m
$Z-$ axis	1.72	Vs^2/m	71.647	Vs/m
$A-$ axis	0.0023	Vs^2/rad	0.022	Vs/rad
$C-$ axis	0.01489	Vs^2/rad	0.100	Vs/rad

the tool-coordinate system:

$$x = 0.01 \sin(2\pi t)(\text{m}),$$
$$y = 0.01 \sin(2\pi t)(\text{m}),$$
$$z = -0.01 \cos(2\pi t)(\text{m}),$$
$$a = \frac{\pi}{9} \sin(\pi t)(\text{rad}),$$
$$c = \frac{\pi}{18} \cos(\pi t)(\text{rad}). \tag{7.22}$$

The equivalent inertia and viscous friction coefficients of the five-axis machine are given in Table 7.1. In addition a disturbance to the control input is applied so that the actual control input $u_{act} = u + d_{dis}$, where $d_{dis} = [0.3, 0.3, 0.5, 0.05, 0.05]^T \sin(0.1t)$ (V) and u is calculated from Eq. (7.8). In this simulation, we compared the proposed controller with and without the disturbance observer under the same controller parameters. The gain matrix F_s is set to diag$\{50, 150, 150, 100, 100\}$. The parameters of the nonlinear function, β and $\bar{k}$, are selected to be [10, 10, 10, 10, 10]^T and [5, 50, 50, 0.3, 1]^T, respectively. The gain matrix K_s is adjusted to diag$\{10, 20, 20, 20, 20\}$. For the disturbance observer parameters, the gain matrices K_d and K_v are selected to be diag$\{100\ 100\ 350\ 0.1\ 0.1\}$ and diag$\{0.5\ 0.5\ 10\ 0.001\ 0.001\}$, respectively.

Figure 7.1 shows the transformed error (tangential, normal and bi-normal error components (i.e. Eq. (6.19))) and the tool orientation contour error components (i.e. Eq. (6.22)). It can be seen that the proposed controller with the disturbance observer achieves a better performance.
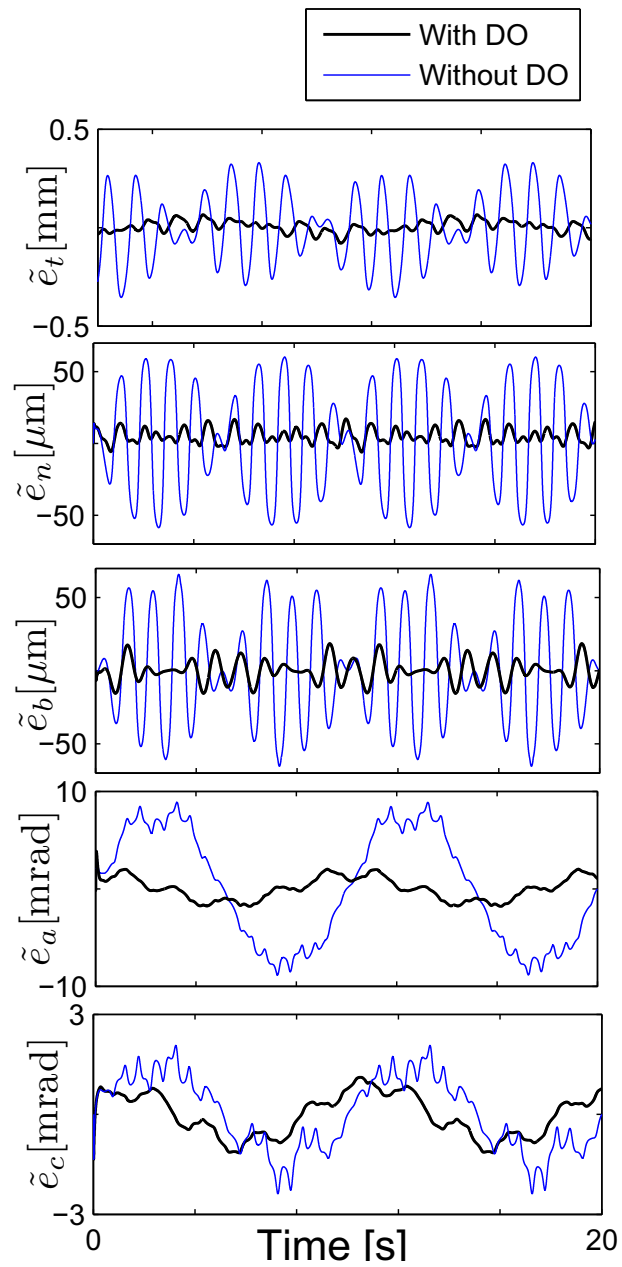
FIGURE 7.1: Simulation results; with/without disturbance observer

7.4   Conclusions

In this chapter, we propose a novel sliding mode contouring controller with a non-linear sliding surface for five-axis machining tasks. The controller aims to reduce the tool tip and tool orientation contour errors. We design a disturbance observer to compensate for the effect of modeling error and external disturbance. The proposed controller with the disturbance observer results in a good performance compared with the conventional controller in terms of tool tip and tool orientation contour errors.

Chapter 8

Conclusions and Future Work

8.1 Conclusions

In modern CNC machines tools, robotics and industrial applications the need for fast response and high precision becomes the concern of the machine tool control community. In order to improve the tracking performance for feed drive systems, and reduce the consumed energy, this dissertation presented sliding mode control with nonlinear sliding surface. In addition, to improve the contouring performance in multi-axis feed drive systems, the dissertation presented a new sliding mode contouring controller with nonlinear sliding surface for biaxial, three-axis and five-axis feed drive system. To examine the effectiveness of the proposed controllers, several free-form contour following tasks experiments and simulation (single-axis, biaxial, three-axis and five-axis feed drive system) were conducted.

The main contributions of the dissertation are as follows:

(1) A model-based predictive contouring controller for biaxial feed drive systems based on error and control input coordinate transformation. To verify the effectiveness of the proposed control approach, we conducted experiments involving circular and non-circular reference trajectories. The results indicated that the proposed controller can significantly improve the contouring accuracy for smooth contour by adjusting the prediction horizon and performance index weighting factors.

(2) In order to improve the tracking performance in feed drive system and reduce
the consumed energy, we presented a sliding-mode controller with a non-
linear sliding surface for ball-screw feed drive systems. Then we have verified
the effectiveness of the proposed controller via experiments. Two cases were
considered: the first case showed the effectiveness of the proposed non-linear
sliding surface at reducing the tracking error, while the second one verified
the ability of the proposed approach to reduce the consumed energy and
control input variation. For the first case, the mean of the tracking error
magnitude was reduced by 35% without the need for additional electrical
energy or control input variation, while in the second case, the consumed
energy and control input variation were reduced by about 12.9% and 19.1%,
respectively.

(3) We have extend the proposed sliding mode controller with nonlinear sliding
surface to consider the contour following in biaxial feed drive systems. A
sliding mode contouring controller with nonlinear sliding surface based on
coordinate transformation is presented. The advantage of the proposed ap-
proach is that the sliding surface varies according to the contour error so
that the damping ratio of the system changes from its initial low value to its
final high value as the contour error changes from high value to small value
and vice versa so that the system simultaneously achieves low energy con-
sumption and a small settling time, resulting in a smaller error. To verify the
effectiveness of the proposed control approach, we conducted experiments for
elliptical reference trajectories. The results indicated that the proposed con-
troller can significantly improve the contouring accuracy for smooth contour
by adjusting the tunning parameters of the nonlinear function without any
additional electrical energy. In addition, the proposed approach reduced the
control input variance and consumed energy on average by about 45.7% and
18.9% (for x and y-axis, respectively) and 29% and 12.5% (for x and y-axis,
respectively), respectively. Moreover, and in order to improve the steady
state performance, the proposed sliding surface can be extended to include
integral action. In order to verify the effectiveness of the proposed nonlin-
ear sliding surface composite with integral action, a sliding mode contouring
controller is designed and compared to the the sliding mode controller with
proportional-integral-derivative (PID) sliding surface presented in [104]. The
proposed sliding surface reduces the contour error with small control input

because of employing the nonlinear function that increases the system damping ratio when the contour error converges to a small magnitude to prevent energy consumption. However, the controller with PID sliding surface provides constant damping ratio that is smaller than the optimal damping ratio when the contour error magnitude is smaller and vice versa.

(4) In addition, a sliding mode contouring controller with nonlinear sliding surface for three-dimensional machining based on iterative contour error approximation and a coordinate transformation approach is presented. The effectiveness of the proposed control approach is demonstrated through experiments and simulation involving a three-dimensional reference trajectory. Two cases of simulation and experiments are conducted; the first experiment is to show the effectiveness of the proposed nonlinear sliding surface a against the linear sliding surface, while the second one is to show the effect of the tuning parameter of the nonlinear term. The results indicated that the proposed sliding surface achieve a good performance compared to linear sliding surface. In addition, contouring performance can be significantly improved by adjusting the tuning parameter of the nonlinear term.

(5) A new definition of tool orientation contour error for five-axis machining tasks is proposed. Unlike the conventional definition of the tool orientation contour error, the proposed model considers the synchronization between the tool tip contour error and tool orientation contour error to avoid a mismatch between the actual tool tip position and orientation. The proposed tool orientation estimation model is compared with the conventional one under the same tool tip contour error and tool tracking controller for a five-axis machine. The experimental results demonstrated the effectiveness of the proposed model to reduce the mismatch between the tool tip contour error and tool orientation contour error which causes overcut or undercut during machining.

(6) Finally, we proposed a novel sliding mode contouring controller with a nonlinear sliding surface for five-axis machining tasks. The controller aims to reduce the tool tip and tool orientation contour errors. In addition, we proposed a disturbance observer to compensate for the effect of modeling error and external disturbance. The effectiveness of the proposed controller with the disturbance observer has been verified through a computer simulation. The proposed controller results in a good performance compared with the

conventional controller in terms of tool tip and tool orientation contour errors.

8.2   Future work

In order to improve the contouring performance in multi-axis feed drive systems, several suggestions for future research are listed below:

(1) We have verified that employing a nonlinear sliding surface of a sliding mode control results in improved tracking and performance. The selection of the nonlinear function of the sliding surface is not unique. However, may be there are other functions that may produce even improved results. Hence, we consider the design of an optimal sliding surface based on the minimization of the tracking/contour error and control input as future work. Based on the above optimal sliding surface, a sliding mode controller will be designed for the feed drive systems.

(2) In the proposed sliding mode control for single, two and three-axis feed drive systems those are presented in Chapters 2, 4 and 5, respectively, the traditional sign function is still utilized in the controller design to drive the system onto the sliding surface. This means that the chattering phenomenon will exist particularly for the feed drive systems. However, such phenomenon and its corresponding influences should be well addressed. Moreover, the cutting force is an important source of disturbance causes contour error in many industrial applications. In order to eliminate the chattering phenomena duo to the discontinues control action and to estimate the cutting force, we consider a design of an adaptive sliding mode disturbance compensator based on the concept of model following control as future work.

(3) Implementation of the proposed approach presented in Chapter 7 for five-axis machine. As presented in Chapter 7, the proposed contouring controller reduce the contour error and compensate for disturbance. Hence the proposed approach is expected to improve the contouring performance in the five-axis machining tasks.

(4) Since the simulation and experimental results verified that employing the nonlinear sliding surface reduces the control input variation and hence reduce

the vibration of the cutting tool, we like to conduct actual cutting process by multi-axis feed drive systems in a future work. It is expected that the consumed energy by the feed drive systems will be much reduced because the control input variation is very high during actual cutting process compared to air cutting.

Appendix A

Appendix A

To tune the servo behaviour of a closed-loop system, the polynomial P is introduced, and two monic polynomials Q_n and Q_d with no common factors are used to examine different performance indices [84]. The performance index (3.11) can be written in terms of tracking errors and control inputs in X and Y direction as follows:

$$
\begin{aligned}
J = \sum_{j=H_m}^{H_P} & \rho_{cn}(e_x^* S - e_y^* C)^T (e_x^* S - e_y^* C) + \rho_{ct}(e_x^* C + e_y^* S)^T (e_x^* C + e_y^* S) \\
& + \rho_n (u_x^* S - u_y^* C)^T (u_x^* S - u_y^* C) + \rho_t (u_x^* C + u_y^* S)^T (u_x^* C + u_y^* S), \\
e_x^* = & \hat{x}^* - x^*, \\
e_y^* = & \hat{y}^* - y^*, \\
x^* = & [P(1)r_x(k + H_m), ..., P(1)r_x(k + H_P)]^T, \\
y^* = & [P(1)r_y(k + H_m), ..., P(1)r_y(k + H_P)]^T, \\
\hat{x}^* = & [P\hat{x}(k + H_m), ..., P\hat{x}(k + H_P)]^T, \\
\hat{y}^* = & [P\hat{y}(k + H_m), ..., P\hat{y}(k + H_P)]^T, \\
u_x^* = & [u_x^*(k), ..., u_x^*(k + H_P - \hat{d} - 1)]^T, \\
u_y^* = & [u_y^*(k), ..., u_y^*(k + H_P - \hat{d} - 1)]^T, \\
u_x^*(k) = & \frac{Q_{nx}}{Q_{dx}} u_x(k), \\
u_y^*(k) = & \frac{Q_{ny}}{Q_{dy}} u_y(k).
\end{aligned} \tag{A.1}
$$

The vectors $\bar{u}_x$ and $\bar{u}_y$ consist of controller output sequence:

$$\bar{u}_x = [u_x(k), \cdots, u_x(k + H_c - 1)]^T. \tag{A.2}$$

$$\bar{u}_y = [u_y(k), \cdots, u_y(k + H_c - 1)]^T. \tag{A.3}$$

The relationships between the vectors $\bar{u}_x$ and u_x and between $\bar{u}_y$ and u_y are

$$u_x = \mathbf{M}\bar{u}_x + \mathbf{N}\check{u}_x,$$

$$\check{u}_x = [u_x(k-1), \cdots, u_x(k + H_c - n_\Phi - n_P)]^T. \tag{A.4}$$

$$u_y = \mathbf{M}\bar{u}_y + \mathbf{N}\check{u}_y,$$

$$\check{u}_y = [u_y(k-1), \cdots, u_y(k + H_c - n_\Phi - n_P)]^T. \tag{A.5}$$

where $\mathbf{M}$ and $\mathbf{N}$ are given in (3.16) and (3.17), respectively. The gradients of (A.1) with respect to $\bar{u}_x$ and $\bar{u}_y$ are

$$\frac{\partial J}{\partial \bar{u}_x} = [(\rho_{cn}S^2 + \rho_{ct}C^2)(\hat{x}^* - x^*) + SC(\rho_{ct} - \rho_{cn})(\hat{y}^* - y^*)]\frac{\partial \hat{x}^*}{\partial \bar{u}_x}$$

$$+ [(\rho_n S^2 + \rho_t C^2)u_x^* + SC(\rho_t - \rho_n)u_y^*]\frac{\partial u_x^*}{\partial \bar{u}_x}. \tag{A.6}$$

$$\frac{\partial J}{\partial \bar{u}_y} = [(\rho_{cn}C^2 + \rho_{ct}S^2)(\hat{y}^* - y^*) + SC(\rho_{ct} - \rho_{cn})(\hat{x}^* - x^*)]\frac{\partial \hat{y}^*}{\partial \bar{u}_y}$$

$$+ [(\rho_n C^2 + \rho_t S^2)u_y^* + SC(\rho_t - \rho_n)u_x^*]\frac{\partial u_y^*}{\partial \bar{u}_y}. \tag{A.7}$$

The partial derivatives $\partial \hat{x}^*/\partial \bar{u}_x$, $\partial \hat{y}^*/\partial \bar{u}_y$, $\partial u_x^*/\partial \bar{u}_x$, and $\partial u_y^*/\partial \bar{u}_y$ are

$$\frac{\partial \hat{x}^*}{\partial \bar{u}_x} = \mathbf{M}^T \mathbf{G}_x^T. \tag{A.8}$$

$$\frac{\partial u_x^*}{\partial \bar{u}_x} = \mathbf{M}^T \mathbf{\Phi}^T. \tag{A.9}$$

$$\frac{\partial \hat{y}^*}{\partial \bar{u}_y} = \mathbf{M}^T \mathbf{G}_y^T. \tag{A.10}$$

$$\frac{\partial u_y^*}{\partial \bar{u}_y} = \mathbf{M}^T \mathbf{\Phi}^T. \tag{A.11}$$

The relationships between $\hat{x}^*$ and $\bar{u}_x$, and between $\hat{y}^*$ and $\bar{u}_y$ are given by

$$\hat{x}^* = \mathbf{G}_x\mathbf{M}\bar{u}_x + \mathbf{H}_x\breve{u}_x + \mathbf{F}_x c_x + \zeta_x + \mathbf{G}_x\mathbf{N}\breve{u}_x. \tag{A.12}$$

$$\hat{y}^* = \mathbf{G}_y\mathbf{M}\bar{u}_y + \mathbf{H}_y\breve{u}_y + \mathbf{F}_y c_y + \zeta_y + \mathbf{G}_y\mathbf{N}\breve{u}_y. \tag{A.13}$$

The relationships between u_x^* and $\bar{u}_x$, and between u_y^* and $\bar{u}_y$ are given by

$$u_x^* = \boldsymbol{\Phi}\mathbf{M}\bar{u}_x + \boldsymbol{\Omega}\tilde{u}_x + \boldsymbol{\Phi}\mathbf{N}\breve{u}_x. \tag{A.14}$$

$$u_y^* = \boldsymbol{\Phi}\mathbf{M}\bar{u}_y + \boldsymbol{\Omega}\tilde{u}_y + \boldsymbol{\Phi}\mathbf{N}\breve{u}_y. \tag{A.15}$$

where $\mathbf{G}$, $\mathbf{F}$ and $\mathbf{H}$, and $\breve{u}$ and c are given by (3.13), (3.23) and (3.24), respectively. A minimum of J with respect to $\bar{u}_x$ and $\bar{u}_y$ can be obtained by setting the gradients (A.6) and (A.7) to zero. This leads to the controller in Eq. (3.12).

Bibliography

[1] C. Okwudire. *Modeling and Control of High Speed Machine Tool Feed Drive.* University of British Columbia, Canada, The University of British Columbia, 2009.

[2] L. Alkafafi. *Time and Frequency Optimal Motion Control of CNC Machine Tools.* Dr. Eng. Thesis, Technical University of Hamburg, Germany, New York, 2013.

[3] N. Ushimi K. Tsuruta, K. Sato and T. Fujimoto. High-speed and high-precision position control using a sliding mode compensator. *Electrical Engineering in Japan,*, 174(2):65–71, 2011.

[4] K. Erkorkmaz and Y. Altintas. High Speed CNC System Design. Part I: Jerk Limited Trajectory Generation and Quintic Spline Interpolation . *International Journal of Machine Tools and Manufacture*, 41(9):1323–1345, 2001.

[5] S. L. Omirou and A. K. Barouni. Integration of New Programming Capabilities Into a CNC Milling System. *Robotics and Computer-Integrated Manufacturing*, 21:518–527, 2005.

[6] M.A. Mannan R. Ramesh and A.N. Poo. Tracking and contour error control in cnc servo systems. *International Journal of Machine Tools and Manufacture*, 45:301–326, 2005.

[7] K. Erkorkmaz and Y. Altintas. High Speed CNC System Design. Part III: High Speed Tracking and Contouring Control of Feed Drives. *International Journal of Machine Tools and Manufacture*, 41:1637–1658, 2001.

[8] Y. Nakatsu Y. Kakino, Y. Ihara and K. Okamura. The Measurement of Motion Errors of NC Machine Tools and Diagnosis of Their Origins by Using

Telescoping Magnetic Ball Bar Method. *CIRP Annals-Manufacturing*, 36: 377–380, 1987.

[9] A. G. Ulsoy and Y. Koren. Control of Machining Processes. *ASME Journal of Dynamic Systems, Measurement, and Control*, 115, 1993.

[10] Masory O. Improving Contouring Accuracy of NC/CNC Systems with Additional Velocity Feed Forward Loop. *ASME Journal of Engineering for Industry*, 104:227–230, 1986.

[11] M. Tomizuka. Zero phase error tracking control. *Journal of Dynamic Systems, Measurement, and Control*, 109(1):65–68, 1987.

[12] Y. Altintas, K. Erkorkmaza, and W. Zhua. Sliding Mode Controller Design for High Speed Feed Drives. *CIRP Annals - Manufacturing Technology*, 49: 265–270, 2000.

[13] A. Kamalzadeh and K. Erkorkmaz. Accurate Tracking Controller Design for High-Speed Drives. *International Journal of Machine Tools and Manufacture*, 47:1393–1400, 2007.

[14] H. Van Brussel and P. Van Den Braembussche. Robust control of feed drives with linear motors. *Annals of CIRP*, 47(1):325–328, 1998.

[15] Y. Koren. Cross-coupled biaxial computer controls for manufacturing systems. *ASME Journal of Engineering for Industry*, 102:265–272, 1980.

[16] Y. S. Tarng Z.-MU Yeh and Y. S. Lin. Cross-Coupled Fuzzy Logic Control for Multi-axis Machine Tools. *Journal of Mechatronics*, 7(8):663–681, 1997.

[17] Jia-Yush Y. H.C. Ho and S.S. Lu. A decoupled path-following control algorithm based upon the decomposed trajectory error. *International Journal of Machine Tools and Manufacture*, 39:1619–1630, 1999.

[18] G.T.-C. Chiu and M. Tomizuka. Contouring control of machine tool feed drive systems: A task coordinate frame approach. *IEEE Transactions on Control Systems Technology*, 9:130–139, 2001.

[19] K.-Han Su M.-Yang Cheng and S.-Feng Wang. Contour Error Reduction for Free-Form Contour Following Tasks of Biaxial Motion Control Systems. *Robotics and Computer-Integrated Manufacturing*, 25(2):323–333, 2009.

[20] Ke-Han Sua and M.-Yang Cheng. Contouring Accuracy Improvement Using Cross-Coupled Control and Position Error Compensator. *International Journal of Machine Tools and Manufacture*, 48(12-13):144–145, 2008.

[21] C. C. Lo and C. Y. Chung. Tangential Contouring Controller for Biaxial Motion Control. *ASME, Journal of Dynamic Systems, Measurements, and Control*, 121:126–129, 1999.

[22] M.Y. Cheng and C.C. Lee. On Real-time Contour Error Estimation for Contour Following Tasks. In *Proc. IEEE/ASME International Conference of Advanced Intelligent Mechatronics*, pages 1047–1052, 2005.

[23] X. Ye, X. Chen, X. Li, and S. Huang. A Cross-Coupled Path Precompensation Algorithm for Rapid Prototyping and Manufacturing. *The International Journal of Advanced Manufacturing Technology*, 20:39–43, 2002.

[24] Y. S. Tarng, H. Y. Chuang, and W. T. Hsu. Intelligent Cross-coupled Fuzzy Feedrate Controller Design for CNC Machine Tools Based on Genetic Algorithms. *International Journal of Machine Tools and Manufacture*, 39: 1673–1692, 1999.

[25] J.-Hua Chin, Y.-Ming Cheng, and J.-Huei Lin. Improving Contour Accuracy by Fuzzy-Logic Enhanced Cross-Coupled Precompensation Method. *Robotics and Computer-Integrated Manufacturing*, 20:65–76, 2004.

[26] Yeh SS and Hsu PL. Adaptive-Feedrate Interpolation for Parametric Curves with a Confined Chord Error. *Computer-Aided Design*, 34(3):229–237, 2002.

[27] S. Jee and Y. Koren. Adaptive Fuzzy Logic Controller for Feed Drives of a CNC Machine Tool. *Journal of Mechatronics*, 14:299–326, 2004.

[28] U. Itkis. *Control Systems of Variable Structure*. Wiley, New York, 1976.

[29] Utkin. Variable Structure Systems with Sliding Mode. *IEEE Transactions on Automatic Control*, 22(2):212222, 1977.

[30] J. Guldner and V.I. Utkin. Tracking the gradient of artificial potential fields: Sliding mode control for mobile robots. *Modern Machinery Science Journal*, 63(3):417–432, 1996.

[31] O.M.E. El-Ghezawi A.S.I. Zinober and S.A. Billings. Multi variable structure adaptive model-following control systems. *Proceedings of IEE*, 129:6–12, 1982.

[32] J.K. Hedrick J.J.E. Slotine and E.A. Misawa. On sliding observers for nonlinear systems. *Transactions of the ASME: Journal of Dynamic Systems Measurement and Control*, 109:245–252, 1987.

[33] S. Drakunov and V. Utkin. Sliding mode observers. tutorial. In *Proceedings of the 34th Conference on Decision and Control,New-Orleans, LA,*, 1995.

[34] B. Drazenovic. The invariance conditions in variable structure systems. *Automatica*, 5(3):287–295, 1969.

[35] K. Furuta. Sliding mode control of a discrete system. *Systems and Control Letters*, 14:145–152, 1990.

[36] H. Sira-Ramirez. Differential geometric methods in variable-structure control. *International Journal of Control*, 48(4):1359–1390, 1988.

[37] S.H. Zak R.A. De Carlo and G.P. Matthews. Variable structure control of nonlinear variable systems: A tutorial. *Proceedings of IEEE*, 76:212–232, 1988.

[38] C. Edwards and S. Spurgeon. *Sliding Mode Control: Theory and Applications*. Taylor and Francis, 1998.

[39] U. Itkis. *Control Systems of Variable Structure*. Wiley, New York, 1976.

[40] V.I. Utkin. *Sliding Modes in Control Optimization, Communication and Control Engineering Series*. Springer-Verlag, 1992.

[41] W. Perruquetti and J.-P. Barbot. *Sliding Mode Control In Engineering*. Springer-Verlag, Berlin Heidelberg, 1 edition, 2009.

[42] F. Deepak B. Bandyopadhyay and K.-S. Kim. *Sliding Mode Control Using Novel Sliding Surfaces*. Springer-Verlag, Berlin Heidelberg, 1 edition, 2009.

[43] I. Eker. Sliding mode control with pid sliding surface and experimental application to an electromechanical plant. *ISA Transactions*, 45(1):109–118, 2006.

[44] Banda S. Lin Z, Pachter M. Toward improvement of tracking performance nonlinear feedback for linear systems. *International Journal of Control*, 70: 1–11, 1998.

[45] S. Mondal and C. Mahanta. Nonlinear sliding surface based second order sliding mode controller for uncertain linear systems. *Commun. Nonlinear Sci. Numer. Simulat.*, 16:3760–3769, 2011.

[46] R. Imani-Asrai S.T. Newman, A. Nassehi and V. Dhokia. Energy efficient process planning for cnc machining. *CIRP Journal of Manufacturing Science and Technology*, 5(2):127–136, 2012.

[47] J.B. Dahmus and T.G. Gutowski. An Environmental Analysis of Machining. In *Proceedings of ASME International Mechanical Engineering Congress R&D Exposition*, page 1319, 2004.

[48] A. Vijayaraghavan and D. Dornfeld. Automated monitoring of machine tools. *CIRP Annals*, 59(1):2124, 2010.

[49] A. Dietmair and A. Verl. Energy consumption forecasting and optimisation for tool machines. *Modern Machinery Science Journal*, page 6267, 2009.

[50] R. Bulpett-A.W. Anson M. Zolgharni, B.J. Jones and J. Franks. Energy efficiency improvements in dry drilling with optimized diamond-like carbon coatings. *Diamond & Related Materials*, 17:17331737, 2008.

[51] A. El Khalick M. *Contouring Controller Design for Multi-Axis Feed Drive Systems*. Master of Engineering Thesis, Toyohashi University of Technology, Japan, 2010.

[52] K. K. Varanasi and S. A. Nayfeh. Dynamics of lead-screw drives: Low-order modeling and experiments. *Transactions of ASME, Journal of Dynamic Systems, Measurement, and Control*, 126(2):388–396, 2004.

[53] M. Weck and G. Ye. Sharp corner tracking using the ikf control strategy. *Annals of CIRP*, 39(1):437–441, 1990.

[54] K.L. Hillsley and S. Yurkovich. Vibration control of a two-link flexible robot arm. *Proceedings of the IEEE International Conference on Robotics and Automation*, 3:2121–2126, 1991.

[55] J.M. Hyde and W.P. Seering. Using input command pre-shaping to suppress multiple mode vibration. *Proceedings of the IEEE International Conference on Robotics and Automation*, 3:2604–2609, 1991.

[56] A.D. Smith. *Ph.D. Thesis: Wide Bandwidth Control of High-Speed Milling Machine Feed Drives*. University of Florida, Department of Mechanical Engineering, Florida, 1999.

[57] A. Illarramendi J.L. Azpeitia M. Zatarain, I. Ruiz de Argandoa and R. Bueno. New control techniques based on state space observers for improving the precision and dynamic behaviour of machine tools. *Annals of CIRP*, 54(1):393–396, 2005.

[58] Y. Altintas. Manufacturing automation: Metal cutting mechanics, machine tool vibrations, and cnc design. *Cambridge University Press*, 2000.

[59] P. Dupont H.B. Armstrong and D.W.C Canudas. A survey of models, analysis tools and compensation methods for the control of machines with friction. *Automatica*, 30(7):1083–1138, 1994.

[60] K. Erkorkmaz and A. Kamalzadeh. High bandwidth control of ball screw drives. *Annals of the CIRP*, 55(1):393398, 2006.

[61] B. Veselic and B. P.-Drazenovic. High-performance position control of induction motor using discrete-time sliding-mode control. *IEEE Transaction on Industrial Electronics*, 55(11):3809–3817, 2008.

[62] W. Gao J.Y. Hung and J.C. Hung. Variable structure control: A survey. *IEEE Transaction on Industrial Electrons*, 4o:2 – 22, 1993.

[63] J. Slotine and S. Sastry. Tracking control of nonlinear systems using sliding surfaces with application to robotic manipulators. *International Journal of Control*, 28(2):465–492, 1983.

[64] A. Rojko and K. Jezernik. Sliding-mode motion controller with adaptive fuzzy disturbance estimation. *IEEE Transaction on Industrial Electrons*, 51 (5):963–971, 2004.

[65] K. Maruyama H. Hashimoto and F. Harashima. A microprocessor-based robot manipulator control with sliding mode. *IEEE Transaction on Industrial Electronics*, IE-34(1):1118, 1987.

[66] O. Kaynak K. Erbatur and A. Sabanovic. A study on robustness property of sliding mode controllers: A novel design and experimental investigations. *IEEE Transaction on Industrial Electronics*, 46(5):10121018, 1999.

[67] W. Chen and M. Saif. Output feedback controller design for a class of mimo nonlinear systems using high-order sliding-mode differentiators with application to a laboratory 3-d crane. *IEEE Transaction on Industrial Electronics*, 55(1):39853997, 2008.

[68] M.J. Jang C.L. Chen and K.C. Lin. Modeling and high-precision control of a ball-screw-driven stage. *Precision Engineering*, 28:483495, 2004.

[69] J. Swevers P. Braembussche and H. Brussel. Design and experimental validation of robust controllers for machine tool drives with linear motor. *Mechatronics*, 28:545–562, 2004.

[70] H.-T. Yau and J.-J. Yan. Adaptive sliding mode control of a high-precision ball-screw-driven stage. *Nonlinear Analysis: Real World Applications*, 10: 14801489, 2009.

[71] H. S-Ramirez and M. R-Bolivar. Sliding mode control of dc-to-dc power converters via extended linearization. *IEEE Transactions on Circuits and Systems*, 41(10):652–661, 1994.

[72] M. Tomizuka A. Jabbari and T. Sakaguchi. Robust Nonlinear Control of Positioning Systems with Friction. In *Proceedings of the American Control Conference, USA*, pages 1097–1102, 1990.

[73] J.-J. Lee. Adaptive tracking controller of dc servomotors. *IEEE Transactions on Consumer Electronics*, 37(4):905–912, 1991.

[74] V.-K. Chu and M. Tomizuka. Sliding Mode Control with Nonlinear Sliding Surfaces. In *International Federation of Automatic Control Congress*, pages 481–486, 1996.

[75] H. Temeltas. A Fuzzy Adaptation Technique For Sliding Mode Controllers. In *IEEE International Symposium on Industrial Electronics*, volume 1, pages 110–112, 1998.

[76] K. Erkorkmaz and Y. Altintas. High speed cnc system design. part ii: Modeling and identification of feed drives. *International Journal of Machine Tools and Manufacture*, 41:14871509, 2001.

[77] J.G. Bekker, I.K. Craig, and P.C. Pistorius. Model Predictive Control of an Electric Arc Furnace off-gas Process. *Control Engineering Practice*, 8: 445–455, 2002.

[78] D. Dumur P. Boucher and K.F. Rahmani. Generalised predictive cascade control (gpcc) for machine tool drives. *Annals of the CIRP*, 39(1):357–360, 1990.

[79] X. Zhang, K. Zhu, and X. Yang. Cross-Coupled Model Predictive Control for Multi-axis Coordinated Motion Systems. In *2009 International Conference on Advanced Computer Control*, pages 158–162, 2009.

[80] D. Dumur, M. Susanu, and M. Aubourg. Complex Form Machining with Axis Drive Predictive Control. *CIRP Annals - Manufacturing Technology*, 57(1):399–402, 2008.

[81] M. Susanu and D. Dumur. Using Predictive Techniques within CNC Machine Tools Feed Drives. In *IEEE Conference on Decision and Control*, pages 5150–5155, 2005.

[82] C.-Li Chen and K.-Chen Lin. Observer-Based Contouring Controller Design of a Biaxial Stage System Subject to Friction. *IEEE Transactions on Control Systems Technology*, 16(2):322–329, 2008.

[83] C. Hu, B. Yao, and Q. Wang. Coordinated Adaptive Robust Contouring Controller Design for an Industrial Biaxial Precision Gantry With Cogging Force Compensations. *IEE Transactions on Industrial Electronics*, 57(5): 322–329, 2010.

[84] R. Soeterboek. *Predictive Control A Unified Approach*. Prentice Hall International Limited, United Kingdom, 1992.

[85] M. Tomizuka. Zero Phase Error Tracking Algorithm for Digital Control. *ASME Jornal of Dynamic Systems, Measurements, and Control*, 109:65–68, 1987.

[86] C. Mohtadi D.W. Clarke and P.S. Tuffs. Generalized predictive control: Part i. the basic algorithm. *Automatica*, 23(2):137–148, 1987.

[87] C. Mohtadi D.W. Clarke and P.S. Tuffs. Generalized predictive control: Part ii. extensions and interpretations. *Automatica*, 23(2):149–160, 1987.

[88] Y. Li and Q. Xu. Development and assessment of a novel decoupled xy parallel micro-positioning platform. *IEEE/ASME Transaction on Mechatronics*, 15(1):125–135, 2010.

[89] J. De Schutter D. Torfs and J. Swevers. Extended bandwidth zero phase error tracking control of nonminimal phase systems. *Journal of Dynamic Systems, Measurement and Control, Transactions of the ASME*, 14:347–351, 1992.

[90] B. Yao C. Hu and Q. Wang. Coordinated adaptive robust contouring controller design for an industrial biaxial precision gantry. *IEEE/ASME Transaction on Mechatronics*, 15(5):728–735, 2010.

[91] S.-S. Yeh and P.-L. Hsu. Estimation of the contouring error vector for the cross-coupled control design. *IEEE/ASME Transaction on Mechatronics*, 7 (1):4451, 2002.

[92] H.-L. Liu S.-L. Chen and S. C. Ting. Contouring control of biaxial systems based on polar coordinates. *IEEE/ASME Transaction on Mechatronics*, 7 (3):329345, 2002.

[93] T. Nakamura N. Uchiyama and H. Yanagiuchi. The effectiveness of contouring control and a design for three-dimensional machining. *International Journal of Machine Tools and Manufacture*, 49:876–884, 2009.

[94] C. Hu B. Yao and Q. Wang. An orthogonal global task coordinate frame for contouring control of biaxial systems. *IEEE/ASME Transactions on Mechatronics*, 17(4):622–634, 2012.

[95] B. Yao C. Hu and Q. Wang. Coordinated adaptive robust contouring control of an industrial biaxial precision gantry with cogging force compensations. *IEEE Transaction on Industrial Electrons*, 57(5):17461754, 2010.

[96] T. H. Ho and K. K. Ahn. Speed control of a hydraulic pressure coupling drive using an adaptive fuzzy sliding-mode contro. *IEEE/ASME Transactions on Mechatronics*, 17(5):976–986, 2012.

[97] M. Zeinali A. Fazeli and A. Khajepour. Application of adaptive sliding mode control for regenerative braking torque control. *IEEE/ASME Transactions on Mechatronics*, 17(4):745–755, 2012.

[98] N. Uchiyama A. El Khalick M. and S. Sano. Reduction of Control Input Variance of Feed Drive Systems Using Sliding-Mode Control with Non-linear Sliding Surface. In *IEEE International Conference on Mechatronics, Vicenza, Italy*, pages 5150–5155, 2013.

[99] Dong Sun Y.X. Su and B.Y. Duan. Design of an enhanced nonlinear pid controller. *Mechatronics*, 15:1005–1024, 2005.

[100] J. Yang and Z. Li. A novel contour error estimation for position loop-based cross-coupled control. *IEEE/ASME Trans. Mechatronics*, 16(4):643–655, 2011.

[101] B. Yao C. Hu and Q. Wang. Contouring Control of Biaxial Based on a New Task Coordinate Frame. In *IEEE/ASME International Conference on Advanced Intelligent Mechatronics, Canada*, 2010.

[102] C.-C. Peng and C.-L. Chen. Biaxial contouring control with friction dynamics usinf a contour index approach. *International Journal of Machine Tools and Manufacturing*, 47:1542–1555, 2007.

[103] George T.C. Chiu and B. Yao. Adaptive Robust Contour Tracking of Machine Tool Feed Drive Systems - A Task Coordinate Frame Approach. In *Proc. of American Control Conference*, volume 5, pages 2731–2735, 1997.

[104] B. Sencer and Y. Altintas. Modeling and Control of Contouring Errors for Five-Axis Machine Tools Part II: Precision Contour Controller Design. *ASME, Journal of Manufacturing Science and Engineering*, 131:031007, 2009.

[105] Chih-Ching Lo. Three-axis contouring control based on a trajectory coordinates basis. *JSME international journal*, 41(2):242–247, 1998.

[106] A. El Khalick M. and N. Uchiyama. Contouring controller design based on iterative contour error estimation for three-dimensional machining. *Robotics and Computer-Integrated Manufacturing*, 27:802–807, 2011.

[107] Einar Hille S.L Salas and John T. Anderson. John Wiley and sons, Inc., 5 edition.

[108] X. Zhang, K. Zhu, and X. Yang. Friction Compensator for Feed Drive Systems Consisting of Ball Screw and Linear Ball Guide. In *The 35th International MATADOR Conference*, volume 13, pages 311–314, 2007.

[109] C.-C. Lo. A Tool-Path Control Scheme for Five-Axis Machine Tools. *International Journal of Machine Tools and Manufacturing*, 41(1):79–88, 2002.

[110] E. L. J. Bohez. Compensating for Systematic Error in 5-Axis Machining. *Computer-Aided Design*, 34:391–403, 2002.

[111] B. Sencer, Y. Altintas, and E. Croft. Modeling and Control of Contouring Errors for Five-Axis Machine Tools Part I: Modeling. *ASME, Journal of Manufacturing Science and Engineering*, 131:031006, 2009.

[112] E.L.J. Bohez. Five-Axis Milling Machine Tool Kinematic Chain Design and Analysis. *International Journal of Machine Tools and Manufacture*, 42:505–520, 2002.

[113] W. Gao J.Y. Humg and J.C. Hung. Variable structure control: A survey. *IEEE Transaction on Industrial Electrons*, 40:2–22, 1993.

[114] Y.K. Wong H.F. Ho and A.B. Rad. Adaptive fuzzy sliding mode control with chattering elimination for nonlinear siso systems. *Simulation Modelling Practice and Theory*, 17(7):1199–1210, 2009.

[115] M. Aghababa and M. Akbari. A chattering-free robust adaptive sliding mode controller for synchronization of two different chaotic systems with unknown uncertainties and external disturbances. *Applied Mathematics and Computation*, 218(9):5757–5768, 2012.

[116] M. Zhihong and D. Habibi. A robust adaptive sliding-mode control for rigid robotic manipulators with arbitrary bounded input disturbances. *Journal of Intelligent and Robotic Systems*, 17:371–386, 1996.

Publications

The contents of this thesis are the results of original research and have not been submitted for a higher degree to any other university or institution.

Much of the work presented in this thesis has been published as journal or conference papers. Following is a list of these papers.

International Journal Papers

(1) A. El Khalick M. and N. Uchiyama, "Model Predictive Approach to Precision Contouring Control for Feed Drive Systems," Journal of Computer Science, vol. 6, no. 8, pp. 844-851, 2010. (*Impact Factor: 1.350*)

(2) A. El Khalick M. and N. Uchiyama, "Discrete-Time Model Predictive Contouring Control for Biaxial Feed Drive Systems and Experimental Verification," Mechatronics, vol. 21, no. 6, pp. 918-926, 2011. (*5-Year Impact Factor: 1.496*)

(3) A. El Khalick M. and N. Uchiyama, "Contouring Controller Design Based on Iterative Contour Error Estimation for Three-Dimensional Machining," Journal of Robotics and Computer-Integrated Manufacturing, vol. 27, no. 4, pp. 802-807, 2011. (*5-Year Impact Factor: 1.668*)

(4) A. El Khalick M., N. Uchiyama and S. Sano, "Sliding Mode Contouring Control Design Using Nonlinear Sliding Surface for Three-Dimensional Machining," International Journal of Machine Tools and Manufacturing, vol. 65, pp. 8-14, 2012. (*5-Year Impact Factor: 2.564*)

(5) A. El Khalick M. and N. Uchiyama, "Estimation of Tool-Orientation Contour Error for Five-Axis Machining," Journal of Robotics and Computer-Integrated Manufacturing, vol. 29(5), pp. 271-277, 2013. (*5-Year Impact Factor: 1.668*)

(6) <u>A. El Khalick M.</u>, N. Uchiyama and S. Sano, "Reduction of Electrical Energy Consumed By Feed Drive Systems Using Sliding-Mode Control with A Non-linear Sliding Surface" IEEE Transaction on Industrial Electronics, Accepted. (*Impact Factor: 5.160*)

International Conferences Papers

(1) <u>A. El Khalick M.</u> and N. Uchiyama, "Model Predictive Contouring Control for Biaxial Feed Drive Systems," Proceedings of the 2010 International Symposium on Robotics and Intelligent Sensors, Nagoya, Japan, 2010.

(2) <u>A. El Khalick M.</u> and N. Uchiyama, "Model Predictive Contouring Control for Biaxial Feed Drive Systems Based on Coordinate Transformation," Proceedings of the 2010 International Symposium on Flexible Automation, ASME, Tokyo, Japan, 2010.

(3) <u>A. El Khalick M.</u> and N. Uchiyama, "Synchronization of Tool Tip and Tool Orientation Contour Errors in Five-Axis Machining," The 2012 American Control Conference (ACC), Montreal, Canada. 2012.

(4) <u>A. El Khalick M.</u>, N. Uchiyama and S. Sano, "Reduction of Control Input Variance of Feed Drive Systems Using Sliding-Mode Control with Non-linear Sliding Surface" IEEE International Conference on Mechatronics, Vicenza, Italy, 2013.

(5) N. Uchiyama, Y. Ogawa, <u>A. El Khalick M.</u> and S. Sano, "Energy Saving Control in Five-Axis Machine Tools Using Contouring Control," The 2013 European Control Conference, Zurich, Switzerland, 2013.

(6) <u>A. El Khalick M.</u>, N. Uchiyama and S. Sano, "Sliding Mode Contouring Controller with a Nonlinear Sliding Surface and a Disturbance Observer for Five-Axis Machining Tasks," The 7th International Conference on Leading Edge Manufacturing in 21st Century, Miyagi, Japan, 2013.

Domestic Conferences Papers

(1) <u>A. El Khalick M.</u>, N. Uchiyama and S. Sano, "Sliding Mode Contouring Control for Feed Drive Systems Using Nonlinear Sliding Surface," The 54th japan Joint Automatic Control Conference, Toyohashi, Japan, 2011.

Abd El Khalick Mohammad Ahmad

Toyohashi University of Technology

November, 2013